Off-grid PV systems for rural electrification

Optimizing the sizing methodology
for off-grid PV systems

TU Delft

Ali Chamseddine

Off-grid PV systems for Rural Electrification

Optimizing the sizing methodology for off-grid PV systems

September 24, 2018

Ali Chamseddine - 4622049

In partial fulfillment of the requirements for the degree of
Master of Science
in Sustainable Energy Technology
at the Delft University of Technology,
to be defended publicly on Friday September 28, 2018 at 3:00 PM.

Mentor	Nishant Narayan	TU Delft
Thesis supervisor	Dr. ir. Z. Qin	TU Delft
Thesis committee	Prof. dr. ir. P. Bauer,	TU Delft
	Dr.ir. J.L. Rueda Torres	TU Delft

Acknowledgements

I would like to first thank Nishant Narayan for his constant and valuable feedback throughout this tough but enriching experience. His motivation, optimism and big-brotherly advice were always welcome and uplifting, especially during the last few weeks. The work done in this thesis exceeded my expectations, and sincerely hope that it'll be a great benefit to his research. Furthermore, I would like to thank Prof. P. Bauer and Dr. Z. Qin for their feedback and insight on my work. I would also like to thank Dr. J. Rueda Torres for his willingness to be a part of my thesis committee.

Now that my two years in TU Delft have come to an end, I would like to thank the many, many people that have provided me with the support throughout the journey, and to all the friends that I have met here who have become my second family. I would like to thank the Happy Tree Friends group who, after 8 years, remained my closest friends no matter where life took each one of us. Esther in particular, thank you for your constant support. I would also like to thank Sam for the memorable times we spent in Kanaalweg, and Mariana, who made my move to Delft be as smooth as it can get.

A very special thanks goes to Guillaume, Michael, Dario and Ines, my Frank Van Borselenstraat family, who along with Liz, Miguel, Joana, Carolina & Ibrahim, have provided great support throughout these two years and made my stay in Delft an amazing experience.

Last but not least, I would like to thank my family, the Chamseddines. My parents, Nisrine, Khalil & Aya, who this opportunity would not have been possible without, and for the tremendous support you have provided over the last few months.

Ali Chamseddine

23-09-2018

Abstract

To this day, 16% of the world's population still has little or no access to electricity. The majority of which is located in rural regions of developing countries, such as India and most countries in sub-Saharan Africa. As a part of the Sustainable Energy for All (SE4All) initiative, a multi-tier framework that aims to categorize and quantify the electricity access of households and rural regions to reach the sustainable development goals by 2030.

Solar Home Systems (SHS) is a potential solution that has emerged to cater for the lighting and power needs of these remote households. SHSs consist of a small stand-alone DC system which are composed of a PV array, battery, and power electronics that are designed to meet the load of a single household. The aim of this study is to propose a universal, optimal sizing methodology for the SHS with respect to cost, reliability (LLP) and battery lifetime for any household in the mutli-tier energy ladder. Moreover, the study aims to anticipate to which extend a stand-alone architecture remains a feasible solution.

In this thesis, a practical model for each of the Solar Home System components was built using MATLAB, then two optimization methods: a classical iterative method, and the Genetic Algorithm, an evolutionary method were used to perform a multi-objective optimization on three case studies in different locations. The results obtained showed that for the lower energy tiers, with a load profile up to a peak load of 155 W, the stand-alone approach is optimal. With an LLP≤2%, an average total upfront cost of 1600$, and a lead-acid battery lifetime of 6.5 years. The results from the higher tiers however show proved that as the household moves up the energy ladder, the stand-alone approach becomes unaffordable and less reliable.

An alternate approach to solve this issue was examined, where several households are interconnected forming a minigrid to share their energy generation and load. The outcome of this study showed that households with sub-optimal sized Solar Home Systems were able to greatly increase their system reliability, the LLP was recorded to drop by up to 50% in some scenarios with an increasing number of interconnected households. The LLP drop however reached a saturation point beyond 25 households.

On this basis, it is recommended that further work should be done to increase the complexity of the component models, notable the battery. Moreover, a more extensive study should be conducted on the interconnected approach, with a multitude of scenarios to optimize the system size in a mini-grid architecture.

Contents

List of Figures

List of Tables

1 Introduction

1.1. Energy Scenario

In the past decades, energy has been key for a nation's economic growth, prosperity, social equity. Access to energy has lead to technological advancement, improved public health, increased education, and social empowerment. Moreover, the energy transition towards renewable sources has been a revolutionary, but necessary milestone towards a sustainable future [86]. In recent years, research and development, firm learning, and economies of scale have been majors factors in the technological development of renewable energy sources, particularly solar and wind. For example, the cost of replacing a coal-fired electricity plant with a solar PV farm has fallen 85% since 2000 [80].

However, even with this technological breakthrough and decreasing trend in energy and renewable source costs, there are still 1.2 billion people around the world that lacked access to electricity in 2011, some 85% of them in rural areas, the majority of them living in Sub-Saharan Africa where the electrification rate is only 31% [43]. This has lead to the formation of the Paris conference in 2015, where 193 members states of the United Nations agreed on ensuring access to reliable and affordable energy for all by the year 2030. Since then, electrification efforts have been increasing where more than 100 million people per year have gained electricity access. The International Energy Agency's (IEA) World Energy Outlook report expects a decline to only 674 million people without access to electricity by 2030, out of which 600 million are in rural areas in Sub-Saharan Africa [1].

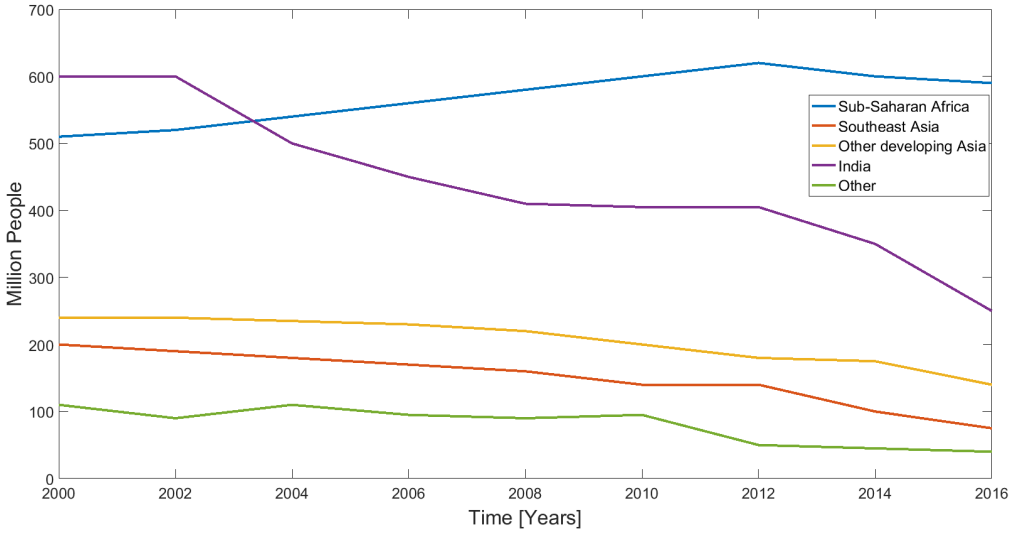

Figure 1.1: Population without access to electricity, *Adapted from* [1].

In several countries, household income and electricity cost are the major concerns for the poorest households, but several other factors contribute to the lack of electrification such as insufficient policy and lack of

infrastructure. In sub-Saharan Africa, around 120 million people live above the poverty line, but still have no access to electricity, and even when they do, the electricity is unreliable as illustrated in figure 1.2.

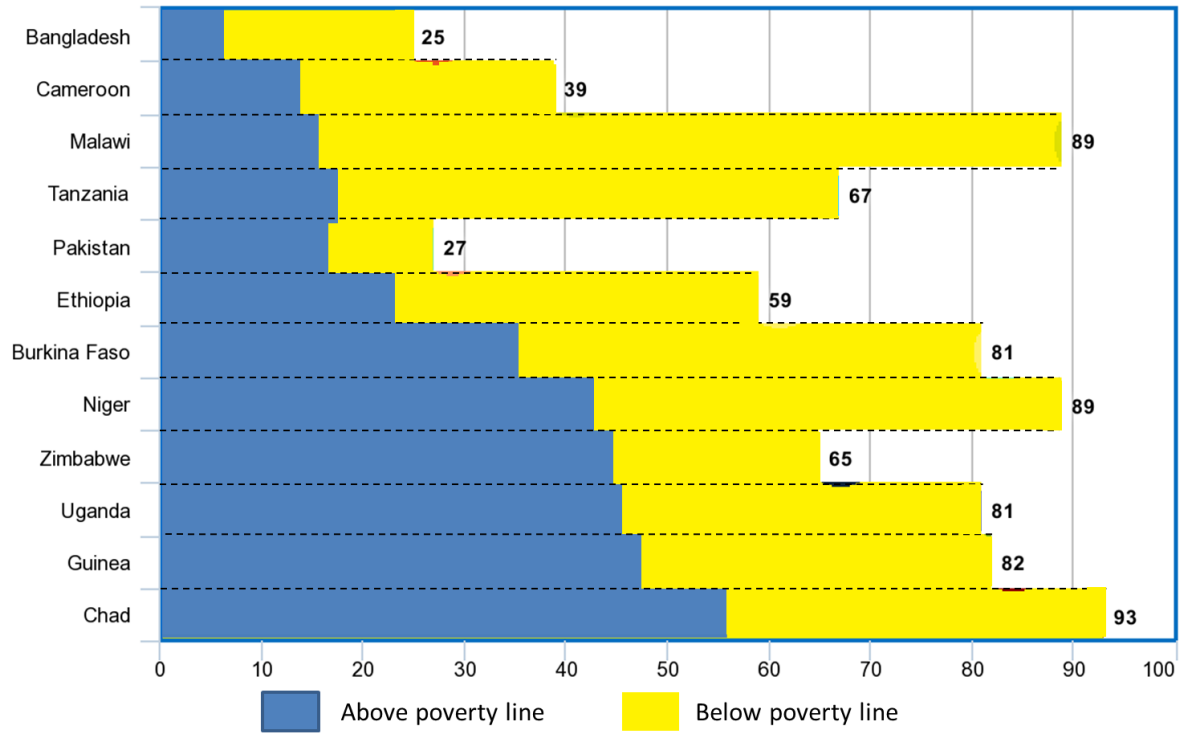

Figure 1.2: Some households that are above the poverty line still lack energy access due to poor infrastructure [1].

Recently, with the emerging of renewable sources and technological innovations, new business models started to take advantage for the situation. Several countries have provided subsidies and policy efforts in order to help the rise of of renewable energy sources, and to the decentralized energy distribution designs. Decentralized energy provides a solution to the long term infrastructure problems, and provides a local and reliable electricity supply source [45]. Many decentralized system architectures and designs have become available, from single household stand-alone pico-grids, to larger micro and mini-grids. These decentralized systems are able to fill the energy gap in most remote and urban areas.

1.2. Role of Solar Energy in Rural Electrification

With the world focusing more on investment and innovations in renewable energy sources, there has been a large increase in their total installed capacity. Wind and solar installed capacity has doubled every three years on average over the past three decades, exceeding the expectations and projections of the IEA [80].

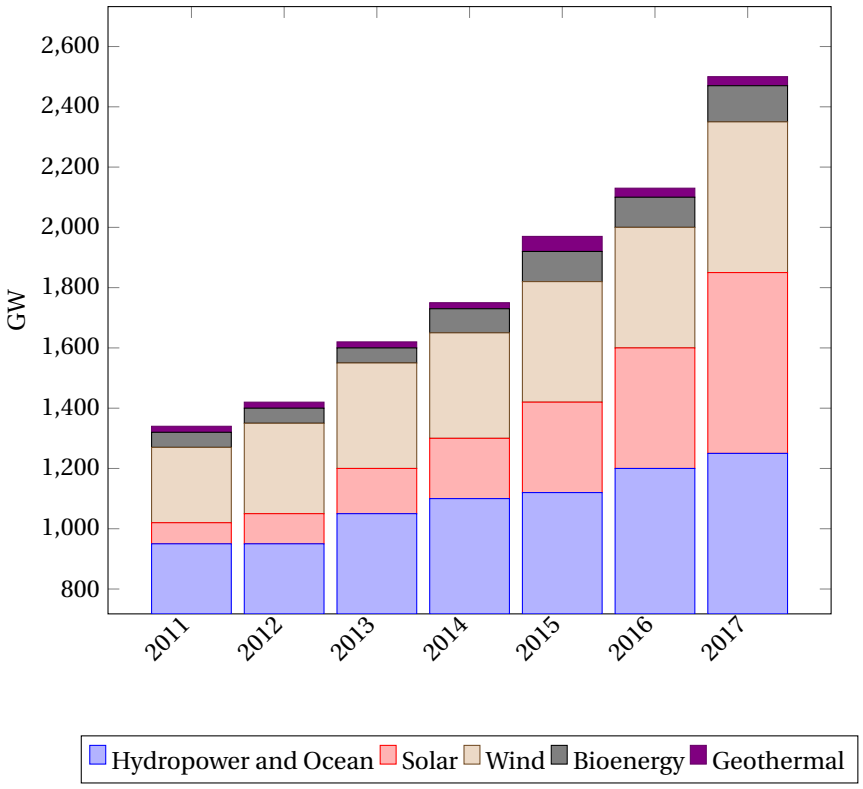

Figure 1.3: Renewable energy generation 2011-2017, *Adapted from* [39].

Solar power notably, has been the leading renewable energy source in terms of installed capacity, PV capacity grew from 6.1 GW to 291 GW between 2006 and 2016. The deployment of new technologies and implementation of new projects allowed manufacturers and to gain experience as they produce the technology, and that was a major factor in increasing the efficiency and improving the production methods which led to the reduction of their cost. Moreover, the global awareness in climate-change issues has led many households to shift towards clean and affordable energy sources. Solar PV was the ideal solution as it can be mounted on the roof of homes, reducing the energy bill costs and CO_2 emissions. Residential and commercial rooftop PV installations grew by around 50% per year from 2008 - 2014 [6, 39]. Figures 1.4 and 1.5 show the increasing grid-connected worldwide installed PV capacity and decrease in the module price for different PV technologies respectively.

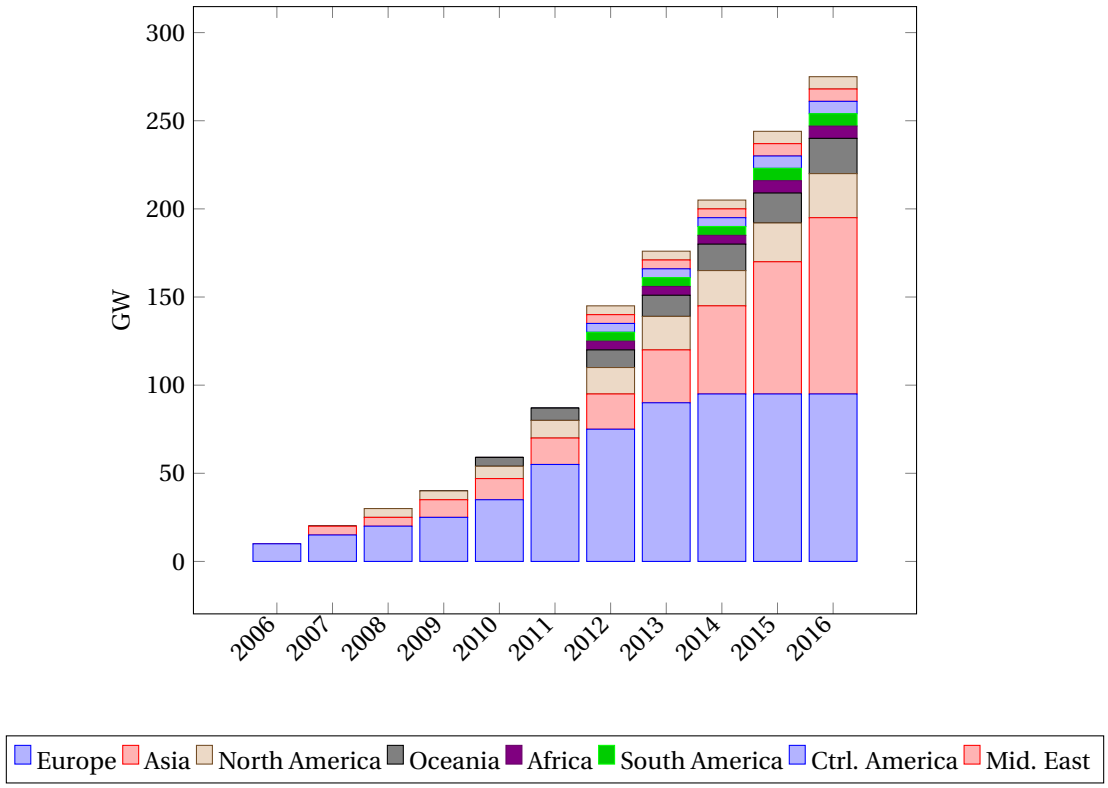

Figure 1.4: Cumulative grid-connected PV capacity 2006 - 2016, *Adapted from* [39].

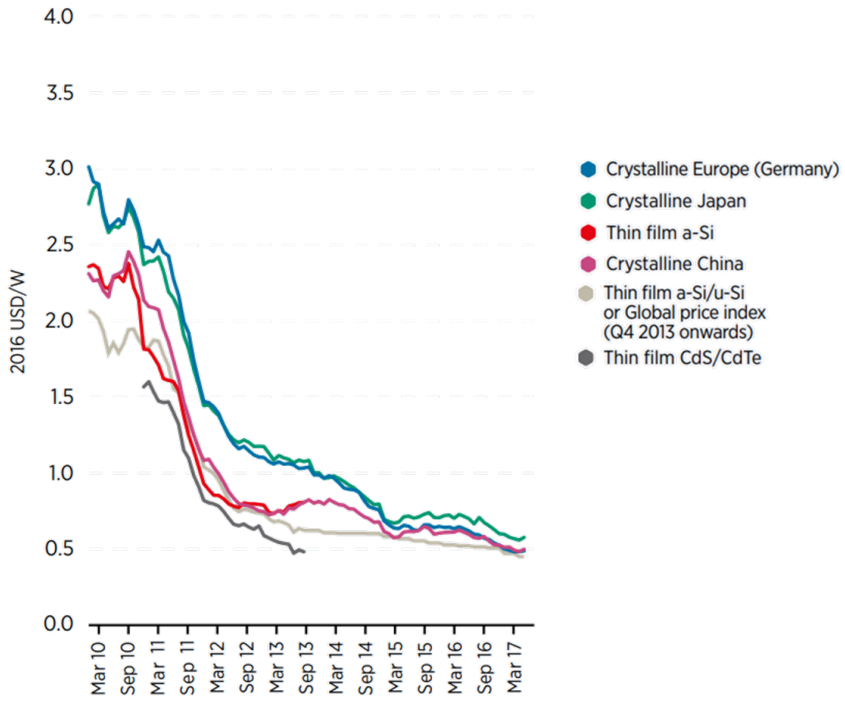

Figure 1.5: Decline in module price for different technologies [39]

The rapid decrease in cost, increased efficiency and reliability of PV modules made the technology ideal in remote and urban areas as a back-up for unreliable grid supply, or as the sole electricity generation source for households. Rural areas in regions with developing countries such as India or sub-Saharan Africa, having low demand density and sparse households, make investment in grid infrastructure and maintenance unattractive, and not a feasible possibility in the coming few years. For these areas, developing off-grid solar systems seems like the most promising and immediate solution for electrification.

Solar Home Systems

Solar Home Systems (SHS) are stand-alone photovoltaic systems that emerged as a solution for off-grid households to cater their lighting and power needs. In rural areas, where grid connection is not feasible, SHSs are typically designed to meet the desired load of a single household and are in the capacity range of 35-100 Wp. A Solar Home System always consists of a PV array, a battery, a charge regulator, and the load consisting of lights and sockets or appliances. In India and sub-Saharan Africa SHS can be considered as an alternative to conventional fuels such as kerosene and candles [19, 71].

To support the rise of SHSs, recent appliance manufacturers have also gained high interest in developing innovative and highly efficient appliances that greatly reduce electricity consumption costs. Figure 1.6 below shows that the use of highly-efficient appliances, even though more expensive themselves, reduce the annual discounted cost by 32%

Solar home systems consists of a PV array, battery storage and Balance of System (BoS) that can be built at any scale to meet the needs of a household.

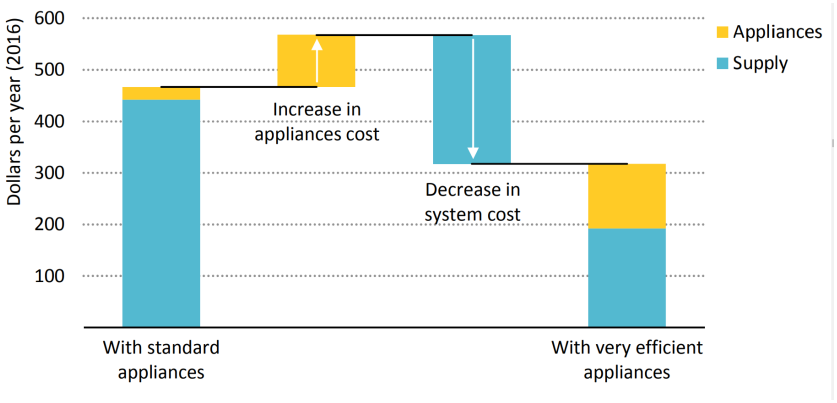

Figure 1.6: Annual discounted cost reductions with the use of highly-efficient appliances [39]

In the following sections, the use of stand-alone SHSs for the electrification of rural areas will be explained.

1.3. Multi-tier framework

With the increasing urgency of action against climate change, and dedication towards reaching a sustainable future and allowing sustainable for 4 all (SE4ALL), a Global Tracking Framework (GTF) call has been made as a call for action for leaders to track, plan and take action in delivering sustainable energy and meeting the sustainable development goals set in the Paris conference in 2015. As per the GTF, a multi-tier framework has been made to categorize households and regions according to their access to electricity. This framework helps quantify both the quality and quantity of electricity access for households. Table 1.1 below shows the classification of the different tiers [81].

Table 1.1: Multi-Tier Framework classification, *Adapted from* [81]

Attribute	Tier 0	Tier 1	Tier 2	Tier 3	Tier 4	Tier 5
Services	-	Task Light Phone charging Radio	Lighting TV Fan	Tier 2 + Other low power appliances	Tier 3 + Medium power appliances	Tier 4 + High power appliances
Peak power capacity	-	>1 W	>20/50 W	>200 W / 500 W	>2,000 W	>2,000 W
Duration	-	>4 hrs	>4 hrs	>8 hrs	>16 hrs	>16 hrs
Evening supply	-	>2 hrs	>2 hrs	>2 hrs	>4 hrs	>4 hrs
Quality [Voltage]	-	-	-	✓	✓	✓

The smallest SHSs, known also as Pico solar installations, comprise a solar panel, battery, one or more LED lamps and mobile phone charging port. Although it is very low, it nonetheless provides significant benefits to those previously without any access such as going from tier 0 to tier 1. This breakthrough from no electricity

access to tier 1 is a low-cost way for people to secure an immediate improvement in their quality of life. However, to provide a significant improvement in the household quality of life, higher energy supplies are needed to feed several appliances that could improve productivity such as refrigerator or televisions. As can be seen from table 1.1, there is a large gap between tier 1 & 3 of over a hundred times in magnitude in peak power capacity. This would require a significantly larger SHS that would be able to sustain these loads at a better voltage quality without compromising system reliability (very few or no blackouts, no-over use of the components and wear prevention). Hence, systems of various sizes and characteristics are needed for each tier, and only through going up the energy ladder can the households reach a significant improvement in quality of life.

1.4. Importance of modular sizing

As mentioned in the previous section, it is only through going up to the higher levels (tier 3 and above), will the households be able to have a significant improvement in their quality of life and increase productivity. However, this poses a problem for the household. On the one hand, after moving from tier 0 to tier 1, with this new access to electric power, households will quickly be eager to increase their investments in more appliances that will help them in their daily life. Nevertheless, the use of the extra appliances will be exceeding the peak power capacity and make the original SHS unfeasible or unreliable. On the other hand, investing in a larger SHS system from the start is not a possibility for most households due to the large increase in the system upfront cost. A tier 1 SHS costs roughly $\leq$ 50$, while a tier 3 system is in the order of a 1000$, hence out of the budget of many households living in poverty. A promising solution for this issue, is the design of flexible and modular SHSs. The basic idea behind these systems is that they consist of blocks of a predetermined SHS with a specific peak power, consisting PV and battery capacity along with the Balance of System (BoS). These basic SHS blocks can be gradually combined together as needed by the household to go from tier to the next, hence, climbing up to the top of the energy ladder.

1.5. Thesis Objective

The objective of this thesis is to design a system that would be optimal for the household in each tier, as they go up the energy ladder. The system needs to maintain optimal performance and reliability, without the compromise of higher cost which would make it unaffordable. Hence, the main objective of this project is to design a SHSs, that will operate at its optimum during the gradual increase in load demand, eventually leading to a large improvement in the quality of life of the household. In short the thesis objective is:

- **Propose an optimal sizing methodology for a SHS with respect to cost, LLP, energy dump and lifetime that would be applicable for the varying load demands in the energy ladder.**

1.5.1. Research Questions

Finding a universal sizing methodology for an optimal SHS is a challenge, and needs to address several issues:

1. What are the best modeling and optimization strategies to optimize the size of a SHS.
   (a) What are the most important parameters that need to be optimized during the sizing process?
   (b) What are the best optimization methods that can be used in the sizing methodology?
2. What is the methodology that can be applied to all tiers to obtain the optimal system size that will be able to cope with the household demand? And at what point does the SHS stand-alone approach become unfeasible?

1.5.2. Contributions

Upon achieving the goal of this thesis, some unique contributions were made during the process that can be implemented during the design of stand-alone Hybrid Renewable Energy Systems (HRESs) as follows:

- A multi-objective optimization approach that incorporates several parameters of the SHS to find the best modular system size taking into account:
  - Maximizing battery lifetime
  - Maximizing the reliability through a minimum LLP
  - Minimizing the upfront cost considering replacement costs and future cost projections.
- A feasibility study between the stand-alone SHS architecture and household interconnectivity for the different tiers.

1.6. Layout of the Thesis

Chapter 1 - Introduction

This chapter consists of a short overview of the thesis topic and defining the objective and research questions as well as the unique contributions of this work.

Chapter 2 - Literature Review

In this chapter, a literature review on the various sizing methodologies of Solar Home System available in studies is presented. Moreover, the critical system parameter as well as the most popular optimization methods during the system sizing are addressed.

Chapter 3 - Modeling & Sizing Methodology

The theory applied to model the different components of the SHS is explained, along with some simulation results to illustrate the performance of each. Then, the system control architecture and performance parameters are presented.

Chapter 4 - Stand-alone SHS sizing

In this chapter, the methodology for the sizing optimization for each tier as the household escalates up the multi-tier energy ladder is explained. Then, two optimization methods: the iterative method and the Genetic Algorithm are used in three case studies to present the findings and results.

Chapter 5 - Sizing interconnected SHS

In chapter 5, a different approach is examined for optimizing the performance of the system over the different tiers. The method consists of a microgrid architecture where several households are interconnected in order to share their electricity generation and demand, hence increasing overall reliability.

Chapter 6 - Conclusions & Recommendations

In the final chapter, the main conclusions drawn from this study are presented, along with recommendations for future works and studies.

2

Literature Review

This chapter introduces the existing research and work done on the topic of off-grid electrification. The typical architecture of a standalone PV system is introduced, followed by determining the most important sizing parameters of the system and component selection. Finally, the existing system sizing and optimization methodologies will be discussed.

2.1. Solar Home Systems Architecture

Renewable energy systems can be split into two types: grid-connected systems and off-grid systems. The majority of residential grid-connected systems include large scale solar and and wind farms, hydro-plants, and most of the residential PV systems, where the surplus energy is sent or sold to the grid [2]. However, remote areas that are located out of the reach of the electricity grids, households have to rely on self-sufficient and standalone Hybrid Renewable Energy Systems or HRESs [70].

2.1.1. HRES Combination

Several studies have been conducted on off-grid HRES combination designs that would work in a reliable and efficient manner. In some studies such as [32, 85], a sizing methodology was presented for HRESs consisting of PV, Battery storage and a diesel generator in Northern Australia and Brazil respectively. The aim was to design a self-sufficient standalone system while minimizing the use of the diesel generator. Other studies, such as [5, 50, 64], did a study on PV, wind turbine and battery storage combinations, making the system completely made out of renewable energy sources, and having the storage system act as a buffer to keep up with the constant load demand during low energy production days. However, a lot of studies such as [9, 18, 89] are focused on the simple combination of a PV array as an energy source, and a battery bank to account for the load fluctuations, night time, and cloudy days.

As the goal of this thesis is the electrification of rural areas through simple, flexible and affordable systems, the Solar array/battery storage combination seems the most promising one. Moreover, these areas such as India and Sub-Saharan Africa are mostly abundant in solar irradiance and have few cloudy days.

2.1.2. Electrical Configuration

Renewable energy systems need to be implemented in a specific interface or architecture following the nature of the energy sources, loads, and battery storage. Typically, there are 3 topologies for a stand-alone renewable energy system [78]:

- **DC-coupled Configuration:** Where the renewable energy sources are connected to the main DC feeder either directly or through a DC/DC converter. The DC feeder connects to the various loads and to the energy storage through DC/AC and DC/DC converters as needed.
- **AC-coupled Configuration:** Where the energy sources (DC or AC) are connected to an AC feeder through AC/AC or DC/AC converter. The AC feeder connects the various sources to the loads and storage devices.
- **Hybrid Configuration:** Where there are two AC and DC feeders connected by a AC/DC converter. AC and DC renewable sources are connected to the AC and DC feeders respectively. The two feeders are

connected by an AC/DC converter. This topology reduces conversion losses if the loads, sources and storage devices are scattered and vary between AC and DC.

The three topologies are shown in figure 2.1 below:

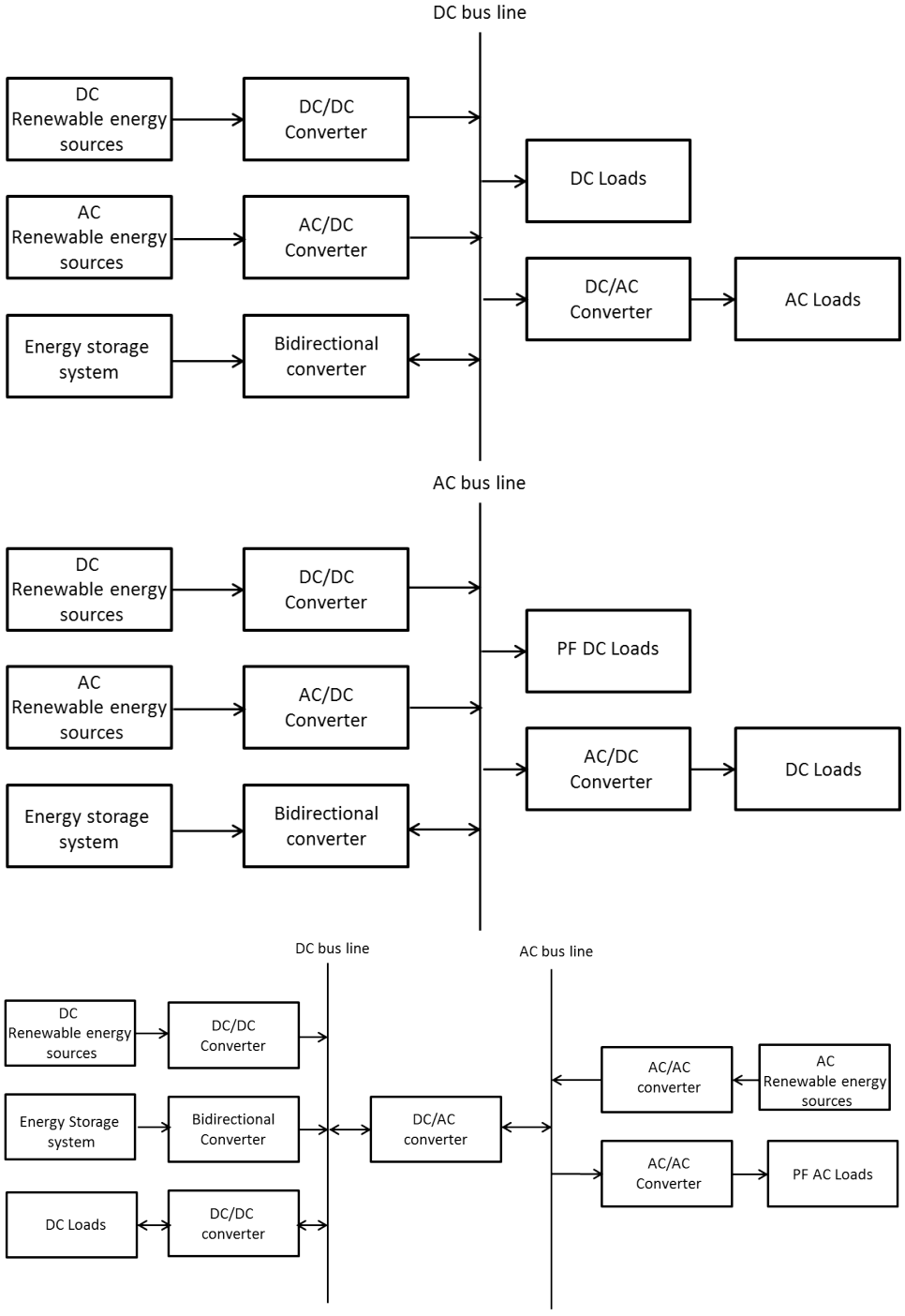

Figure 2.1: (a)DC-Coupled Configuration. (b) AC-Coupled Configuration. (c) Hybrid Configuration [78].

As the Solar Home System consists uniquely of DC components, being solar modules, batteries, and DC loads, the simple DC topology was selected as the system architecture. The power electronics in this architecture consist uniquely of a charge controller that is responsible for regulating the battery charge/discharge and adjusting the voltage of the PV modules and batteries to the DC load. The typical architecture of the proposed system is as shown in figure 2.2 below.

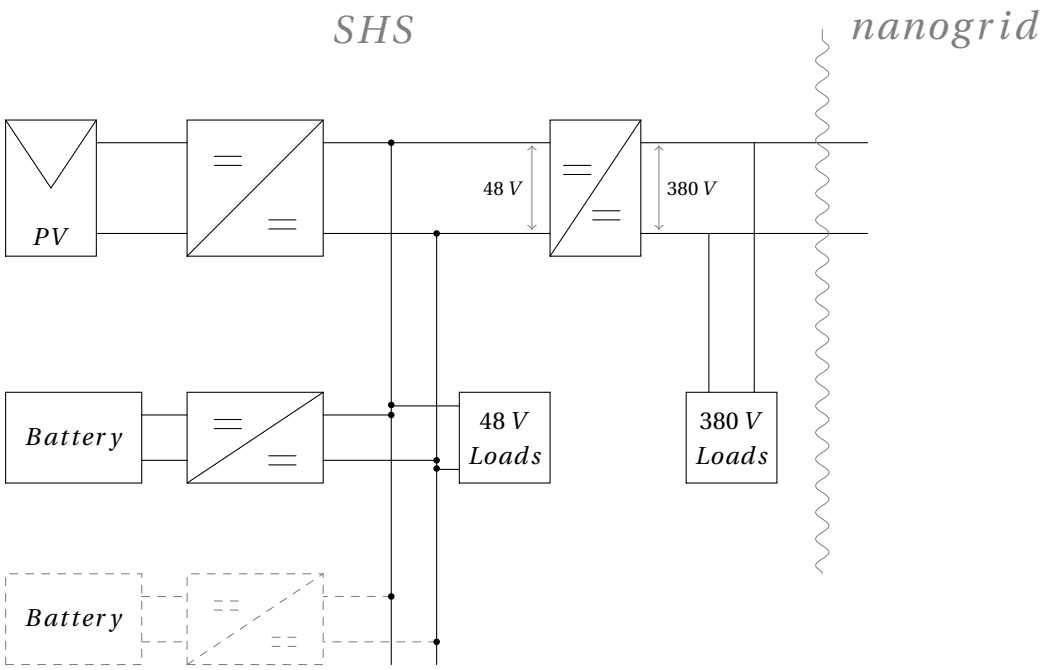

Figure 2.2: SHS architecture, with a possibility of interconnecting several households for a modular growth option.

2.2. System Parameters

With the basic system architecture identified, the system parameters or criteria on which the system needs to be sized have to be identified. Most research discusses optimal sizing of the integrated SHS to find a good trade-off between system performance and reliability, and initial cost. Some studies such as [7] and [9] focused mainly on the economic analysis of the system, for example, [9] presented a methodology for the proper sizing of a PV unit and storage through an economic point of view by optimizing the system size according to the payback period and net present value. While [70] tried to determine the effectiveness of the SHS solution of different households falling in different tiers by comparing the monthly cost to a regular subscription to the grid in Uttar Pradesh and Bahar in India, which have less than 40% household electrification rate.

Table 2.1: Monthly cost of grid connected systems VS SHS for different tiers, *adapted from [70]*

Tier	**Grid**		**Solar Home System**				**Competing**
	Capacity Shortage [%]	**Monthly cost [USD]**	**Capacity Shortage [%]**	**Lifetime [years]**	**Specs**	**Monthly cost [USD]**	
0	81,8	UP: 24,92/43,04 Bihar: 23,33/25,65	10 15	15 10	PV: 111W PV: 101 W	2,39 2,29	Yes
1	78	UP: 27,68/45,21 Bihar: 25,94/27,82	10 15	15 10	PV: 175 W PV: 155 W	3,35 3,13	Yes
2	57	UP: 46,23/53,91 Bihar: 50,58/52,46	40	15	PV: 579 W	7,58	No
3	21	UP: 102,75/43,04 Bihar: 87,10/41,88	40	15	PV: 2180 W	22,04	No

While other studies focused both on reliability and on costs. In the study in [37], an optimal sizing on a HRES consisting of PV modules, a wind turbine and fuel cells in Iran to achieve a highly reliable system at the best cost of energy or COE. The system reliability was measured by a parameter called the Loss of Load Probability or LLP. Battery lifetime is also an important parameter that was the main focus of some studies. In [17] an economic analysis was performed on a system consisting of PV-Diesel Generator-Batteries was performed. The goal was to find a trade-off between minimizing the full system cost, and hence the diesel generator operating cost and the number of battery replacements. The more the battery was being used, the faster it was degrading leading to the need to change it more frequently. Following the studies introduced above, the main parameters, or design criteria that need to be met in the proposed SHS are the following:

Loss of Load Probability

The loss of load probability (LLP) is the essential parameter for quantifying the overall system reliability. The LLP value indicates the the relative period of time in which the PV and battery combination failed to satisfy the load demand over the studied period [79]. A higher LLP value means a less reliable system. For example, an LLP of 0.05 or 5% in a year, means that throughout this year, the system was down during 5% of the time, or 18 days. This LLP is defined as the Level of Autonomy (LA) in some studies, where it is expressed as one minus the LLP. Hence, a higher LA means a more reliable system [25]. Other studies such as [48] define the LLP as the fraction of the load that is not supplied by a stand-alone system over the whole yearly load. The equations of both definitions are shown in equations 2.1 and 2.2 below.

$$\mathrm{LLP} = \frac{\mathrm{t_{downtime}}}{\mathrm{T_{total}}} \tag{2.1}$$

$$\mathrm{LLP} = \frac{\mathrm{E_{fail}}}{\int_{\mathrm{year}} \mathrm{P_L(t)dt}} \tag{2.2}$$

$$\mathrm{LA} = 1 - \frac{\mathrm{T_{downtime}}}{\mathrm{T_{Total}}} \tag{2.3}$$

In this study, the interest in reliability is focused more on simply supplying the load at all times, and not at the amount of load that is supplied. So the first definition and equation 2.1 will be used for the LLP from here on-wards.

System Cost

The system cost is another important parameter that needs to be addressed in the sizing optimization. A focus on cost minimization eliminates the need to oversize the system components just to make the system reliable. There are multiple ways to calculate the system cost [11, 22], the chosen method consists of calculating the system capital cost and component replacement replacement cost over the lifetime of the system, which is usually equal to the lifetime of the PV module, being the longest of around 20 years [49].

$$\mathrm{Q_{system}} = \mathrm{Q_{cap}} + \mathrm{Q_{rep}} \tag{2.4}$$

$$\mathrm{Q_{cap}} = \mathrm{N_{PV}}.\mathrm{Q_{PV}} + \mathrm{C_B}.\mathrm{Q_B} + \mathrm{S_C}.\mathrm{Q_C} \tag{2.5}$$

$$\mathrm{Q_{rep}} = \mathrm{C_B}.\mathrm{Q_B}.\sum_{\mathrm{n=1}}^{\mathrm{T_B}} \frac{1}{(1+\mathrm{i})^{\mathrm{T_L}\times \mathrm{n}}} + \mathrm{S_C}.\mathrm{Q_C}.\sum_{\mathrm{n=1}}^{\mathrm{T_C}} \frac{1}{(1+\mathrm{i})^{\mathrm{T_L}\times \mathrm{n}}} \tag{2.6}$$

Where the different variables are shown in table 2.2 below.

Table 2.2: System cost variables

Variable	Definition
$\mathrm{Q_{system}}$	System cost
$\mathrm{Q_{cap}}$	Capital cost
$\mathrm{Q_{rep}}$	Replacement cost
$\mathrm{N_{PV}}$	Number of PV modules
$\mathrm{Q_{PV}}$	Cost of PV module
$\mathrm{C_B}$	Battery capacity
$\mathrm{Q_B}$	Cost per kWh
$\mathrm{S_C}$	Converter/inverter size
$\mathrm{Q_C}$	Converter cost per kW
$\mathrm{T_B}$	Battery lifetime
$\mathrm{T_L}$	System lifetime
i	inflation rate
$\mathrm{T_C}$	Converter lifetime

As shown in equations 2.4 to 2.6, the smaller the system size, being number of PV modules, converter size and battery capacity, the lower the cost. Moreover, the longer each component lasts, the lower are the replacement costs.

Battery lifetime

Batteries degrade and experience capacity loss as they age. This is due to the irreversible chemical and physical changes that occur with usage[10]. Each battery type is affected by different aging processes. Some of the causes for aging for Li-ion and lead-acid batteries are discussed below:

- **Li-ion batteries:** Different processes contribute to their aging such as electrolyte decomposition, and the formation of surface films on both electrodes [69].
- **Lead-acid batteries:** Over-charge in lead-acid batteries leads to anodic corrosion, and positive active mass degradation and loss of adherence are caused by high cycles and increased depths of discharge [73].

In a stand-alone SHS, batteries or energy storage systems are typically the most expensive component [61], their lifetimes vary greatly from one project to another. Proper use and maintenance of batteries could increase their lifetime considerably, while poor maintenance and charging/discharging could reduce the lifetime to even less than 1 year. Lead-acid batteries typically have a rated lifetime of around 4 years, but if they perform at low charge/discharge cycles their lifetime could increase to up to 15 years [23]. Li-ion batteries on the other hand, have a higher typical lifetime. In fact, most electric vehicle car manufacturers give nowadays give a lifetime of 8 - 10 years for the Li-ion batteries in their EVs [82]. The figure below shows the overall cost distribution of an off-grid SHS where the battery accounts for 14 - 69% of the total installed costs of the various SHSs that are below 1 kW [38].

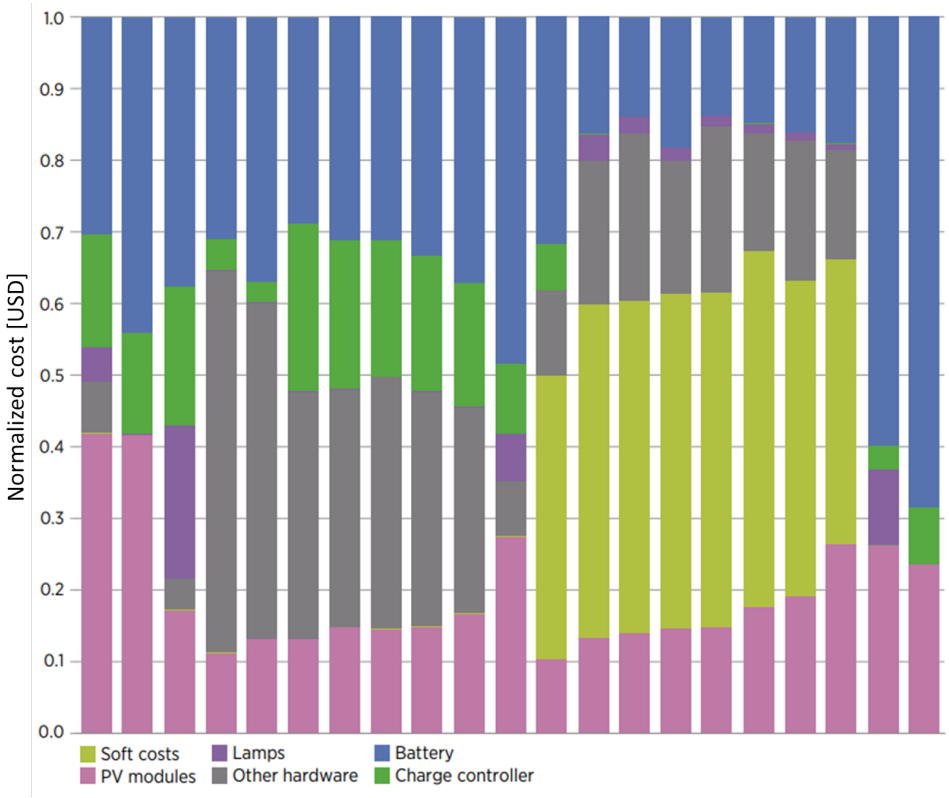

Figure 2.3: Normalized total installed cost for various < 1 kW off-grid Solar Home Systems in Africa [38].

2.3. Existing Sizing methods

In general, to find the size of a stand-alone system, the main data required are the system load data, and the meteorological data of the location. Based on that, the different components can be sized accordingly. In literature, different sizing methods have been used, and are categorized as either intuitive methods, or optimization methods.

2.3.1. Intuitive Methods

Intuitive methods rely on quick and simple "rule-of thumb" calculations to size the SHS. This method employs the use of average daily, monthly or yearly meteorological data, and the use of safety factors during design to estimate the size of the PV arrays and batteries [47]. This method gives and idea about the order of the system size, but has the disadvantage of over or under sizing the system due to the many assumptions.

In this method, the performance and efficiency of the different components are assumed as constants, and does not take into account the dynamic interaction between them. The size of the PV array and batteries can be calculated via:

$$\mathrm{P_{PV}} = \frac{\mathrm{E_{Load}}}{\eta_{\mathrm{PV}}.\eta_{\mathrm{C}}.\mathrm{ESH}}.\mathrm{S_f} \tag{2.7}$$

$$\mathrm{C_B} = \frac{\mathrm{E_{Load}}.\mathrm{DOA}}{\mathrm{V_B}.\mathrm{DoD}.\eta_{\mathrm{B}}} \tag{2.8}$$

Where E_{Load} is average daily load, S_f, V_B and DoD are the battery voltage and depth of discharge respectively. η_{PV},η_C and η_B are the efficiencies of the PV, power electronics and batteries respectively. The factor ESH means the Equivalent Sun Hours, which depends on the location. The safety factor S_f and battery Days of Autonomy (DOA) are chosen according to the users preferences. The DOA accounts for how many days will the battery be sized to run during days with no energy generation, such as cloudy days, winter, and nights. Typically, the DOA is taken to be 2-5 days depending on the sun abundance of the location, and S_f is usually chosen to be 10% [79]. This intuitive method was used in various studies to size stand-alone PV systems, in [13, 26, 77], average daily load demand and solar radiation has been used to size the PV system and batteries while limiting system cost over the life cycle as explained in equation 2.4. However, the system performance and reliability cannot be taken into account in this method. The average daily irradiance and loads do not account for seasonal and daily variations, which make the system design very rough. Moreover, the DOA and S_f are subjective values, and can lead to an undersized or highly over sized system compromising reliability and cost.

2.3.2. Optimization Methods

Optimization is the defined as the "discipline which is concerned with finding the maxima and minima of functions, possibly subject to constraints [33]". The optimization problem can be defined by specifying a set of optimization or decision variables, an objective function to be minimized or maximized while abiding to a set of constraints. Designing efficient SHSs is a tough task, due to the intermittent power production from the energy sources such as solar and wind, finding an appropriate battery storage size, as well as the relatively high present cost of investment are the main challenges encountered during the design stage. This led to numerous research on finding and forming optimal sizing methodologies for off-grid renewable energy systems.

A thorough overview on the currently available optimization techniques for SHSs was preformed in [2] and categorized in the following manner:

- **Classical Techniques:** These techniques are very useful to obtain the optimal solution of problems with continuous and differentiable functions. These methods are usually analytical and employ iterative, probabilistic and graphical methods. Differential calculus is usually employed to derive and find the maximum and minimum points for both constrained and unconstrained continuous objective functions [2, 28].
- **Modern Techniques:** Modern methods use heuristic search and can determine the global optimum system even in non-linear functions. In modern techniques, a better convergence rate has been achieved that leads to more accurate, global optimum solutions.
- **Computer software:** Optimization software are tools that employ a mix of classical and modern techniques and are specific for designing and optimizing HRESs are becoming popular and widely used. These tools can find the optimal design for different locations worldwide, and subjecting it to various environmental, reliability and social constraints. HOMER and iHOGA which employ hybrid and genetic optimization algorithms are two of the most popular software.

Classical Techniques

Most of the studies that have been to optimize off-grid HRESs using classical techniques employ numerical and iterative methods. In [12, 74] for example, iterative methods were used to design a HRESs at a minimum

cost while maintaining a very low loss of power, or low LLP. The mathematical formulation of the problem was defined as follows:

-*Objective Function:* Minimize the cost $Obj = mincost$ where the cost function is as defined in equation 2.4

-*Constraint:* Maintain a low LLP value, such as 2% as in the study done by [12].

These analytical and iterative methods have proven to have given accurate optimum results, but have not been widely used in recent years due to the fact that they require long computational time to find the solutions.

Modern Techniques

Modern techniques have been implemented in several recent studies due to their numerous advantages, notably the fact that they can handle multi-objective optimization problems, where there is a set of objective functions that are sometimes conflicting. Artificial techniques are thus able to provide an optimal solution set as opposed to a single solution.

The Genetic Algorithm (GA) is powerful heuristic optimization algorithm that has been widely used in studies to optimize HRESs [63, 88]. For example, the optimization of the allocation of the different renewable sources consisting of a wind turbine, solar panels, a diesel generator and a storage system to solve a multi-objective optimization by minimizing the cost, and maximizing the penetration of renewable sources (RF) in the system was done in [88]. A similar study performed in [14] used another well known multi-object algorithm called Multi Objective Particle Swarm Optimization (MOPSO) to optimize the allocation of a system consisting of PV panels, wind turbines and a diesel generator, the problem had 3 objective functions which are.

$$\mathrm{COE}(\frac{\$}{\mathrm{kWh}}) = \frac{\mathrm{Total\quad Net\quad Present\quad Cost(\$)}}{\mathrm{E_{Yearly\quad Load}(kWh)}} \tag{2.9}$$

$$\mathrm{LLP} = \frac{\sum(\mathrm{P_{load}} - \mathrm{P_{PV}} - \mathrm{P_{wind}} + \mathrm{P_{Battery}} + \mathrm{P_{Diesel}})}{\sum \mathrm{P_{load}}} \tag{2.10}$$

$$\mathrm{RF}(\%) = (1 - \frac{\sum \mathrm{P_{diesel}}}{\sum \mathrm{P_{PV}} + \sum \mathrm{P_{wind}}}) \times 100 \tag{2.11}$$

Equations 2.9 through 2.11 ensure that the allocation of the different sources results in a highly reliable system at a minimal cost, while also minimizing the use of the diesel generator as shown in 2.11.

Some of the most recent techniques employ hybrid algorithms, which are a combination of two or more single classical or modern techniques to achieve even faster and more accurate results [2], they have been also widely used in stand-alone systems that have multitudes of renewable energy sources leading to a more complex solution. Notable studies are [44] in which a combination of GA and exhaustive-search technique was used, and in [24] a mix of Multi-objective evolutionary algorithm and GA were used to optimize their stand alone renewable energy systems.

Computer Software

Several licensed software tools that specialize in optimizing renewable energy systems in a specific location given a set of data are being used. HOMER, the most popular software, is able to optimize systems in both grid-connected and standalone modes using meteorological data. The software runs the simulation over a year at a 1 hour interval, and the output is includes the optimal size allocation of the components, monthly demand limits, and advanced battery analysis. Moreover, it can be connected to MATLAB making it highly versatile. The main disadvantage of this software is that it performs only single objective optimization which is cost minimization. iHOGA is another popular software, that uses the genetic algorithm to find the optimal system size using single or multi-objective optimization techniques [2]. Finally, Mathworks developed an optimization toolbox for MATLAB which includes several optimization algorithms from linear programming to multi-objective genetic algorithms.

2.3.3. Chosen optimization method: The Genetic Algorithm

The Genetic Algorithm (GA) is the selected optimization technique used in this study, it was chosen as it is a power artificial optimization technique, that can handle multi-objective optimization problems [2], and has been used in many studies for optimizing hybrid renewable energy systems and Solar Home Systems with great computational speed and accuracy in reaching the global optimum. The terminologies and working principle of the GA algorithm used will be explained in the following sections.

Genetic Algorithm: Definition

The GA takes the working principle of natural selection in genetics that stimulates biological evolution. It belongs to the class of Evolutionary Algorithms (EA) and is able to generate accurate solutions to optimization and multi-objective optimization problems using bio-inspired operators such as mutation, selection, and crossover. The GA can handle several optimization problems that classical techniques are not able to solve such as non-differentiable, stochastic or non linear function. Following the process of natural selection, the population of solutions evolves towards an optimal solution [20, 52, 53].

Genetic Algorithm: Terminologies

- ***Fitness function:*** Which is the function, or set of functions that the algorithm has to optimize. It is also known as the objective function in classical optimization methods. In our study, the fitness functions consist of a set of 3 functions [20, 53]:
  1. The system cost function
  2. The system reliability or LLP
  3. The battery lifetime
- ***Population:*** Which is the set of individuals, or candidate solutions to the problem. The size of the population is assigned by the user initially.
- ***Generation:*** After each iteration, the computations made on the initial population produce a new population, this new population is called a new generation, or a new set of candidate solutions.
- ***Diversity:*** The diversity in a population is the average distance between the set of individuals in the population. Initially, the population has a high diversity and tends to decrease with newer generations at each iteration as illustrated in figure 2.4.
- ***Crossover:*** Genetic crossover, or recombination is a genetic operator in the GA is a way to stochastically generate a new "child" solution from two "parent" solutions from the previous generation.
- ***Mutation:*** Which is another genetic operator that randomly alters the values some of the "child" population values to maintain some variability.
- ***Best Fitness Value:*** At each iteration, when the algorithm determines the fitness value of every individual in the population, the best fitness value is the smallest fitness value for one of the individuals in that population.
- ***Dominance:*** The term dominate is equivalent to the term 'inferior'. An individual *'x'* in the population dominates *'y'* when:
  - $f_i(x) \leq f_i(y)$ for all i
  - $f_j(x) \leq f_j(y)$ for some j

  Dominating individuals have a higher chance of selection during the calculations for the newer generation.
- ***Pareto set:*** The Pareto set of solutions, is the set of individuals with fitness functions that are non-dominated by any other individual in the search space as shown in figure 2.5 below.
- ***Spread:*** Which is the measure of the movement of the pareto set of dominating solutions, with each iteration, the spread becomes smaller as the dominating individuals get closer to the best fitness function, and stopping the algorithm iterations.

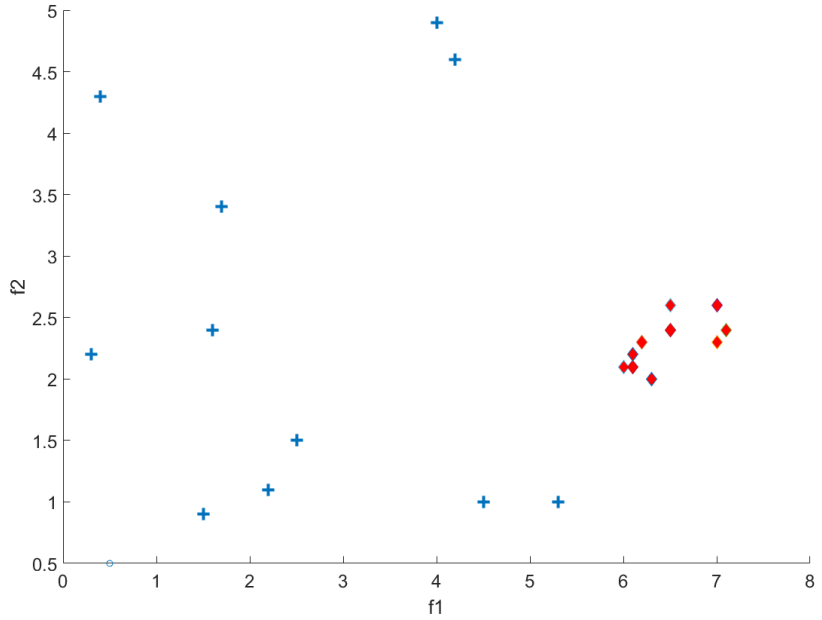

Figure 2.4: Population diversity: Low diversity population (Red) VS High diversity population (Blue) [53]

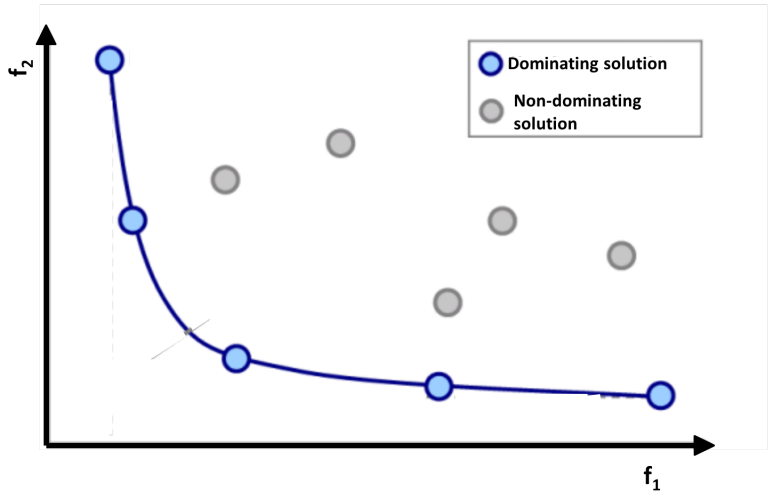

Figure 2.5: Pareto front in the feasible region where f_1 and f_2 are the objective functions to be minimized

With the basic terminologies of the GA defined, the principle of operation and the steps taken during each iteration are explained in the section below.

Genetic Algorithm: Working principles

1. ***Initialization:*** The process of creating an initial random population is the first step in the GA. The population size is set by the user, and the population is randomly created to fit within the bounds and constraints of the search space.
2. ***Selection:*** At each generation, some of the individuals in the population are selected for the new generation. Individuals with the most optimal fitness functions and are within the defined constraints are more likely to be selected.

3. ***Crossover and mutation:*** From each pair of "parents" solutions selected in step 2, a "child" solution is produced using crossover and mutation. Hence, the new generation created shares many of the properties from the parents, with some slight changes due to the genetic operators.
4. ***Fitness evaluation of the children:*** The fitness values of the children are evaluated just as was done to the initial population, and from which a new generation is created.
5. ***Stopping conditions:*** The iteration in the GA keeps happening until one of the following stopping conditions occur:
    - Maximum number of generations that was set by the user is reached.
    - The relative change in the spread of the solutions becomes smaller than as set by the user.
    - No feasible solution or set of solutions found.
    - Time limit exceeded.

Genetic Algorithm: Numerical example

In order to explain mathematically explain the working principle of the GA, a numerical example is presented in this section. Let us suppose a function of x and y for which we have to find the minimum for $0 \leq x \leq 10$ and $0 \leq y \leq 10$:

$$f(x,y) = x\sin 3x + 2y\sin 2y \tag{2.12}$$

The first step is to set the initial population, which will be composed of 10 individuals or chromosomes, each with n parameters as such: chromosome = $[p_1, p_2..p_n]$. In this case, since there are only two variables, each chromosome will have two parameters: chromosome$_i$ = $[x_i, y_i]$. The initial x and y values of each individual are generated randomly, then the fitness of each is calculated using equation 2.12. The initial population along with its fitness is presented in table 2.3 below:

Table 2.3: GA numerical example: Initial population

Individual	**x**	**y**	**Fitness** $f(x,y)$
1	6,78	6,94	20,18
2	7,58	3,17	-4,80
3	7,43	9,5	0,66
4	3,92	0,34	-2,40
5	6,55	4,39	9,98
6	1,71	3,82	5,90
7	7,06	7,65	11,19
8	0,32	7,95	-2,77
9	2,77	1,87	0,38
10	0,46	4,89	-2,95

Following that, the selection process of the parent individuals takes place to produce the offspring. Each set of two parents produces two offspring, hence, to keep the population at 10 individuals, only 50% of the initial population is chosen and these are the fittest individuals being:

Table 2.4: GA numerical example: Surviving population

Rank	**x**	**y**	**Fitness** $f(x,y)$
1	7,58	3,17	-4,80
2	0,46	4,89	-2,95
3	0,32	7,95	-2,77
4	3,92	0,34	-2,40
5	2,77	1,87	0,38

The probability of the chromosomes of the table above for being selected as a parent depends on its ranking, the highest rank having the highest probability and so on. Following that, the crossover between the two parent chromosomes takes place to produce the offspring. One method to achieve this is through Haupt's method [16, 35]. Taking two chromosomes d and m as parent chromosomes, with values:

$$d = [x_d, y_d] \tag{2.13}$$

$$m = [x_m, y_m] \tag{2.14}$$

The x values of the offspring are:

$$x_{new1} = (1-\beta)x_m + \beta x_d \tag{2.15}$$

$$x_{new2} = (1-\beta)x_d + \beta x_m \tag{2.16}$$

Where β is a random value between 0 and 1. The remaining parameter y of the offspring is same value as the parents. Taking the first two ranking chromosomes for example with a β value of 0.312 we will have:

$$\text{offspring}_1 = [(1-0.312) \times 7.58 + 0.312 \times 0.46, 3.17] = [2.54, 3.17] \tag{2.17}$$

$$\text{offspring}_2 = [(1-0.312) \times 0.46 + 0.312 \times 7.58, 3.17] = [4.76, 4.89] \tag{2.18}$$

Hence, offspring from the parents are generated until a new population of 10 individual is obtained. The GA continues repeats the above steps until either the number of preset generations is reached, or if the fitness value of the highest ranking chromosome remains the same for several generations, meaning that the solution converged to the global minimum [16, 35]. Using MATLAB's optimization toolbox, the genetic algorithm was used for a multi-objective optimization to find the minimum system cost, LLP, while maximizing battery lifetime as will be shown in chapters 4 & 5.

2.4. Conclusions

Through the literature review performed, a clear framework of the SHS design and optimization process was identified. The system in study consists of PV modules, a storage system, and the power converters in a DC coupled configuration. The main system parameters and design objectives were also identified, being the minimization of the system cost while not compromising reliability through maintaining a low LLP value, and maximizing the battery lifetime. Finally, following a thorough review on the currently used optimization methods, two techniques seemed to be the most promising and flexible for implementation: the classical iterative technique, and the Genetic Algorithm, an evolutionary technique that is inspired by the process of natural selection for multi-objective optimization problems. Through these objectives and optimization techniques, an affordable, reliable and robust SHS can be sized.

3

Modeling & Sizing Methodology

In order to find an optimal solution for the SHS size, the components that compose the system, as well as the interconnection between them needs to be modelled accurately. In this chapter, the yearly household load profile used to develop the component models is introduced first, then the mathematical model for the PV module, battery and power converter built using MATLAB is discussed in detail, finally the performance analysis to evaluate the obtained results is shown.

3.1. General methodology

The general sizing methodology from extracting the load and meteorological data to finding the system size will be explained in this section. First, the yearly load profile for the household is obtained for every minute of the year, and is used as the load for the SHS system to feed. Then, the geographical location for the household is selected, and from that the meteorological data is extracted using Meteonorm. Following that, the irradiance data is used as an input for a MATLAB algorithm to obtain the output of the PV array along with its dynamic efficiency. Finally, the battery storage and power electronics are sized according to the system peak power and performance criteria. The overall methodology is shown in figure 3.1 below.

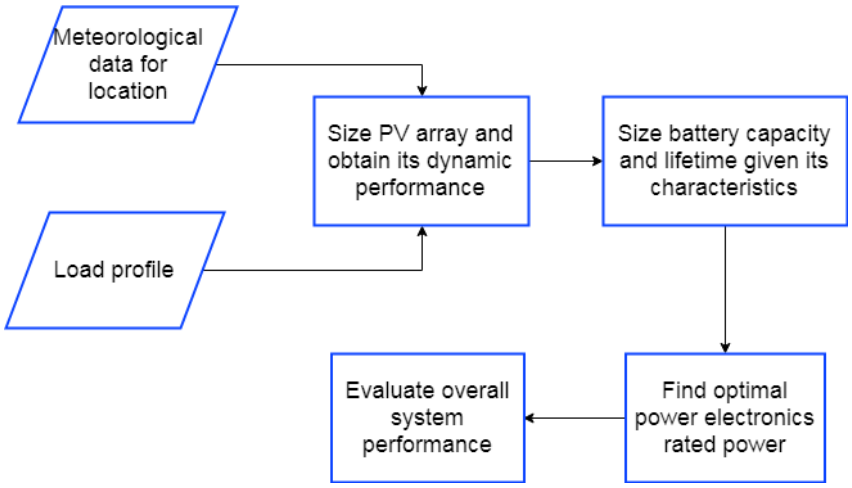

Figure 3.1: General sizing methodology flowchart

3.2. Load profile

Following the introduction to the multi-tier load profiles and households in section 1.3. One of the main inputs required to construct working mathematical models for the SHS components, and evaluate their performance, is the load profile. The load profile consists of the yearly energy consumption of a household through the use of typical household appliances, such as lights, phone charging, television, etc. These appliances are used during

different times of the day to simulate the behavior of the residents of an actual household. The power ratings for the appliances used, and the obtained yearly load profile characteristics are shown in the tables below.

Table 3.1: (a) Load profile appliances power rating. (b) Load profile characteristics.

Appliance	Power Rating [W]
Fan	15
Fridge	21
Laptop	60
Led lights	10
Phone Charger	3
Radio	5
Tab	18
TV	12

Load profile data	
Data resolution	Minute
Data length	525600
Peak load [W]	185.0
Yearly energy consumption [kWh]	453.2
Average daily consumption [kWh]	1.2

This load profile will serve as the testing ground for the modeling of the components, as well as the evaluation and sizing metrics of the system. The load profile over a typical week is shown in figure 3.2 below.

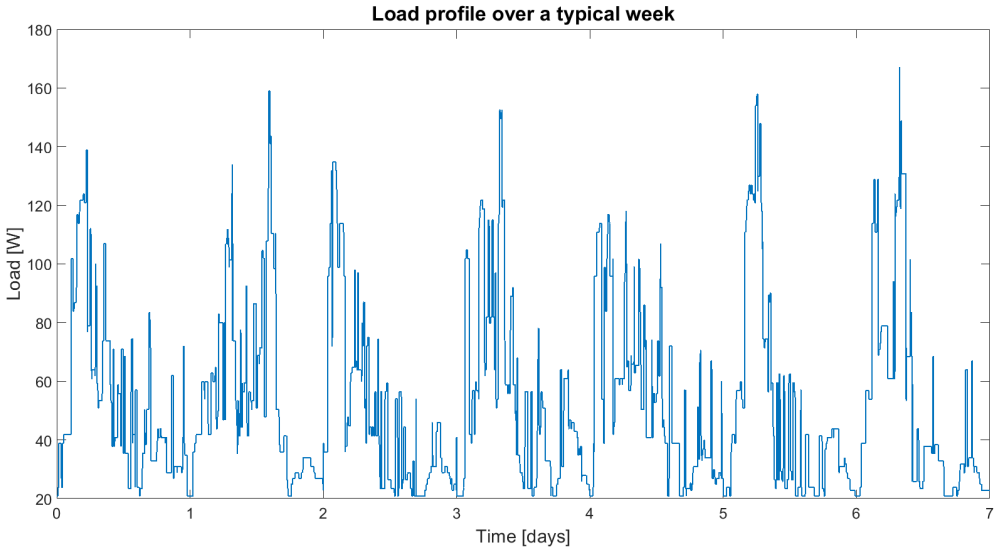

Figure 3.2: Test case: load profile over a typical week

3.3. Components

The dynamic model for each of the main performance components was obtained through literature and implemented in MATLAB in the form of functions at a first stage. These different components were linked at later stage to obtain the system size and parameters for a given load profile and input meteorological data.

3.3.1. Photovoltaic Module

The working principle of a solar cell is based on the photovoltaic effect, where a potential difference is generated across the cell following electromagnetic radiation [79]. The amount of power that a PV module depends on the incoming solar irradiation and on the module's characteristics. In the following sections, the steps for sizing the solar module and computing its net output will be explained as summarized in figure 3.3 below.

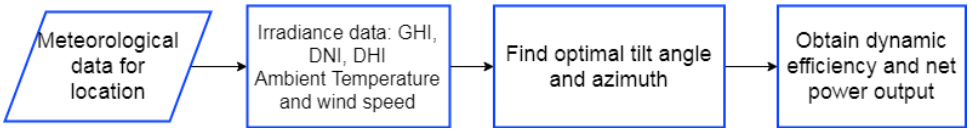

Figure 3.3: Methodology for PV module modeling

Modeling the Irradiance on the PV Module

The irradiance on a PV module is composed of 3 components:

- Direct Irradiance: which is the direct irradiance that is directly striking the PV module.
- Diffuse irradiance: which is the scattered light that hits the module due to the earth's atmosphere.
- Ground Irradiance: which is the irradiance reflected from the ground on the module.

The total irradiance arriving on the module is then $G_{Tot} = G_{dir} + G_{Diff} + G_{Grnd}$.

G_{dir}, G_{grnd}, and G_{Diff} can be found through the following equations is the product of the Direct Normal Irradiance (DNI) and the angle of incidence γ which is defined as [79]:

$$\mathrm{G_{dir}} = \mathrm{DNI} \times \cos\gamma \tag{3.1}$$

$$\gamma = \cos^{-1}[\sin(\theta_\mathrm{M})\cos(\mathrm{a_s})\cos(\mathrm{A_M} - \mathrm{A_S}) + \cos(\theta_\mathrm{M})\sin(\mathrm{a_S})] \tag{3.2}$$

$$\mathrm{G_{grnd}} = \mathrm{GHI} \times \alpha \times (1 - \mathrm{SVF}) \tag{3.3}$$

$$\mathrm{G_{diff}} = \mathrm{DHI} \times \mathrm{SVF} \tag{3.4}$$

$$\mathrm{SVF} = \frac{1 + \cos\theta_\mathrm{M}}{2} \tag{3.5}$$

Table 3.2 below summarizes the different variables used.

Table 3.2: Irradiance Parameters

Symbol	Description
DNI	Direct Normal Irradiance
γ	Angle of Incidence
θ_M	Module tilt angle
A_M	Module azimuth
a_s	Solar altitude
A_S	Solar Azimuth
GHI	Global Horizontal Irradiance
α	surface albedo
DHI	Diffuse Horizontal Irradiance
SVF	Sky View Factor

Power output modeling

The power output of a PV array is found via

$$\mathrm{P_{out}[W]} = \mathrm{N} \times \mathrm{G_{Tot}} \times \mathrm{Area_M} \times \eta_\mathrm{M} \tag{3.6}$$

Where A_M and η_M are the module's area and efficiency respectively, and N is the number of modules in the array. The efficiency of the module is directly related to the module temperature, which fluctuates over the course of the day. The efficiency given by the manufacturer on the module data-sheet is typically the efficiency value during Standard Test Conditions (STC) at $1000 W/m^2$ and $25^o C$ module temperature. However, during the day, and during warmer months, the irradiance on the module increases its temperature, and hence reducing its efficiency. A fluid dynamic (FD) model was developed based on [30] for estimating the module temperature at each time interval given various meteorological data as input such as: ambient temperature, wind speed, ground temperature, etc. as in the following equation:

$$\mathrm{T_M} = \frac{\alpha.\mathrm{G} + \mathrm{h_c}.\mathrm{T_a} + \mathrm{h_{r,sky}}.\mathrm{T_{sky}} + \mathrm{h_{r,gr}}.\mathrm{T_{gr}}}{\mathrm{h_c} + \mathrm{h_{r,sky}} + \mathrm{h_{r,gr}}} \tag{3.7}$$

$$\eta_\mathrm{M} = \eta_\mathrm{M,STC}.(1 - \kappa.(\mathrm{T_M} - 25)) \tag{3.8}$$

Table 3.3: Module efficiency parameters

Symbol	Description
α	Absorptivity coefficient
G	Irradiance
h_c	Back side convection
T_a	Ambient temperature
$h_{r,sky}$	Air convection coefficient
T_{sky}	Sky temperature
$h_{r,gr}$	Ground convection coefficient
T_{gr}	Ground temperature
T_M	Module temperature
η_M	Module efficiency
$\eta_{M,STC}$	Module efficiency at STC

Meteoroligical data

Besides the detailed mathematical model for the module performance, credible and exhaustive meteorological data had to be obtained in order to estimate the module and system's performance correctly throughout the year. In this research, the meteorological data was obtained from Meteonorm, which offers access to data from ground stations and satellites. It also offers unique access to the Global Energy Balance Archive (GEBA), which meets the quality criteria of the World Meteorological Organization (WMO) [54]. Moreover, the user has a choice of extracting data over a year ranging from a monthly basis, to a minute basis. In the models used in this research, all the calculations were done minute by minute over a year. Hence, all the fast variations of the irradiance during the day were taken into account, making the obtained optimum size more accurate.

In this chapter, the meteorological data used for the testing and evaluation of the developed were taken from the weather station in Pune, India through Meteonorm. This location was chosen due to the fact that it is located in India, hence it has very similar meteorological data as the remote villages in the case studies. Moreover, the data extracted is highly accurate to the presence of the weather station at its location. The data extracted are arrays representing the various irradiance and meteorological data at every minute over a year. The coordinates at the location are 73^o 50' 60"N and 18^o 31' 58.8"E.

Module Orientation

As mentioned previously, the direct irradiance incoming on the PV array depends on γ, the angle of incidence of the sun rays on the module. As seen in equation 3.2, γ depends on the position of the sun at each instant and on the tilt angle and orientation of the module. The module tilt angle and orientation can be adjusted depending its geographical location in order to receive the maximum amount of direct irradiance over the year. For example, the rule of thumb for the module or array orientation is to point south in the north hemisphere, and north in the southern hemisphere in order to be directed towards the sun [79]. The tilt angle however, depends greatly on the latitude on longitude of the location of the module, and leads to a large variation in the total energy yield of the array. In order to find the optimal angle and orientation at which the PV array needs to be placed, an iterative algorithm was developed on MATLAB that calculated the yearly energy yield for all the different combinations of module azimuth and tilt angle. First, the position of the sun is computed as in [79] for every minute at the given latitude and longitude, then the direct irradiance is found at that instant, in order to obtain the total energy yield at each specific angle as shown in equation 3.9

$$\text{Yield}_{(\theta_{\text{M,i}},\text{A}_{\text{M,j}})} = \sum_{\text{t=1}}^{525600} \text{G}_{\text{Tot}_\text{t}} \times \text{Area}_{\text{module}} \tag{3.9}$$

The module azimuth ranges from 0^o (North) to 180^o (South), while the tilt angle ranges from 0^o where it's flat on the ground to 90^o being perpendicular to the ground. Figure 3.4 illustrates the angles that characterize a PV module's orientation.

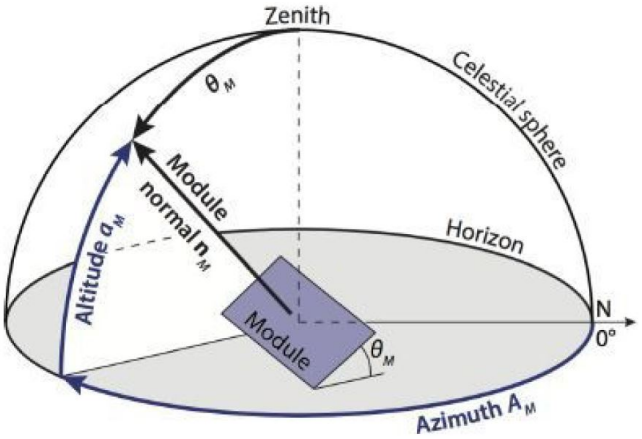

Figure 3.4: The angles characterizing a PV module (θ_M, A_M) [79]

In figure 3.5 below, the total yearly irradiance as a function of the module azimuth and tilt angle is shown. The module is located in Pune, India as mentioned in section 3.3.1, with the load profile shown earlier. As can be shown in the figure, the optimal module azimuth and tilt angle are 180^o and 13^o respectively. This procedure will be followed for each of the locations of the study cases in section 4.3.

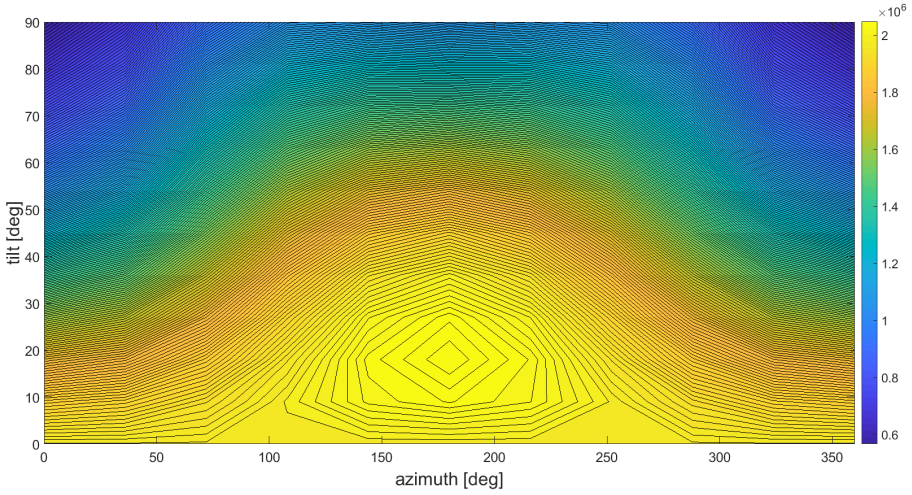

Figure 3.5: Total Irradiance as a function of module Azimuth and tilt angle in Pune, India. Optimal tilt angle azimuth: 13^o and 180^o.

Module Characteristics

In order to accurately find the optimal size of the PV array for a given load profile, smaller modules are preferred in order to decrease the Watt Peak increment of the system. The Watt Peak (Wp) is defined as the power generated by the PV array at STC [79]. Hence, a 20 Wp solar module was selected, from which the PV array power output will consist of $N \times 20Wp$. The main module characteristics are found in table 3.4 and taken from the manufacturers datasheet [72]. Figures 3.6 to 3.9 below show the module temperature, efficiency, and net output for the selected module.

Table 3.4: Renogy 20 Wp module characteristics

Electrical and Mechanical Data	
Maximum Power at STC [W]	20
Optimum Operating Voltage (V_{mpp}), [V]	17.5
Optimum Operating Current (I_{mpp}), [A]	1.14
Module Efficiency [%]	12.33
Dimensions [mm^3]	345 x 470 x 25
Nominal Operating Cell Temperature (NOCT) [^oC]	47
Lifetime [years]	25

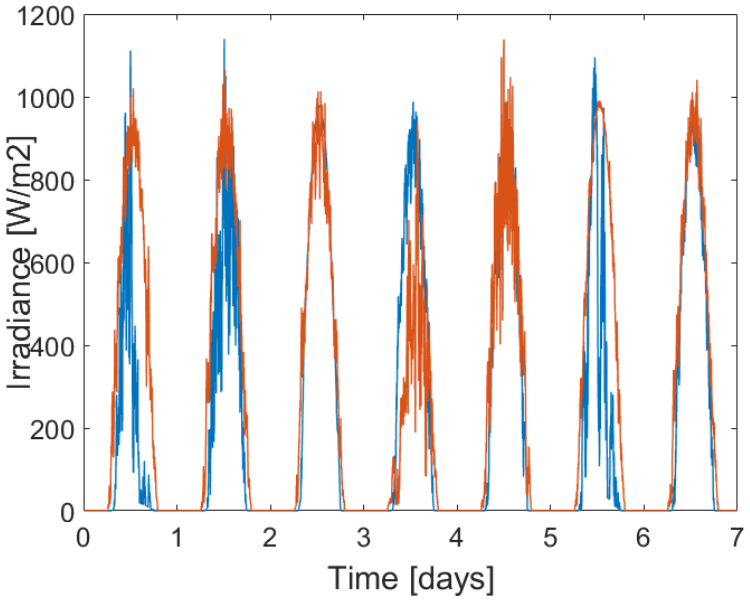

Figure 3.6: Incoming irradiance over a week in the summer and winter

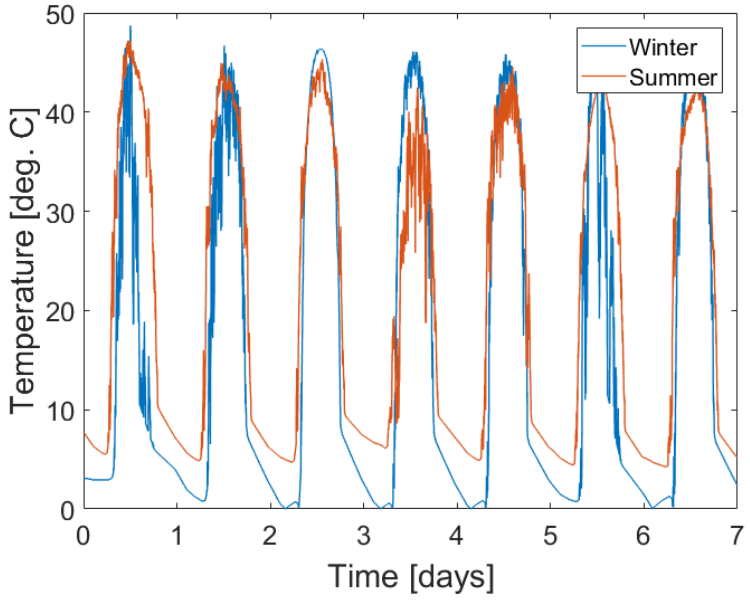

Figure 3.7: Module temperature over a week in the summer and winter

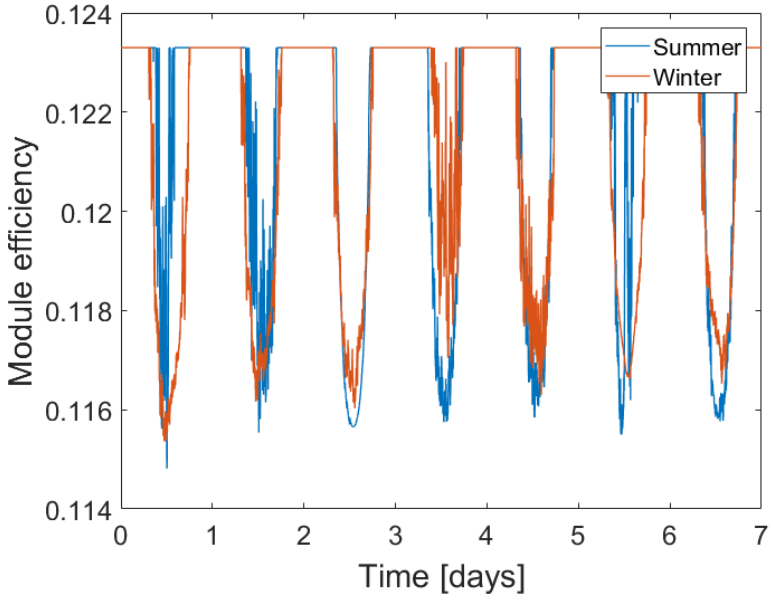

Figure 3.8: Module efficiency over a week in the summer and winter

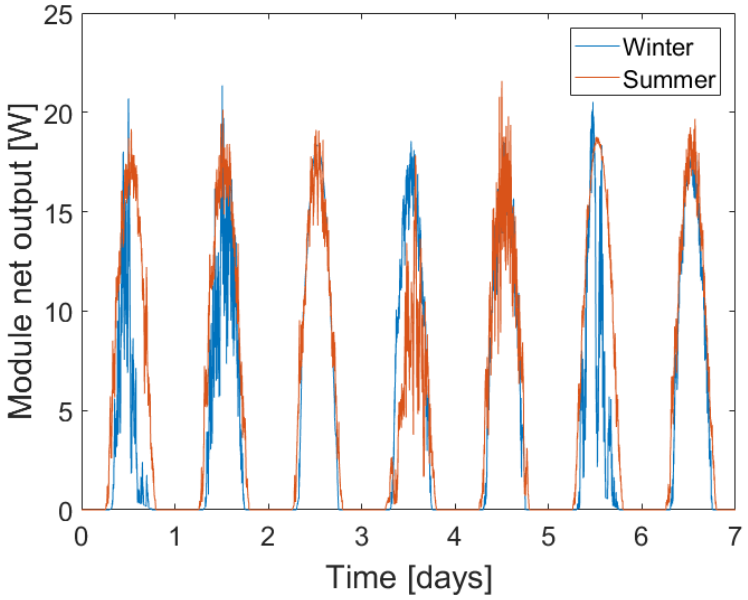

Figure 3.9: Module net output over a week in the summer and winter

3.3.2. Batteries

Batteries are a crucial component in a solar home system, as previously mentioned in section 2.2. Having a low lifetime of 4 - 8 years compared to the typical system lifetime of 25 years and having the largest cost among the system components, makes modeling and sizing batteries an important task. To reproduce a battery model, the important parameters that affect the behavior of the battery are identified at first, then followed by the proposed model. Finally, the battery aging and lifetime estimation models are presented.

Battery Parameters

This section discusses the main parameters that represent the dynamic operation of the battery, and that will be used during the modeling.

State of Charge The battery State of Charge, commonly referred to as SoC, represents the relative capacity of the battery at a certain moment. For example, a 10,000 Ah 75% SoC means that a battery is at three-quarters of its full capacity, or at 7,500 Ah [75]. A common method for calculating the SoC is the Ampere hour counting, which depends on the withdrawn current during discharge, and intake current during charge [68]:

$$\mathrm{SoC} = \mathrm{SoC}_0 + \frac{1}{\mathrm{C_B}} \int_{\mathrm{t_0}}^{\mathrm{t}} (\mathrm{I_{batt}} - \mathrm{I_{loss}}) \mathrm{d}\tau \tag{3.10}$$

Where SoC_0 is the initial battery SoC, I_B is the battery current, and I_{loss} is the lost current due to the battery side reactions.

In practical applications a simpler way is commonly used via the following equation [79]:

$$\mathrm{SoC} = \frac{\mathrm{C_{B,t}}}{\mathrm{C_{Nom}}} \tag{3.11}$$

Where $C_{B,t}$ and C_{Nom} are the battery capacity at time 't' and the rated battery capacity respectively. The latter equation will be used in this study. It is generally recommended by manufacturers to keep the battery 15% < SoC < 20% in order to avoid damage during excessive charge or discharge, hence preserving the battery health and extending its lifetime.

Depth of Discharge The Depth of Discharge (DoD) indicates the relative amount of which the battery has been discharged, a 100% means that the battery is completely empty. Knowing the battery SoC, the DoD can be easily found via [79]:

$$\mathrm{DoD} = 1 - \mathrm{SoC} = 1 - \frac{\mathrm{C_{B,t}}}{\mathrm{C_{B,Nom}}} \tag{3.12}$$

Life cycle The life expectancy of batteries is rated using the number of cycles that battery can perform. These cycles refer to the number of times the battery can be charged and discharged before it reaches its end of life (EoL). The battery reaches its EoL usually when its capacity reaches 80% of its initial nominal capacity [60].

Energy Throughput The energy throughput is the total amount of energy that is processed by the battery, in other words, it is the sum of the energy intake and discharge by the battery [56, 60].

Voltage efficiency Which is the ratio between the charging and discharging voltage of the battery and is defined via:

$$\eta_{\mathrm{V}} = \frac{\mathrm{V_{discharge}}}{\mathrm{V_{charge}}} \tag{3.13}$$

Coulombic efficiency Which is the total charge extracted from the battery to the charge input to the battery:

$$\eta_{\mathrm{C}} = \frac{\mathrm{Q_{discharge}}}{\mathrm{Q_{charge}}} \tag{3.14}$$

Battery efficiency The battery round-trip efficiency, is defined at the ratio of energy output to the energy input.

It is the product of the voltage efficiency and the coulombic efficiency. The battery efficiency equation is derived as follows [79]:

$$\eta_{\mathrm{batt}} = \eta_{\mathrm{V}} \times \eta_{\mathrm{C}} = \frac{\mathrm{V_{discharge}}}{\mathrm{V_{charge}}} . \frac{\mathrm{Q_{discharge}}}{\mathrm{Q_{charge}}} = \frac{\mathrm{E_{out}}}{\mathrm{E_{in}}} \tag{3.15}$$

However, in this study, the battery round-trip efficiency will be used as a constant value for practicality.

Battery Lifetime

In stand-alone solar home systems, particularly in small scale systems, the battery storage usually takes the largest share in the total system cost [67]. In the figure below, the breakdown of the SHS retail price for different types of appliances is shown, for a household with standard appliances in 2014, the battery takes one third of the price of the whole system.

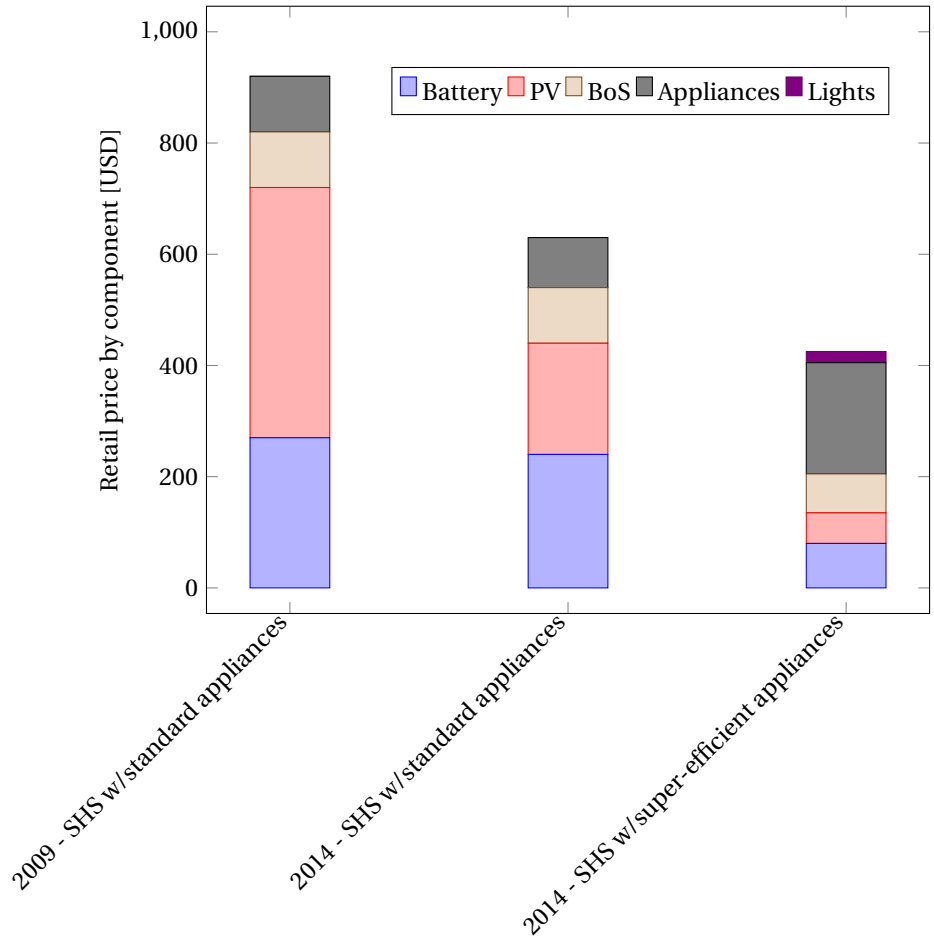

Figure 3.10: Renewable energy generation 2011-2017, *Adapted from* [39].

Moreover, batteries typically are the component with the lowest lifetime in the SHS, table 3.5 below shows the typical lifetime of the two most available batteries types on the market [3].

Table 3.5: Lifetime of Lead-acid and Li-ion batteries [3, 51]

	Lead-acid 25^oC	**Lead-acid** 33^oC	**Lithium-ion**
Size [kWh]	100	100	62.5
Cycle Life	1,000 @ 50% DoD	500 @ 50% DoD	1,900 @ 80% DoD
Calendar life [Years]	4-6	3-5	6-8

The SHS lifetime is equal to the lifetime of the solar array, which is typically 20 - 25 years. This means that the number of battery replacements during the project lifetime is around 4 - 5 times for lead-acid and 3 - 4 times for Li-ion batteries. In order to maximize the battery lifetime during the simulation and optimization, an accurate algorithm and lifetime model has to be constructed first to simulate the battery capacity degradation and calendar life. In [60], a practical methodology is used to model and estimate the battery lifetime. The methodology used in the study takes into account the two main factors that influence the battery lifetime: the cell temperature, and the DoD range of operation during battery cycling. Figure 3.11 below shows the effect of each of the two factors on the battery lifetime.

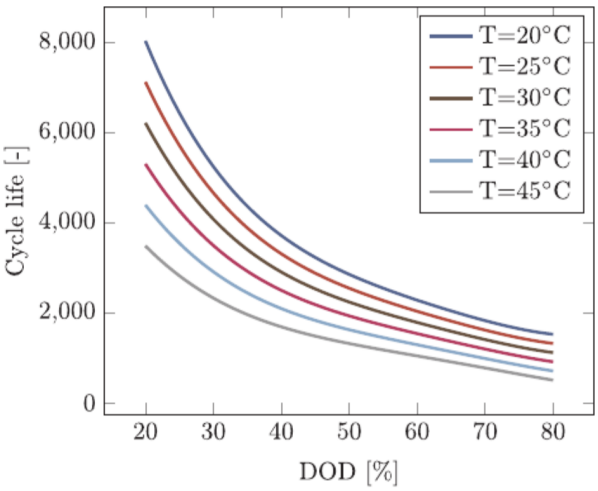

Figure 3.11: Effect of DoD and cell temperature on battery lifetime [60]

The first step in this method consists of extracting the relevant lifetime data from the datasheets given by the battery manufacturers. These datasheets, similar to figure 3.11, give the lifetime of the battery with respect to the temperature and DoD. The battery curves are extracted from the datasheet, and using a curve-fitting tool, a polynomial function can be obtained to approximate the lifetime based on the battery DoD in the SHS. As shown in figure 3.11, there is a linear dependency of the life cycle for temperature variations. Hence, during the simulation, a linear factor is added to interpolate the battery cycle life for temperatures in the range $20-45^{o}C$. A 4^{th} degree polynomial was found to be a good fit for calculating the cycle life accurately, resulting in the following equations [60, 65]:

$$n(T, DoD) = n(T_{ref}, DoD) - f(T_{avg} D_n(DoD) \tag{3.16}$$

$$n(T_{ref}) = p_4 D^4 + p_3 d^3 + p_2 d^2 + p_1 d + p_0 \tag{3.17}$$

$$f = p_{l1} T_{avg} + p_{l0} \tag{3.18}$$

$$D_n = p_{d4} D^{d4} + p_3 d^{d3} + p_2 d^{d2} + p_{d1} d + p_{d0} \tag{3.19}$$

Table 3.6: Variable description for fitting polynomial

Variable	Description
n(T,DoD)	Cycle life for a given T and DoD
f	Linear factor for temperature dependency
D_n	Difference between two temperature curves
$p_0 - p_4$	Polynomial fitting coefficients at T_{ref}
p_{l1}, p_{l0}	Coefficients for determining linear factor
$p_{d0} - p_{d4}$	Fitting coefficients for temperature difference curves
T_{avg}	Average battery operating temperature
T_{ref}	Reference operating temperature
d	Battery DoD

Now that the cycle life can be calculated using the battery operating temperature and DoD as inputs, the next step is to find the average DoD during operation. The study discusses two approaches to obtain the DoD, the coarse average approach, and the zero-crossing approach, which proved to be more accurate and reliable. Thus, in this study, the zero-crossing approach will be used as follows.

The zero-crossing approach is based on only recording the micro-cycles where the battery is charging and discharging. It is based on considering only the active battery DoD and not taking into account the time intervals where the battery is not in operation. This results in fewer effective cycles than the coarse DoD method that is employed in most other studies. The micro-cycle where the active DoD is recorded, is the period between two consecutive zero-current crossings as illustrated in figure 3.12 below. Hence, the total average DoD is calculated by summing only the average DoD in every cycle as shown in equation 3.20 [57, 60].

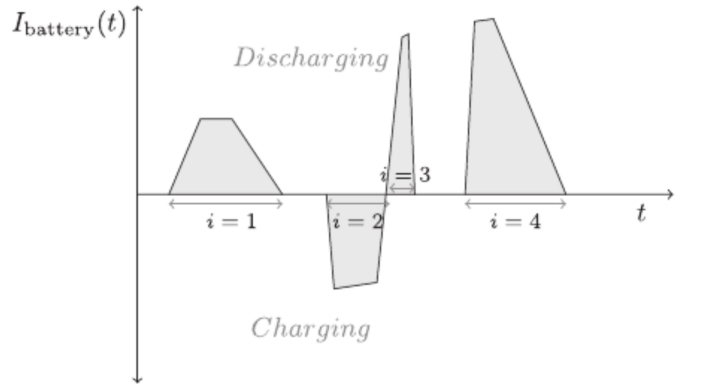

Figure 3.12: Battery current waveform showing the micro-cycles during charge and discharge [60]

$$\overline{\text{DOD}} = \frac{\sum_{\text{i=1}}^{\text{N}} \overline{\text{DOD}_\text{i}}.\text{E}_{\text{thr,i}}}{\sum_{\text{i=1}}^{\text{N}} \text{E}_{\text{thr,i}}} \tag{3.20}$$

Where $\overline{DOD}$ is the combined average active DOD due to all the micro-cycles, DOD_i: Average active DOD in the i^{th} micro-cycle, $E_{thr,i}$ is the total energy throughput in the i^{th} micro-cycle and N is the total number of ZC-based micro-cycles.

The same principle can be applied for calculating the average cell temperature by summing up the temperature at each micro-cycle as in the following equation:

$$\text{T} = \frac{\sum_{\text{i=1}}^{\text{N}} \text{T}_\text{i}.\text{T}_{\text{ZC,i}}}{\sum_{\text{i=1}}^{\text{N}} \text{T}_{\text{ZC,i}}} \tag{3.21}$$

Finally, once $\overline{DOD}$ and T_{avg} are known, equations 3.16 through 3.19 can be used to find the cycle life of the battery. The battery calendar life in years (L) can then be found through [57]:

$$\text{L} = \text{n} \times \overline{\text{DOD}} \times \frac{2 \times \text{E}_{\text{nom}}}{\sum_{\text{i=1}}^{\text{N}} \text{E}_{\text{thr,i}}} \tag{3.22}$$

Battery Model

Through the parameters and equations from the previous sections, two sets of parameters were used to model the battery as a charge counter with a chosen energy capacity C_{Nom}. The two models are for lead-acid and Li-ion batteries, the characteristics, parameters and lifetime data were extracted from [60, 65] and are summarized in appendix A in table A.1. Figure 3.13 below shows the battery degradation and life for their SUN valve regulated lead-acid (VRLA) batteries:

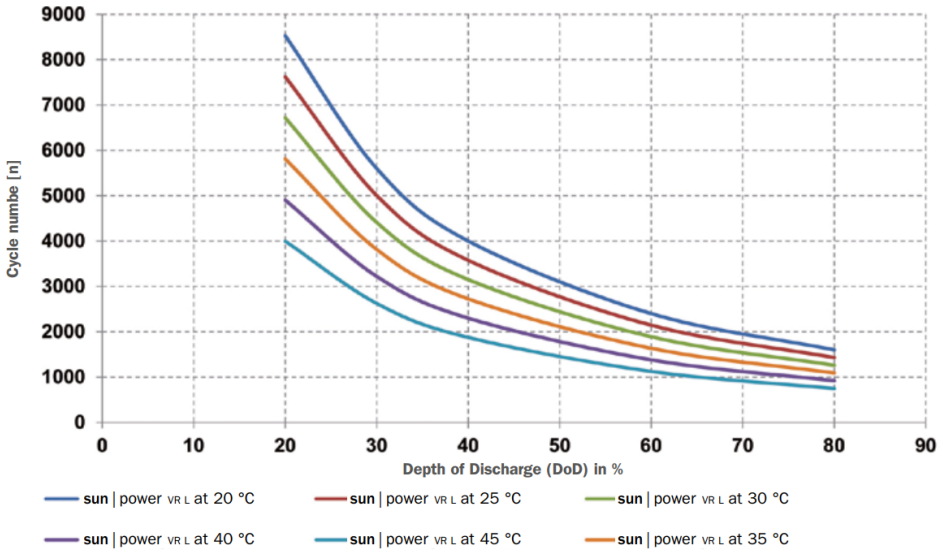

Figure 3.13: Endurance in cycles of sun VRLA batteries depending on DoD and temperature [36]

Using the curves above, a curve reconstruction was made and a 4^{th} degree polynomial algorithm was built on MATLAB to find the number of cycles over which the battery will operate before it reaches its EoL, or 80% of its original nominal capacity.

Battery cost

The upfront battery cost consists of the largest part of the total upfront SHS cost. Moreover, being the component with typically the shortest lifetime, both the upfront and replacement costs of the battery during the system need to be taken into account [58]. The upfront cost is the cost of purchase of a battery of a certain size and technology and can be defined as:

$$Q_{upfront} = Q_0.C_{nom} \tag{3.23}$$

Where ${Q_0}^T$ is the battery cost in \$/Wh at year 0, and C_{nom} is the nominal capacity.

The replacement costs occur at a later stage when the installed battery reaches its EoL. However, the cost of the battery during its replacement after some years depends on two factors: the discounting of future replacement cost to the present, and the forecasting of the future battery technology costs. Discounting future costs depends on the discounting factor r that varies according to the location's macroeconomic climate as follows [58]:

$$Q_{present} = \frac{Q_{future}}{(1+\frac{r}{100})^n} \tag{3.24}$$

As the battery costs trends are showing a general decline, the future replacement costs will be lower or equal to the initial cost at t=0. In order to estimate the purchase cost of the batteries at later years, a the data from a future costs projections for the years 2015 - 2040 based on experience rates was used. Figure 3.14 below, which was adapted from [76], shows a projection in a decrease in the costs of the lead-acid and Li-ion batteries for the upcoming two decades which is due to the increase in total installed capacity worldwide, and gained experience from manufacturers. The curves were fitted into a 3^{rd} degree polynomial using MATLAB, and a cost function was used to find the cost at that year. Taking into account the discounting factor mentioned previously, the total upfront battery cost including future replacements is:

$$Q^{Total}_{upfront} = Q_0.C_B + \sum_{i=1}^{n} \frac{Q_{future,i}.C_B}{(1+\frac{r}{100})^n} \tag{3.25}$$

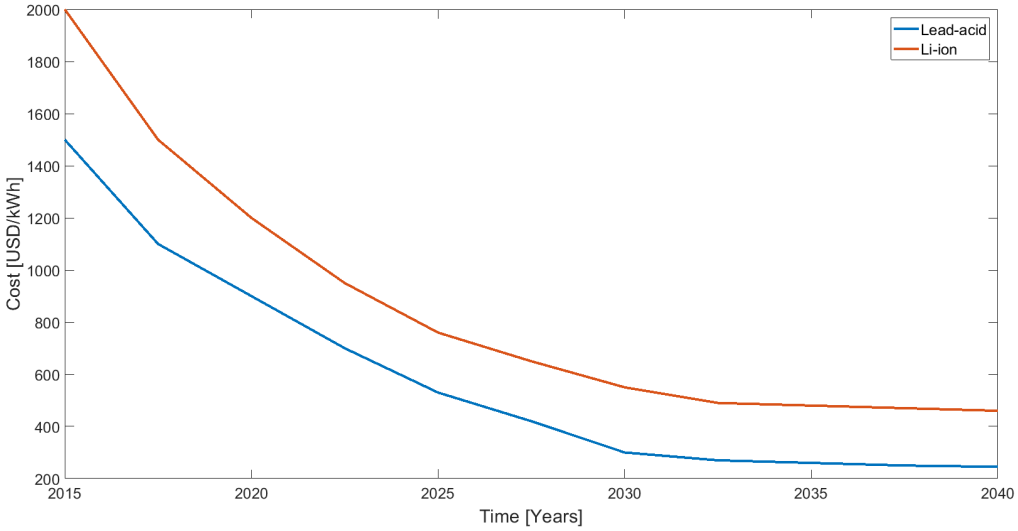

Figure 3.14: Future cost forecast for lead-acid and Li-ion batteries, *Adapted from* [76].

3.3.3. Power Electronics

The power electronics are the core of a solar home system. They are the main connection between the PV array, batteries and load. For the standalone, DC coupled architecture SHSs that are under study in this research, the main power electronics devices needed are charge controllers and DC/DC converters [79]. The converters in the system serve the following purposes:

- The charge controller connected to the PV array regulates the voltage output and current output of the array to ensure that it is always running at the Maximum Power Point (M_{PP}) [46].
- The converter connected to the load regulates the output voltage from the array and battery as required by the loads.
- The controller connected to the battery controls their charging and discharging to prevent damage through under or over charge.

Hence, a converter working properly increases the reliability and efficiency of the whole system, as well as preventing damage to the components [34]. In figure 3.15 below, the household converters are shown connected to their respective components, first the Maximum Power Point Tracker (MPPT) ensures the PV array operates at its optimal output, then the power output feeds the DC loads and battery depending on the system state [31].

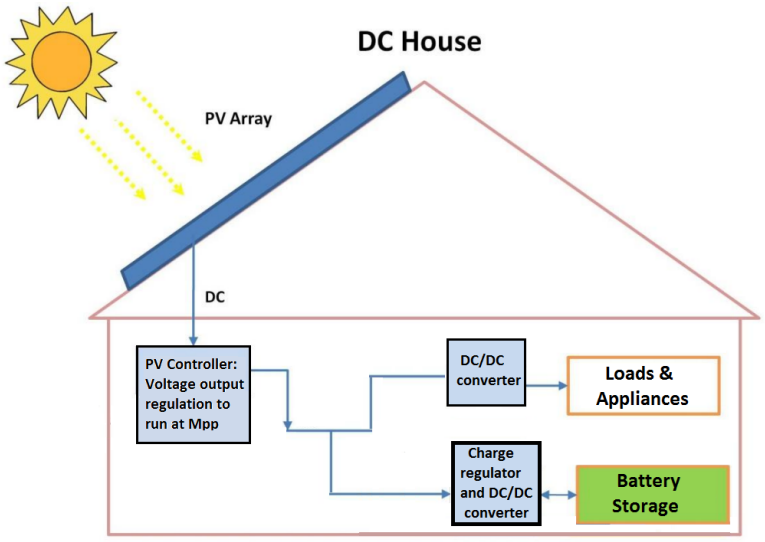

Figure 3.15: Typical DC house with DC/DC converters. *Adapted from [31].*

DC/DC converter parameters

All controllers have the same basic parameters that are provided by manufacturers. The most important parameters in sizing a converter are its operation limits, such as the peak power and voltage input from the PV array or battery, the maximum load currents, and possible load operation voltage. The controller also has set points that control the charging and discharging of the battery, most importantly the following [34]:

- **Voltage Regulation set point (VR):** which is the maximum allowable voltage value to be reached by the battery. After reaching this value, the battery is disconnected to prevent overcharge.
- **Low Voltage Disconnect (LVD):** The minimum voltage the battery is allowed to reach while discharging before being disconnected, to prevent excessive discharge. This voltage defines the minimum allowable State of Charge of the Battery.

In this study, the set points of the charge controller are assumed to be implemented according to the battery specifications, while the characteristics and operation limits are chosen according to the system size and load profile and summarized in table 3.7 below.

Table 3.7: Converter main characteristics

Converter characteristics	
PV DC input voltage [V]	P_{PV}
Max PV input current (A)	$I_{DC,max}$
Nominal input power [W]	$P_{conv,N}$

DC/DC converter model

In literature, the papers discussing the power electronics modeling in renewable energy or solar home systems assume a constant operation efficiency for the the charge controller and DC converters, and in case of the use of AC loads or grid-connection, use an inverter model for the DC to AC conversion. However, both inverters and DC converters have very similar efficiency curves, with peak efficiencies ranging from 90 to 98% as shown in figure 3.16 below where the output efficiency of each is shown as a function of the normalized $\frac{P_{in}}{P_{Nominal}}$ ratio. Hence, in this study, the converters were assumed to have the same behavior as an inverter, and were modeled using the available models in literature.

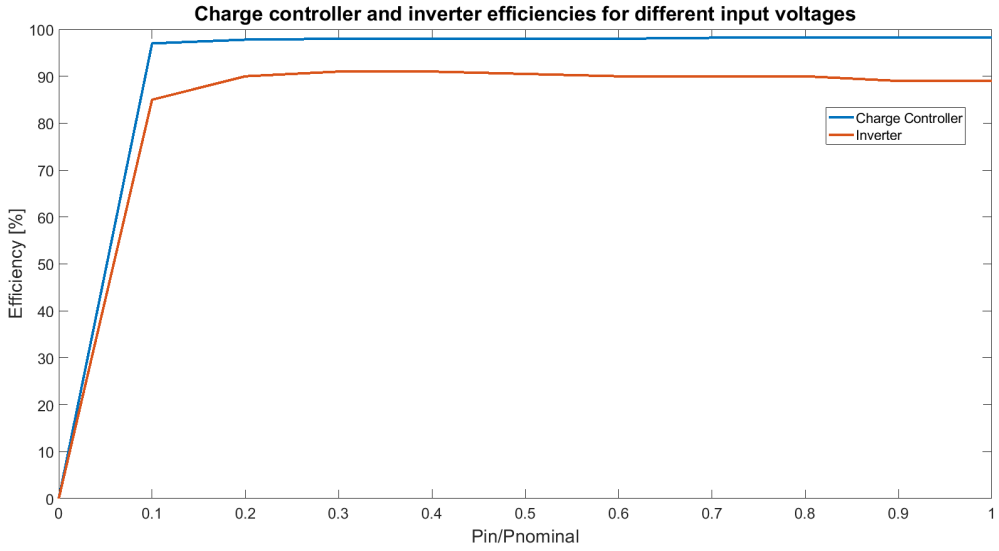

Figure 3.16: Efficiency curve of a typical inverter and charge controller *Adapted from [15, 55]*

The performance and sizing of the converter depends on two main parameters: the efficiency η_C and the nominal input power $P_{conv,N}$. Sizing the charge controller commonly depends on the sizing Ratio R_S [83]:

$$R_S = \frac{P_{PV,P}}{P_{conv,N}} \tag{3.26}$$

Where $P_{PV,P}$ is the peak power (Wp) of the PV array. Under-sizing the converter than the PV capacity (R_S>1) usually leads to better economy especially if the duration of peak irradiance values is low and therefore the higher rating of the converter is rarely used. Moreover, η_C depends on the instantaneous input and is typically lower at partial loads, hence affecting the performance[66]. Figure 3.16 illustrates the typical η_C VS the DC input P_{PV}. It is clear that higher, ideal operating efficiencies are achieved at higher partial loads or full loads (0.3 - 1), hence a highly oversized converter is not desired.

Converter efficiency

For practical modeling purposes, the converter power losses can are divided into a constant self-consumption loss (b_0), a linear load dependent loss (b_1) and losses dependent on the output power (b_2) as in the following equation [21, 66, 83]

$$\eta_{conv} = b_0 . \frac{P_{conv,N}}{P_{mp(t)}} + b_1 + b_2 . \frac{P_{mp(t)}}{P_{conv,N}} \tag{3.27}$$

Jantsch et al. [42] gathered a set of 35 commercial inverters, and studied their efficiency and performance through a various set of loads to obtain a range of practical and usable values for b_0, b_1 and b_2, these values were adopted in other studies such as [21, 66, 83] for the converter modeling and sizing for renewable energy systems. Table 3.8 below shows the values of the parameters for 3 different inverter classes.

Table 3.8: Parameter values for different converter classes

	b_0	b_1	b_2
Low efficiency converter	-0,05	0,915	-0,15
Average efficiency converter	-0,02	0,975	-0,08
High efficiency converter	-0,0035	0,995	-0,01

Hence, the output power of the converter can be expressed as:

$$(b_0 . \frac{P_{conv,N}}{P_{mp(t)}} + b_1 + b_2 . \frac{P_{mp(t)}}{P_{conv,N}}) . P_{mp}(t) \qquad for \quad 0 < P_{mp}(t) < P_{conv,N} \tag{3.28}$$

$$(b_0 + b_1 + b_2) . P_{conv,N} \qquad for \quad P_{mp}(t) > P_{conv,N} \tag{3.29}$$

Equation 3.29 above shows that any input power from the PV array that is above the rated power is rejected. In this study, for the practical use and sizing of the converter, the equation 3.27 will be used with the parameter values of a high efficiency converter to model the converter performance.

PV array converter sizing

In some studies, such as [40], under sizing the converter for the PV array is recommended for low power systems. The study consists of calculating the yearly energy yield of the system while varying the converter size. The reason behind undersizing the inverter is that during the year, the frequency of the PV array reaching its maximum output capacity is very low, hence, sizing the inverter according to those occasional peaks results in a high cost to energy yield ratio. In the study, it is concluded that if the sizing is decreased from 1.25 to 1 (increasing the inverter size by 20%), the energy yield will increases by a mere 2% as indicated in figure 3.17.

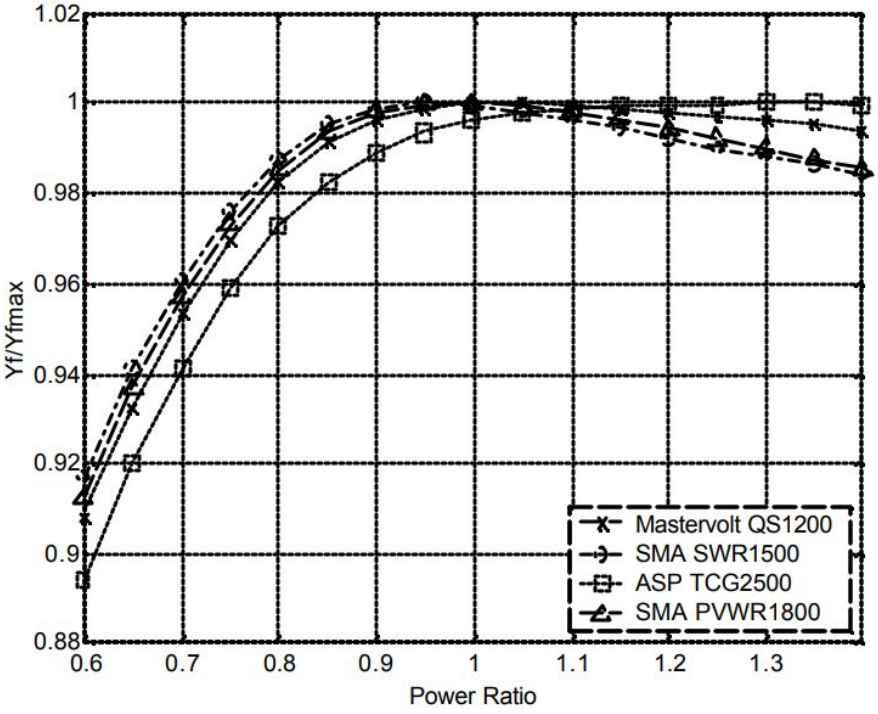

Figure 3.17: Energy yield VS sizing ratio for various inverters [40].

Another study also examined the energy yield of the inverter through a range of sizing ratios experimentally, it was found that the optimal sizing ratio range in terms of yearly energy yield is between 0.85 and 1.18, with a peak yield at 1.08 as shown in figure 3.18 below [15].

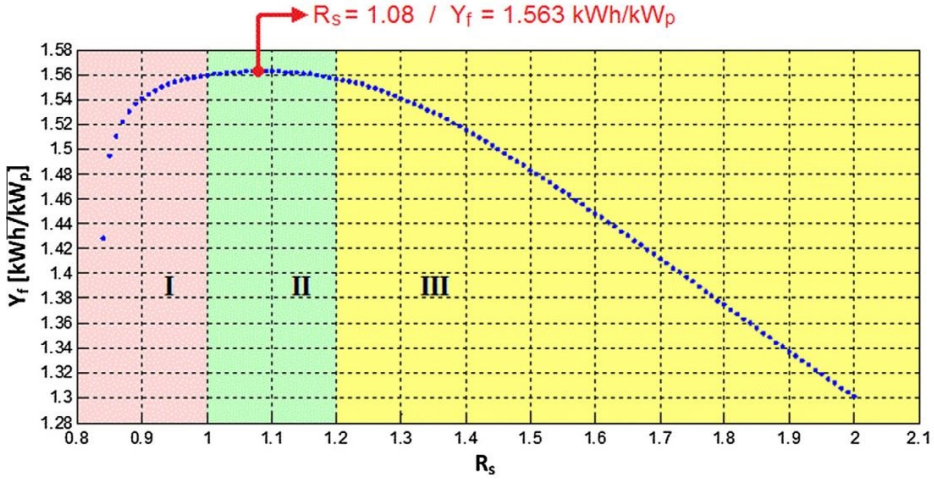

Figure 3.18: Obtained values of Yield Y_f as a function of R_S [15].

Both studies come to the same conclusion of undersizing the inverter, however, there is no absolute optimal R_S that can be chosen, it depends both on the PV array size and the meteorological data. Hence, in this study, the same approach is proposed: for each location, and system size, a preliminary iterative algorithm is to be built and run to find the optimal sizing ratio in terms of yearly energy yield and inverter cost. The methodology is as follows: for a chosen PV array capacity (W_p) the yearly energy yield is to be computed over a range of converter sizes ranging from $0.7W_p < P_{conv,N} < 2W_p$, or a sizing ratio $0.5 < R_S < 1.4$. Following that, the optimal converter size with respect to energy yield and cost is chosen. The iterative algorithm was performed on the 20 W_p module mentioned before, at the chosen location in Pune using the yearly irradiation data. The probability of occurrence of the various output values of the module throughout the year are shown in figure 3.19 below.

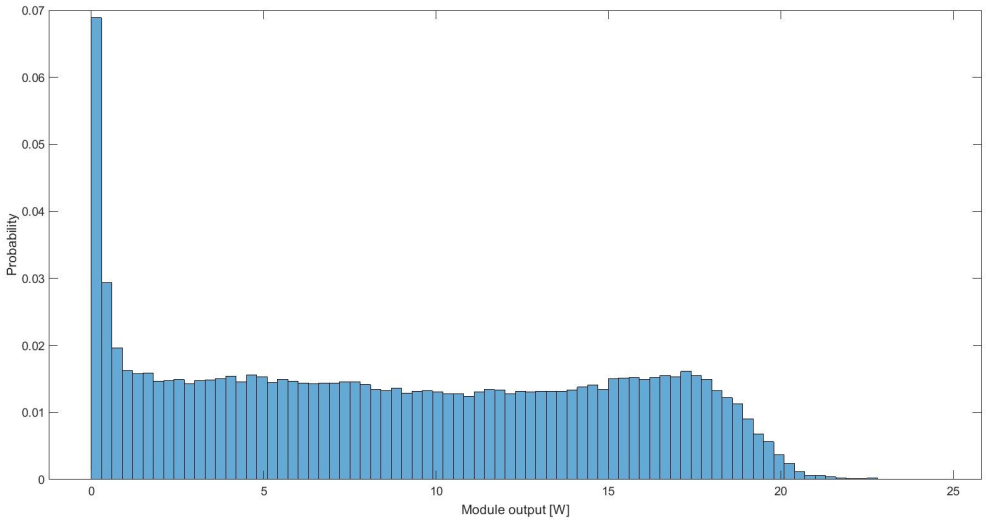

Figure 3.19: Probability density function for the 20 W_p module power output

The figure shows that during the year, the probability of the PV module having an output equal or larger than its rated W_p is very low (<1%). Hence proving the reason for undersizing. Table 3.9 below summarizes the occurrence probability of some irradiance values.

Table 3.9: Irradiance probability of occurrence

Module output	**Probability of occurrence**
20 W or higher	<1%
>14 W (70% of W_p)	6%
>15 W (75% of W_p)	3.8%
>16 W (80% of W_p)	1.4%

Figure 3.20 below shows the normalized yearly energy yield as a function of the sizing ratio R_s for the given module. The maximum energy yield at an $R_s = 1.14$ is 5% higher than the yield at $R_s = 1.38$ or $P_{Nom} = 72\%.W_p$. Hence, an increase in the converter size by 15% leads to only a 5% increase in yield.

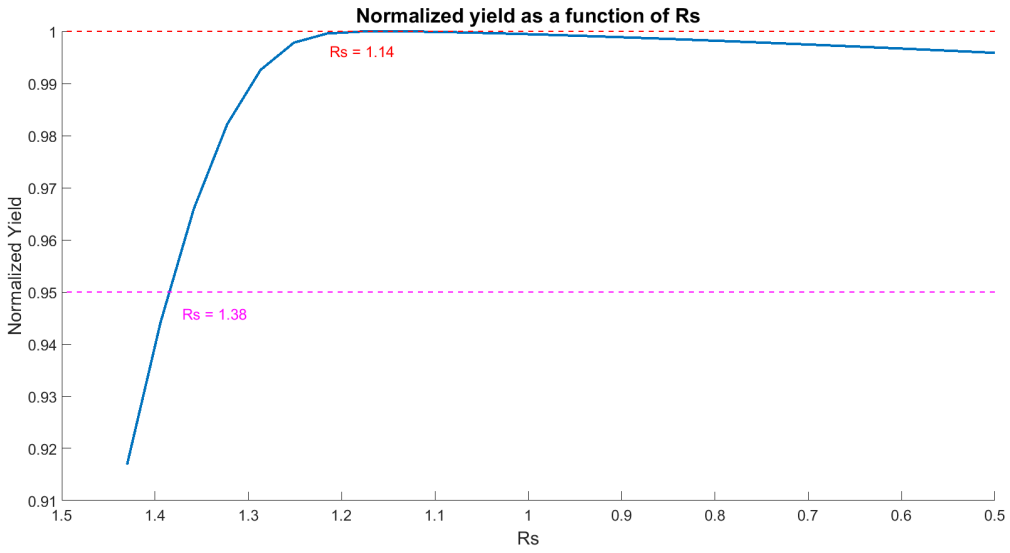

Figure 3.20: Normalized yearly energy yield as a function of the sizing ratio R_S

The converter can thus be chosen to be at 72% the capacity of the PV array, saving 28% of the cost with a less than 5% compromise to energy yield. This procedure to size the charge controller will be followed at the beginning of the optimization methodology in each of the locations in the case studies discussed in section 4.3.

Sizing the converter for the DC loads

The DC/DC converter that feeds the loads is responsible of adjusting the input voltage to the desired output load voltage, and stabilizes the power flow to prevent any damage to the appliances. The sizing of this converter depends on the load profile of the household, the converter should always be able to supply enough power to feed the load, hence, $P_{Nom,Load}$ should be at least equal to the yearly peak load in the load profile.

$$P_{Nom,Load} = \max(Load_{household}) \tag{3.30}$$

With the rated power known, the same equations and procedure described in section 3.3.3 can be used to obtain the converter efficiency curve, and the dynamic operating efficiency during the year according the the load.

Sizing the converter for the battery

As shown in the control strategy in figure 3.22, the battery's role is to supply the load deficit during the time instances where the PV array cannot meet the demand, and to charge and store the excess energy when the array is over-producing. Hence, at each instant i, the energy equations are as follows:

$$PV_{Outpout,i} - \frac{Load_i}{\eta_{Conv,Load,i}} > 0 \qquad P_{excess,i}; \quad \text{Battery} \quad \text{charges} \tag{3.31}$$

$$PV_{Outpout,i} - \frac{Load_i}{\eta_{Conv,Load,i}} < 0 \qquad P_{deficit,i}; \quad \text{Battery} \quad \text{discharges} \tag{3.32}$$

Using the above equations, the highest value of $P_{deficit}$ and P_{excess} can be found, which correspond to the highest amount of power the battery will be charging or discharging at an instant i during the year. The higher value of these two needs to be met by the battery converter in order to avoid power clipping and shortage. Hence:

$$P_{Nom,Battery} = \max(\max(P_{deficit}), \max(P_{excess})) \tag{3.33}$$

After obtaining the rated power for the battery converter, the dynamic efficiency of the power converter can be obtained from each of the $P_{deficit}$ and P_{excess} arrays to obtain $\eta_{Conv,discharge}$ and $\eta_{Conv,charge}$. The flowchart

3.21 below shows the overall sizing methodology going from the meteorological and load data as input to obtaining the sizing parameters of the various power converters.

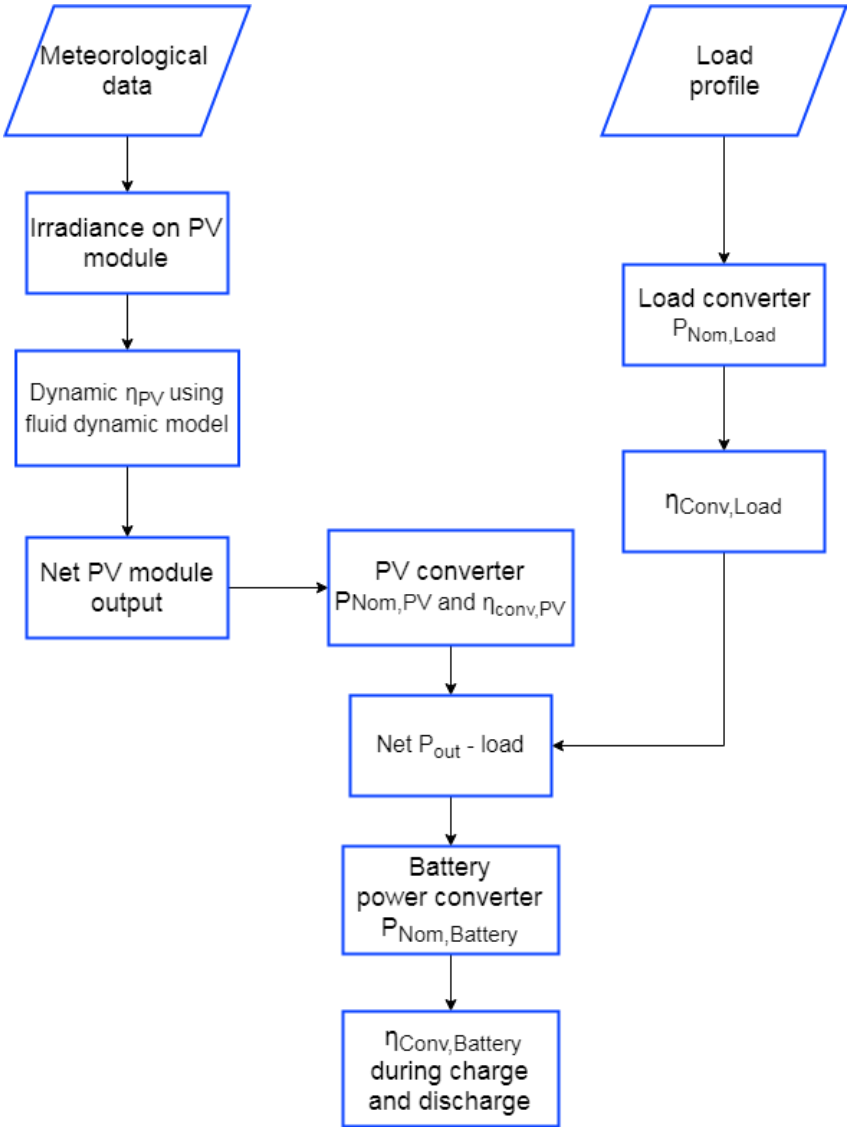

Figure 3.21: Converter sizing methodology flowchart

3.4. Complete System Design

After modeling the different components in the SHS on MATLAB, the different functions were compiled together in a larger code with a control strategy that simulates the behavior of the whole system. The model is designed in a way to take the location meteorological data and component characteristics as input for a given PV and battery size or range of sizes, and output the different performance parameters for each combination. The important parameters are the yearly energy dump and deficit, and the LLP as mentioned in section 3.5.

3.4.1. Control Strategy

The system control strategy designed is an iterative algorithm over the 526600 time steps, representing the minutes in a year, where the power output from the PV array is computed, and an energy balance is performed whether the load requirement is met with excess or deficit. The control strategy is illustrated in figure 3.22.

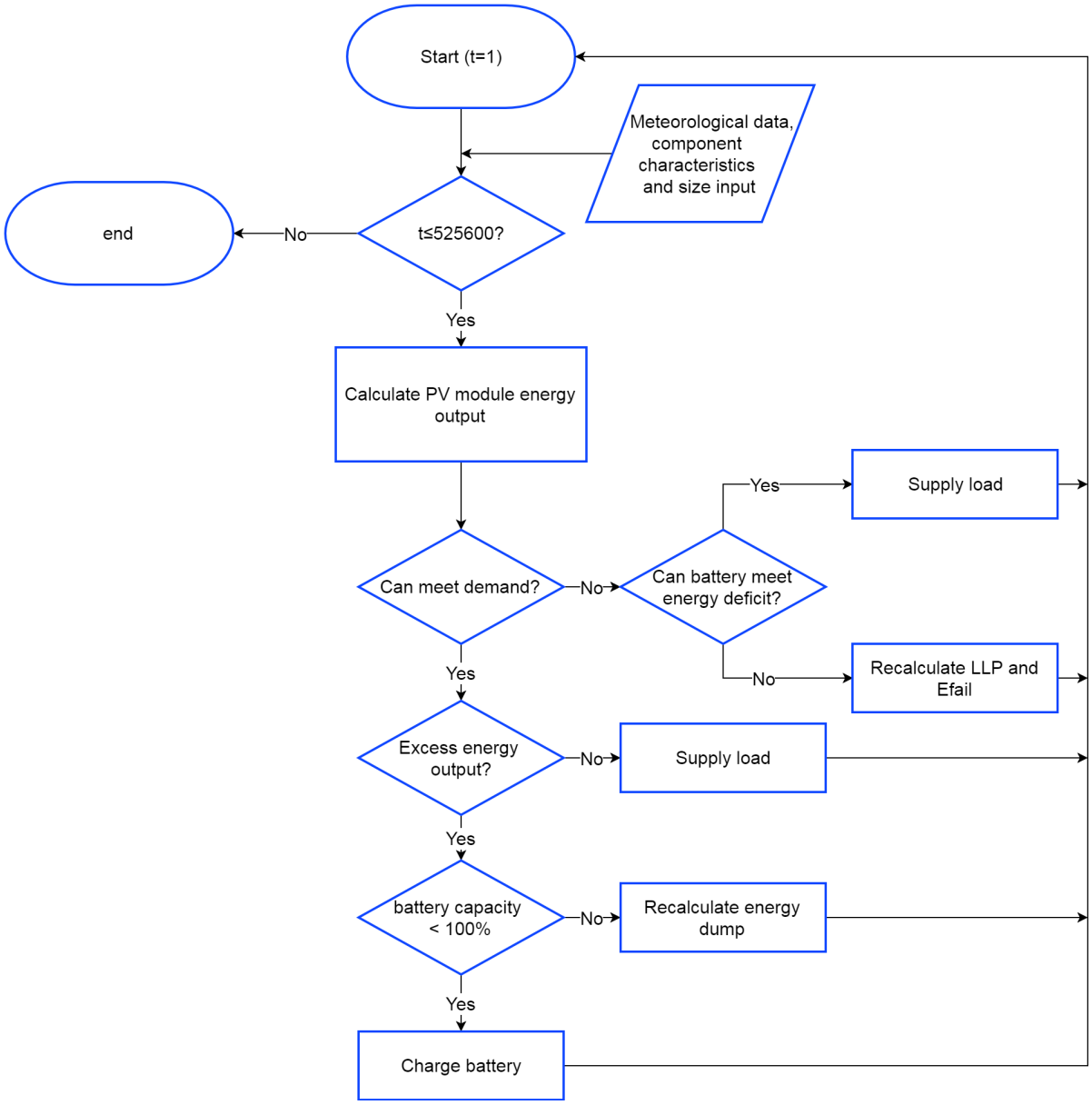

Figure 3.22: SHS control strategy flowchart

At every time step, the battery capacity is calculated, whenever the battery is completely depleted or full,the LLP, E_{Dump} and E_{fail} are recalculated. At the end of the simulation, the system size can be evaluated by the user by assessing the before mentioned parameters.

3.5. System Performance/size Analysis

Now that a MATLAB model for each of the main system components has been constructed, the next step is to assess the performance and feasibility of a given system size or set of system sizes. A set of different parameters can help classify the system, whether it is oversized, undersized, or optimal. In this section, some of the most common sizing strategies will be discussed and analyzed.

3.5.1. LLP as a reliability measurement tool

As mentioned in section 2.2, the LLP is the most commonly used parameter to assess the reliability and performance of a stand-alone renewable energy system over a certain duration. The LLP value, which indicates the amount of system downtime, is normally set by the user as a constraint, such as in [12] where the value

was set to 2% of a year. This is equivalent to a downtime of 7.3 days. In this study, the LLP was obtained as a summation of every minute where there was a blackout over the total amount in a year as follows:

$$\text{LLP} = \frac{\sum_{\text{i}}^{\text{N}} \text{T}_{\text{downtime,i}}}{\text{N}} \tag{3.34}$$

Where $T_{downtime,i}$ has a value of 1 at instant i if there is a blackout, and 0 if the load is being fulfilled. N has a value of 525,600 which is the total number of minutes in a year. The LLP value is directly affected by the PV array and battery size. A higher PV array output allows meeting the load demand during the day, and a higher battery capacity makes it more possible to supply the energy deficit at night or in the absence of sun. Figure 3.23 and 3.24 show the LLP over a year as a function of the battery size and PV array capacity respectively for the load profile discussed earlier.

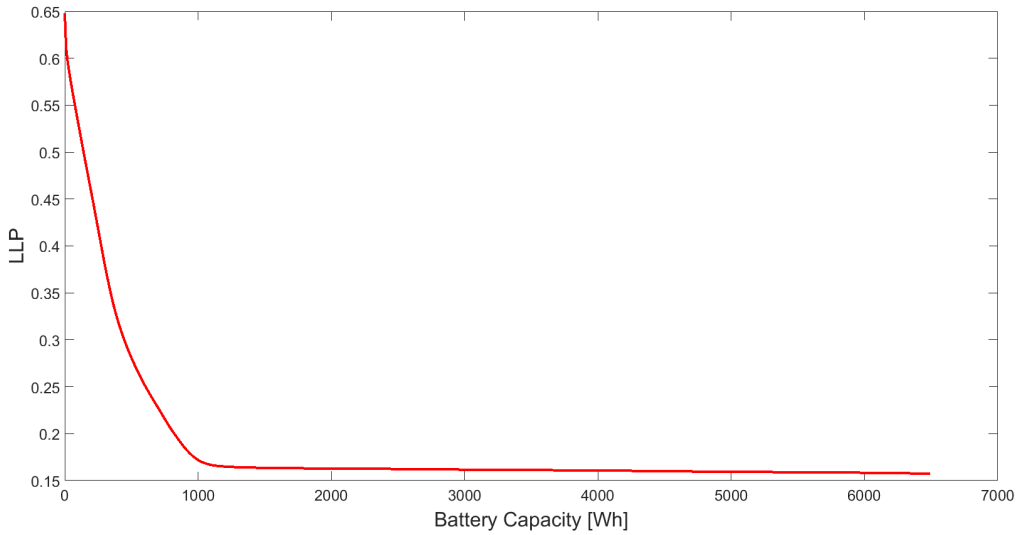

Figure 3.23: Influence of battery size on LLP.

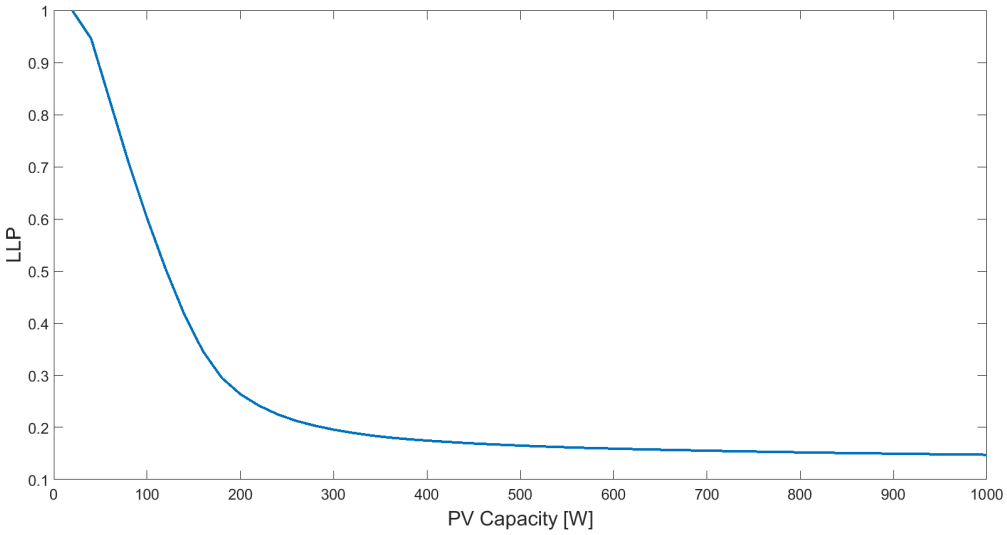

Figure 3.24: Influence of PV array capacity on LLP.

From the figures, it can be concluded that although increasing the capacity of only one of the components decreases the LLP, but it does reach a plateau. So in order to reach a low and desired LLP value without over sizing one of the components, an optimal combination of both has to be selected.

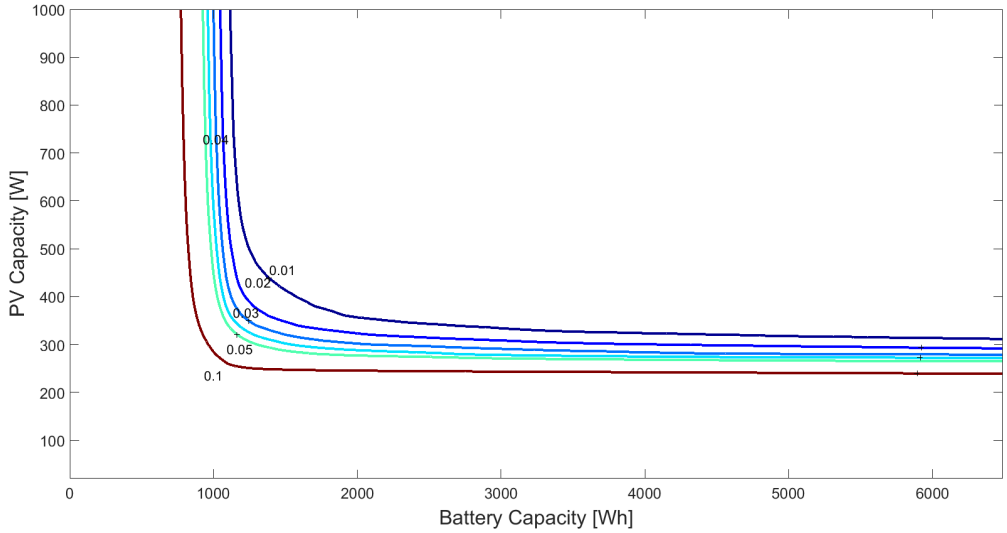

Figure 3.25: Contour showing different values of LLP for PV/battery combinations

In figure 3.25 above, the contour plot shows the various possible combinations of PV and battery for a certain LLP value, ranging from 1% to 10%. The lower the LLP value needed, the higher the PV and battery capacities need to be.

3.5.2. Energy Dump

Energy dump is another useful parameter for evaluating the size of a PV system. Energy dump is the yearly amount of excess energy that was produced by the PV array in excess to the load, and could not be stored by the battery due to being fully charged.

$$E_{Dump} = \sum_{i}^{N} E_{excess,i} \tag{3.35}$$

Where $E_{excess,i}$ is the excess energy at each minute i during the year. Energy dump is also directly related to the capacity of the PV and batteries. A combination high PV array capacity with a low battery storage results in lots of dumped energy that cannot be stored by the battery. Thus, in order to have an efficient system and prevent over sizing, the yearly energy dump should be minimized. In this study, to have a more tangible feel about the amount of energy dump in each system, the parameter relative dump is introduced which is

$$E_{RelDump}[\%] = \frac{E_{Dump}}{E_{Yearly\quad Load}} \times 100 \tag{3.36}$$

In this manner, the energy dump value is relative to the load profile and system size, and not just an absolute value. Figure 3.26 below shows a contour plot of the relative yearly energy dump for the same system described in 3.5.1.

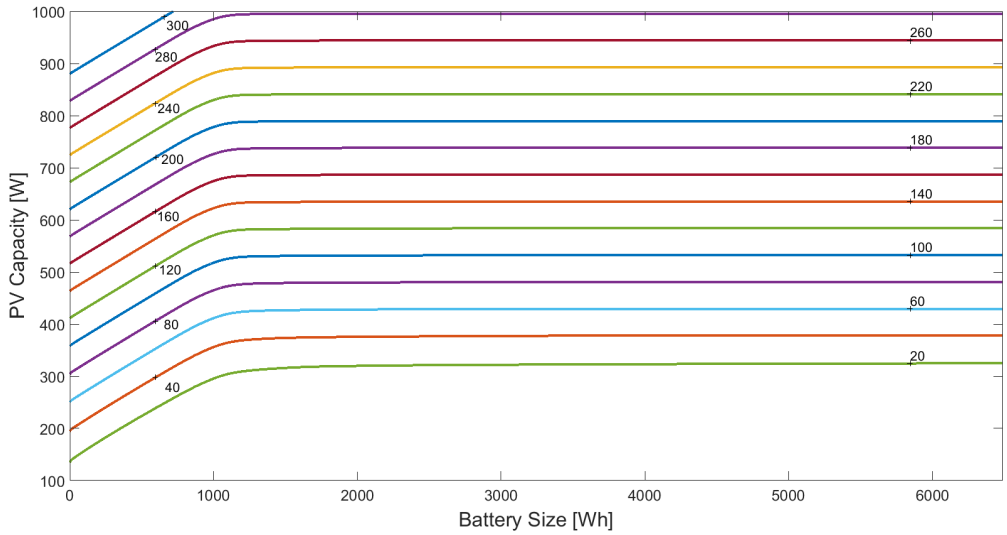

Figure 3.26: Relative dump for different battery and PV capacities

The amount of energy dump is shown to be rapidly increasing with increased PV array capacity, and stabilizing when the battery capacity increases.

3.5.3. Days of Autonomy

The Days of Autonomy (DOA) parameter, is a popular intuitive sizing parameter as described in section 2.3.1. This parameter involves multiplying the size of the battery by the number of days the system is expected to run autonomously in case of adverse weather conditions. The size of the battery for one day of operation is found through equation 2.8, and multiplied by the DOA according to rules of thumb or the user preferences. To illustrate the impact of this parameter, a the battery size for the given system and load profile was calculated for different DOAs. Figure 3.27 below, similarly to 3.25, shows the LLP values at different PV and battery capacities, the LLP contour lines range from 0.01 to 0.05. The vertical lines represent the size of the battery at different DOAs. For DoD = 80% and η_B = 90%, 1 DOA = 1724 Wh.

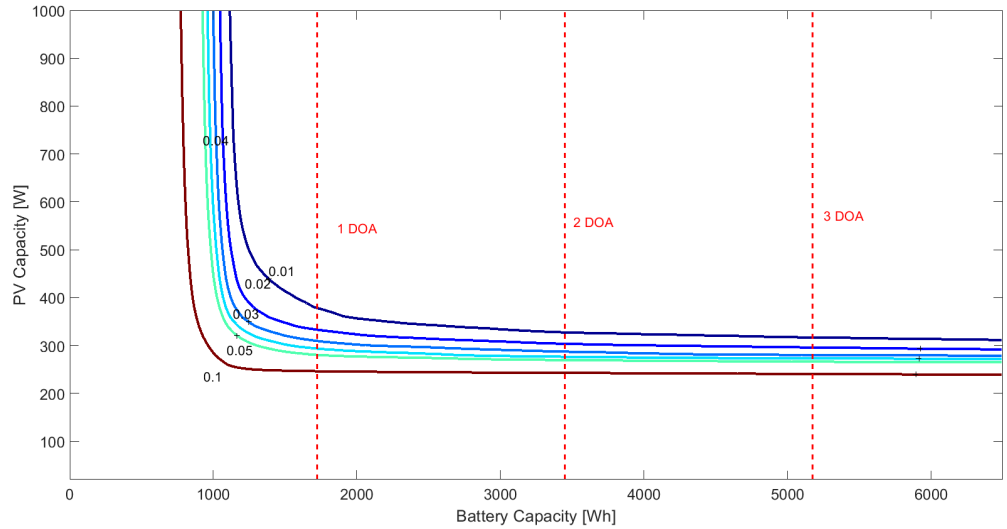

Figure 3.27: LLP at different PV and battery capacities using Days of Autonomy

The large gap between the DOAs shows that this method follows rough sizing and can lead to over or under sizing of the two components. For example, if 1 DOA is chosen during sizing, a very large PV array size is needed to keep the LLP within boundaries. Moreover, following the typical 2-3 DOA rule, the battery bank

capacity increases greatly, with little reduction in PV size. It also be seen that over a certain DOA value, 3 in this case, the LLP reaches a plateau making the battery storage highly over sized. The optimal size for the PV and battery storage for all LLP values falls somewhere between the 1 and 2 Days of Autonomy, where the smallest capacity combination of battery and PV can be used while maintaining the required value of LLP. In order to accurately find locate minimum, a numerical, more precise method needs to be used.

3.5.4. Night of Autonomy

As the Days of Autonomy sizing approach proved to be a very rough approach that leads mostly to over sizing the storage, an attempt was made to increase the accuracy of this approach, and shorten the large capacity gaps between each day of autonomy. The parameter behind this approach is called Night of Autonomy (NOA). The idea behind this approach, is that on any night the battery bank is the only source of power, should be able to satisfy the load during that time reliably. Hence, the battery size should be sized according to the average load during the night, and not during both day and night, especially that the typical households in this study are in areas with year round sunlight abundance. Thus, equation 2.8 can be reformulated into:

$$C_B = \frac{E_{NightLoad}}{V_B.DoD.\eta_B}.NOA \tag{3.37}$$

Where $E_{Night\ \ Load}$ is the average load during the night and NOA is an integer that is subjective to the user, and represents the number of average nights the battery should be capable of. The average night load was obtained by summing up the load at all the instants where there was 0 irradiance on the module over the whole year, and finding the daily average.

Figure 3.28 below shows the difference in the sizing gaps between different DOAs and NOAs for the same system and load profile. One NOA is equal to 111.5 Wh. The amount of NOAs as indicated in vertical blue lines over the capacity range of the battery (0 - 1,200 Wh) is more than the double of the DOAs as indicated in red lines. From the figure, one can conclude that using the average night load only as a basis for sizing the battery capacity leads to a more correct result, and reduces over sizing. However, the gap between two NOAs is still large for any desired LLP. Hence, this method can also be refuted for optimizing the system sizing.

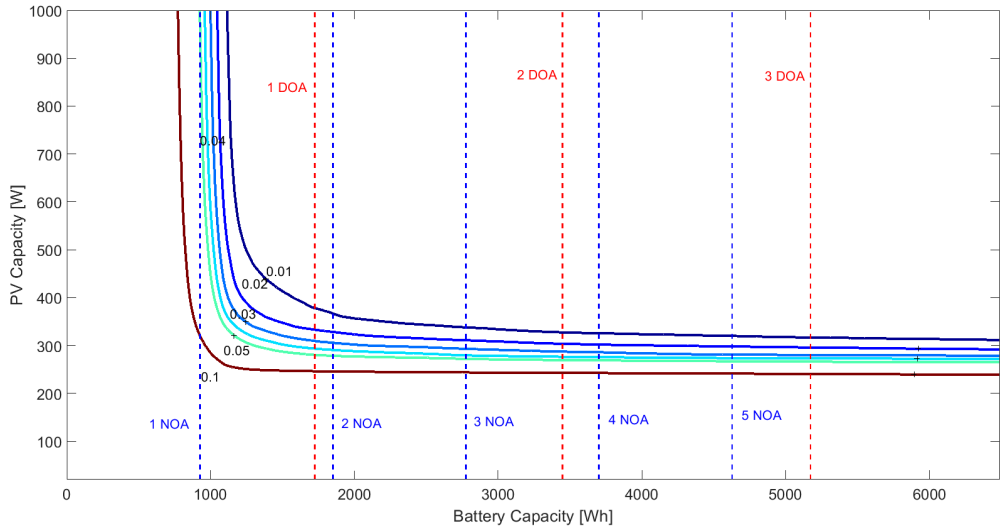

Figure 3.28: LLP at different PV and battery capacities using Nights of Autonomy

3.5.5. Bundled Parameter

The various parameters described above depend highly on the user preferences, whether it is the maximum allowable LLP and energy dump values by the system, or the number of NOAs or DOAs. Moreover, the conflict between the LLP and energy dump leads to a large increase in one of the parameters whenever the other is minimized. i.e. A very low LLP leads to a very high energy dump, and a system with low energy dump leads to an unreliable system with high LLP. Hence, in this study, an attempt at combining these parameters has been made by creating a unit-less bundled parameter U.

$$U = \frac{E_{Dump}}{1 - LLP} \tag{3.38}$$

Using the LLP definition from equation 2.2, the equation above can be reformulated to:

$$U = \frac{E_{Dump}}{E_{YearlyLoad} - E_{fail}} \tag{3.39}$$

As can be seen from the equation above, the bundled parameter is unit-less and with the E_{Dump} and E_{fail} values both needing to be minimized, an optimized and reliable system size is expected to be obtained. In figure 3.29 below, the bundled parameter is plotted for the system in study for different battery and PV capacities.

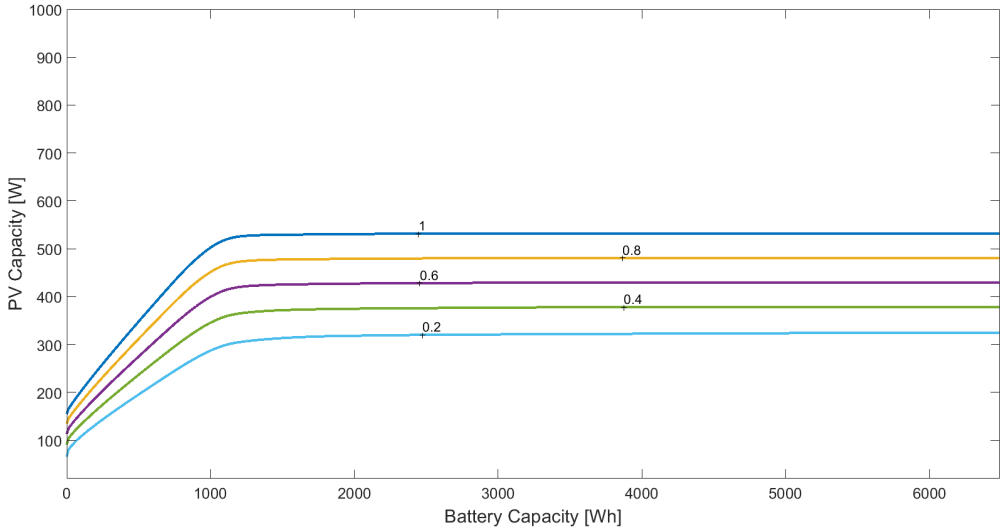

Figure 3.29: Bundled parameter at different PV and battery capacities

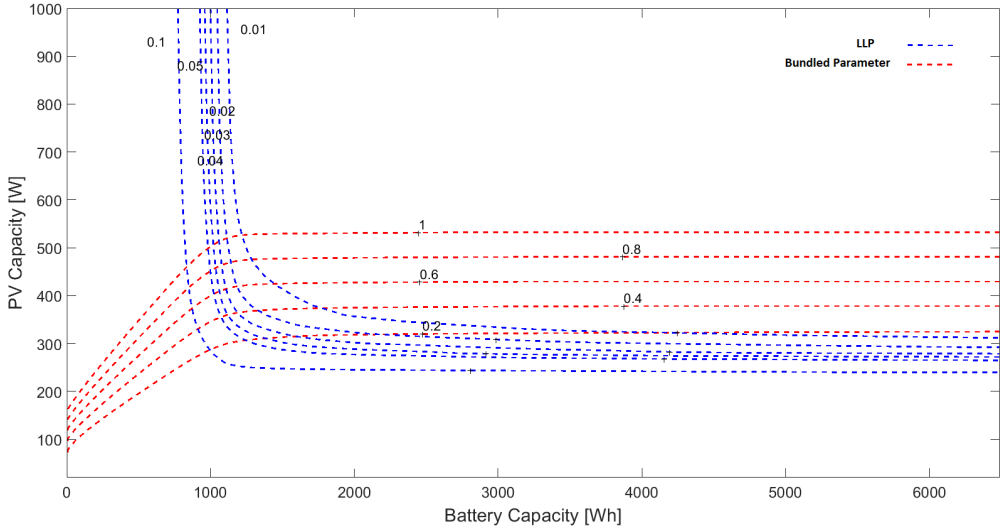

Figure 3.30: Bundled parameter and LLP at different PV and battery capacities

As shown in figure 3.30, an optimal sizing range for the PV and battery capacity using the LLP and U contour lines. The user needs to simply choose the desired maximum LLP and U values, and obtain a small range of the possible system sizes to be used. For example, if the desired system criteria are to have an LLP $\leq$ 2% and a U $\leq$ 0.6, the user can choose any of the PV/battery combinations that are in the dashed area shown in the figure below.

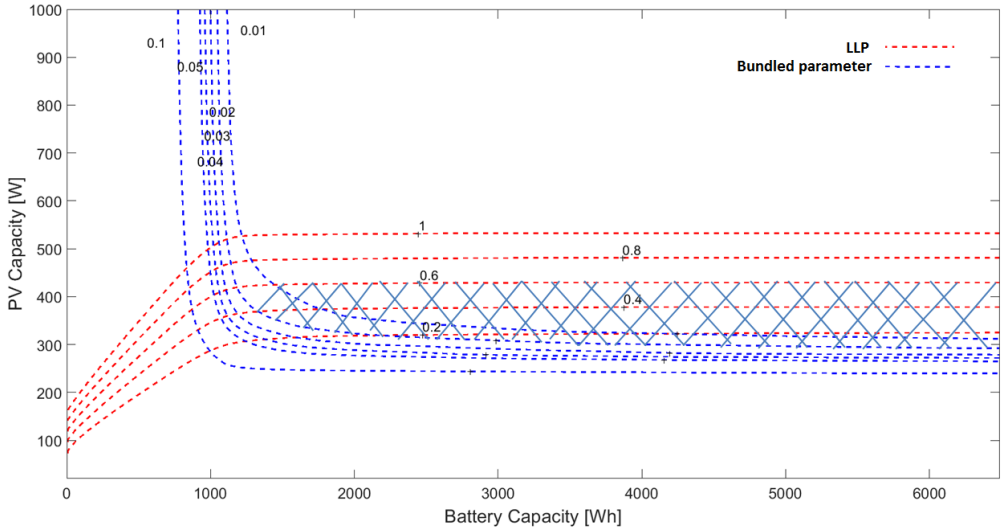

Figure 3.31: Bundled parameter and LLP at different PV and battery capacities with range of system sizes.

The graphical methods shown in this section are very useful to narrow down or find the optimal system sizes following the required design criteria. However, these methods, relying mostly on graphical interpretation, can only handle optimizing up to two parameters at a time. Optimizing a system with respect to upfront cost, LLP, energy dump and battery lifetime cannot be done graphically, as it results in highly inaccurate and poorly represented results. To be able to optimize the system accurately while taking multiple parameters into account, a multi-objective optimization method is required as will be discussed in chapter 4.

3.5.6. Design Assumptions and Limitations

The designed system is able to provide an accurate and reliable solution due to the use of minute based data, dynamic efficiency for the module and power converters, and battery lifetime.Nonetheless, several assumptions were made during the component modeling and system design phase and are listed below:

- The MMPT tracker of the charge controller is assumed to be ideal, hence the PV array output is always at P_{mpp}.
- The self-discharge of the battery is not considered.
- The battery itself is assumed to be an energy counter, where the capacity is just dependent on the energy balance and not the voltage and charging/discharging current.
- The modeling of the DC/DC converters in the system is based mostly on the modeling of inverters found in literature.
- The battery temperature was assumed to be the ambient temperature during the lifetime modeling due to the lack of experimental data.

3.6. Conclusions

In this chapter, the methodology for modeling, sizing and conducting the performance analysis for each of the SHS components was done. Then the effect of the component sizes on the system metrics was analyzed:

- The system LLP greatly depends on the battery capacity, but saturates after a certain limit.
- The energy dump increases with the increase of PV capacity.
- The battery lifetime increases largely with the increase of capacity, and decreases when the PV capacity increases.
- The conventional sizing methods, such as the DOA provide very rough and over-sized system estimations, and are far from being useful in optimization.

Moreover, at the end of this chapter, it became clear that the complexity of the different metrics makes it difficult to find optimal system sizes using graphical methods. To be able to assess the effect of the system size on the different metrics simultaneously, a multi-objective optimization approach needs to be used to address the following metrics:

1. **LLP:** The overall system LLP needs to be minimized and is defined as:
   - $\text{LLP} = \frac{T_{downtime}}{T_{Total}}$
2. **Cost:** The total system upfront cost needs to be minimized and is defined as:
   - $Q_{system} = Q_{PV}.C_{PV} + Q_{Conv}.C_{Conv} + Q_0.C_B + \sum_{i=1}^{n} \frac{Q_{future,i}.C_B}{(1+\frac{r}{100})^n}$
3. **Battery Lifetime:** The battery lifetime, as mentioned earlier, depends greatly on the operating temperature and the number of cycles it undergoes. Typically, the larger the battery, the higher its lifetime. The battery lifetime needs to be maximized, minimizing the number of replacements and hence the overall system cost.
4. **Energy dump:** The yearly energy dump by the system needs to be minimized, hence avoiding an oversized system.

With the above criteria in mind, chapter 4 discusses two multi-objective approaches used in this study to find the optimal SHS size.

4

Stand-alone SHS sizing

In this chapter, the multi-tier framework will be discussed, where the different household load profiles for each tier will be introduced. Then, the procedure for finding the optimal system size at each tier will be elaborated using two optimization methods, an iterative method and the Genetic Algorithm, which is one of the many evolutionary algorithms discussed in 2.3.2. Finally, the optimization methods will be evaluated through three case studies at different locations where rural electrification is in great need.

4.1. Multi-tier framework

The International Energy Agency (IEA) and the World Bank were able to measure and quantify the energy access of different households and countries by combining the average country's electrification rate with the average residential electricity consumption. The proposed household categorization methods is the multi-tier framework. This method is able the access to electricity supply of households through attributes such as: peak available capacity, evening supply, affordability, etc.Moreover, it measures the electric services used of each tier based on the ownership of different levels of household appliances. For example, tier 1 has access to the basic and essential appliances such as lighting and phone charging, and the ownership of appliances increases from tier 2 and above. Tier 0 corresponds to no access to electricity, where many households use kerosene lamps and stove for lighting and cooking, or other forms of solid biomass which emit harmful pollutants. Tables 4.1 and 4.2 below summarize the attributes and appliances used in each tier [4].

ATTRIBUTES	TIER 0	TIER 1	TIER 2	TIER 3	TIER 4	TIER 5
Quantity (peak available capacity)	—	>1W	>50W	>200W	>2,000 W	>2,000 W
Duration of supply (hours)	—	>4	>4	>8	>16	>22
Evening supply	—	>2	>2	>2	4	4
Affordability (of a standard consumption package)	—	—	Affordable	Affordable	Affordable	Affordable
Legality	—	—	—	Legal	Legal	Legal
Quality (voltage)	—	—	—	Adequate	Adequate	Adequate

Figure 4.1: Electricity supply attributes for different tiers [4]

	TIER 0		TIER 1		TIER 2		TIER 3		TIER 4		TIER 5	
				Watts		Watts		Watts		Watts		Watts
Likely feasible applications (May not be actually used) (Wattage is indicative)			Radio Task lighting Phone charging	1 1 1	Radio Task lighting Phone charging General lighting Air circulation Television Computing Printing Etc.	 18 15 20 70 45	Radio Task lighting Phone charging General lighting Air circulation Television Computing Printing Air cooling Food processing Rice cooking Washing machine Etc.	 240 200 400 500	Radio Task lighting Phone charging General lighting Air circulation Television Computing Printing Air Cooling Food processing Rice cooking Washing machine Water pump Refrigeration Ironing Microwave Water heating Etc.	 500 300 1,100 1,100 1,500	Radio Task lighting Phone charging General lighting Air circulation Television Computing Printing Air Cooling Food processing Rice cooking Washing machine Water pump Refrigeration Ironing Microwave Water heating Air conditioning Space heating Electric cooking Etc.	 1,100 1,500 1,100
Possible electricity supply technologies	Dry cell Solar lantern Rechargeable batteries Home system Mini-grid/grid		— Solar lantern Rechargeable batteries Home system Mini-grid/grid		— — Rechargeable batteries Home system Mini-grid/grid		— — — Home system Mini-grid/grid		— — — Home system Mini-grid/grid		— — — Home system Mini-grid/grid	

Figure 4.2: Electricity supply appliances for different tiers [4]

In the following section, the load data used for each tier in the energy ladder will be elaborated.

4.1.1. Load Data for each tier

With the multi-tier household classification method, in the study done in [59]were stochastic methods were used to construct load profiles for each tier using different household DC appliances. The load profiles were used in this thesis to size the optimal SHS for each tier. The load profile for a typical week of each tier is shown in the figures below.

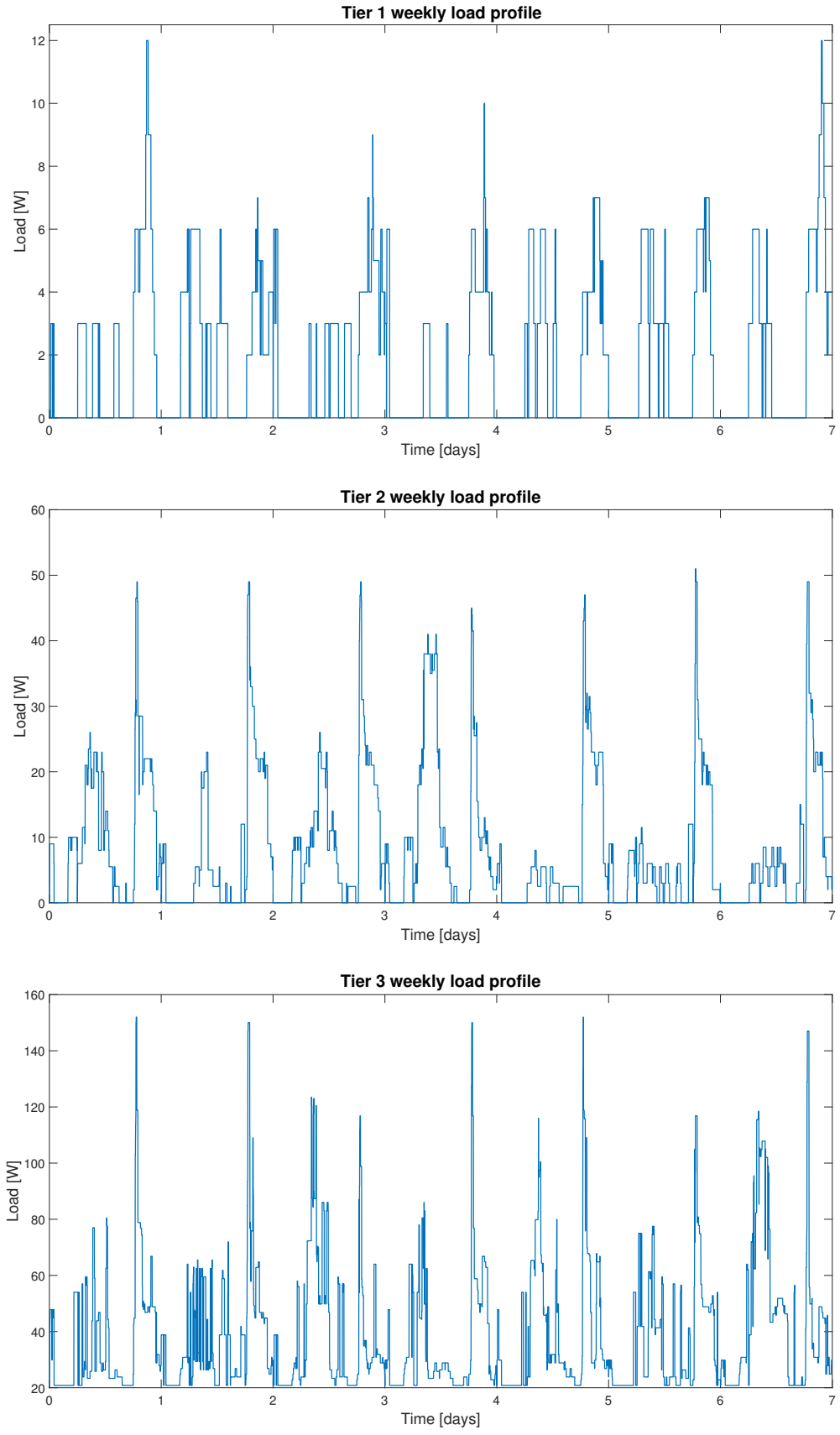

Figure 4.3: Typical weekly load profile for tier 1-3 [59]

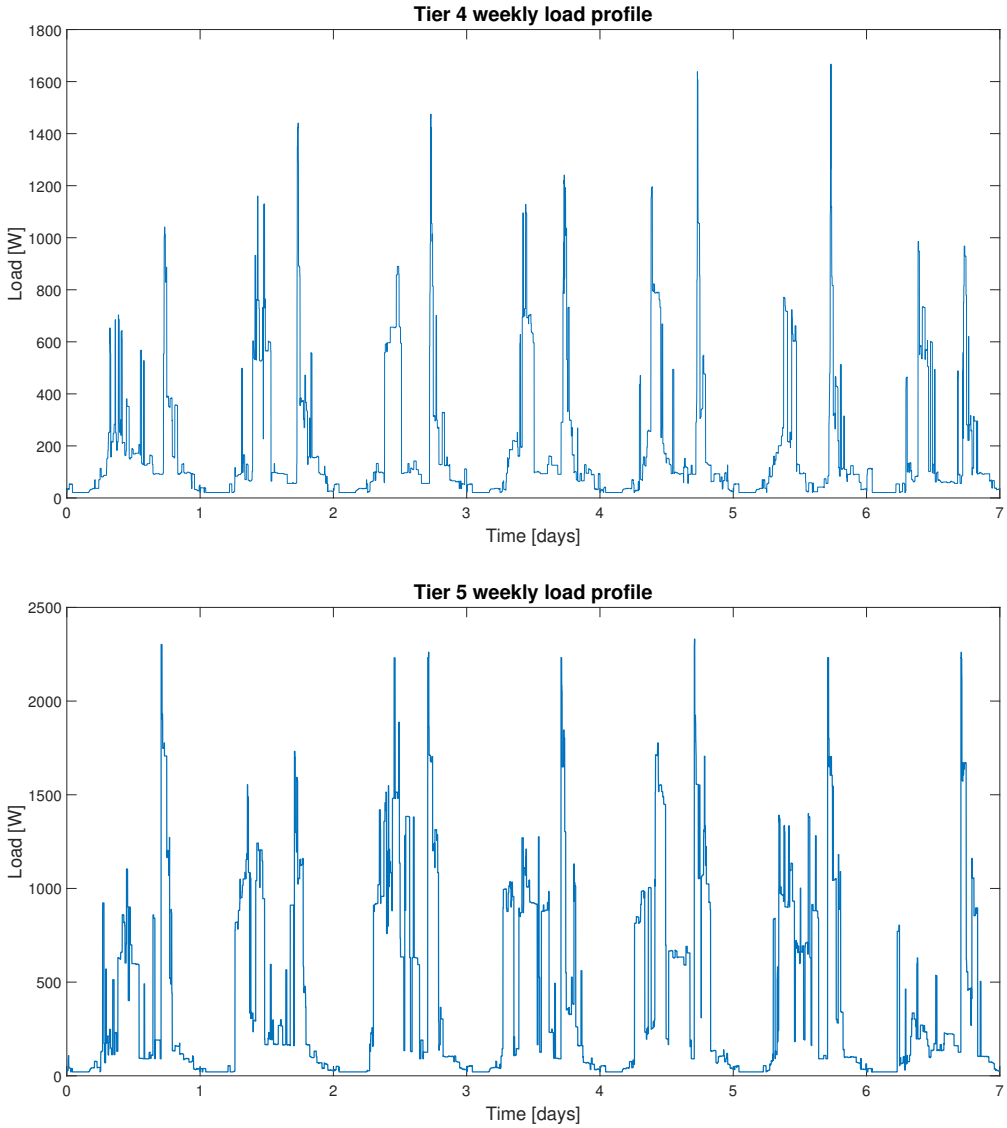

Figure 4.4: Typical weekly load profile for tiers 4 and 5 [59]

From the load profile data, the main characteristics of the load profile of each tier is summarized in table 4.1 below.

Table 4.1: Load profile summary for the different tiers

Tier	Peak power [W]	Yearly energy consumption [kWh]	Average daily load [Wh]
1	12	18.1	49.6
2	51	79.5	217.9
3	154	358.2	981.5
4	1670	1442.6	3952.5
5	3081	3478.8	9530.9

From table 4.1, it is shown that there is a large gap between the load profiles between tier 2 and 3, and an even larger gap between tiers 3, 4 and 5. This larger increase in electricity consumption can be linked to the ownership of high consumption appliances by the household such as refrigerators, washing machines, etc. as summarized in figure 4.2 before. This large increase in yearly energy load will reflect in the SHS size, which is also expected to have a similar rate of increase.

4.2. Modeling

In this section, the modeling methodology and optimization methods used will be explained, in sections 3.3 and 3.4.1, the component modeling was detailed, and the performance of a single system size was evaluated in section 3.5. However, the optimal size in regards of performance, cost, and battery lifetime requires an optimization process to be obtained as will be disclosed below.

4.2.1. Methodology

The optimization methodology consists of five steps starting from choosing a location, up until finding the optimal SHS size and are as follows:

Step 1: Choosing the Location

The first step in the optimization method is the choice of the location in which the SHS size needs to be optimized for the load profiles in each of the 5 tiers. The location choice is important as the meteorological data vary greatly from one geographical location to another. As a first step, to elaborate on the performance of the energy algorithm the same location used in section 3.3.1 with the meteorological data extracted from Meteonorm will be used.

Step 2: Obtain output of the solar module

Using the meteorological data as an input, the yearly net power output of a single 20 W_p solar module using the irradiance data and dynamic efficiency model. The capacity of the PV array for the system to be optimized will consist of a multitude of the 20 W_p modules, hence the total nominal capacity becomes $N_{module} \times 20 W_p$.

Step 3: Selection of capacity range for the PV array and batteries

In order to narrow down the possibilities during the optimization, a range of capacities for both the PV array and battery storage for the given load profile has to be selected. This has two advantages, first, it eliminates all the PV/battery combinations that are insignificant. For example, having a SHS combination of PV/Battery of 40 W_p / 100 Wh for the load profile in tier 5 is highly irrelevant, as the system will be unreliable (LLP > 0.6). Secondly, with the narrowing of the range of possibilities, the MATLAB optimization algorithm becomes less time consuming. The intuitive methods discussed in 2.3.1 are a great tool that can be used to obtain a rough and preliminary system size, from which the capacity range for each of the two components can be found. The equations used to find the rough minimum system size are repeated below for convenience.

$$\mathrm{P_{PV,min}} = \frac{\mathrm{E_{Load}}}{\eta_{\mathrm{PV}}.\eta_{\mathrm{con}}.\mathrm{ESH}}\mathrm{S_f} \tag{4.1}$$

$$\mathrm{C_{batt,min}} = \frac{\mathrm{E_{Load}}.\mathrm{NOA}}{\mathrm{V_{batt}}.\mathrm{DoD}.\eta_{\mathrm{batt}}} \tag{4.2}$$

The safety factor is taken to be unity for finding the minimum PV array size, and the NOA approach explained in section 3.5.4 is used to find the battery size, as it proved to provide a more accurate size than the DOA method. For each of the two components, the maximum capacity is taken to be 4 times the minimum calculated capacity, hence limiting the range of possible combinations.

Step 4: Finding the optimal size of the DC/DC converters

As mention in section 3.3.3, the optimal sizing of the converters depends greatly on the meteorological data, the PV module output, and the load profile, which affects its efficiency. Hence, the size of the converters needs to be obtained. In this case, as seen previously the converter sizes are:

- PV array converter: 72% the PV array capacity.
- Load converter: Peak load power.
- Battery converter: Peak energy deficit or excess

Step 5: Running the optimization algorithm

The fifth and final step is using the above mentioned data as inputs for the optimization algorithm to find the best PV/battery combination for each tier. The optimization algorithm aims to find the best combination in terms of reliability by minimizing LLP, affordability by minimizing cost, and battery lifetime which means a fewer number of replacements during the system lifetime. The two optimization strategies used in this study will be explained below, along with the results obtained for the default system case used previously. The 5 steps

of the optimization methodology are summarized in the figure below:

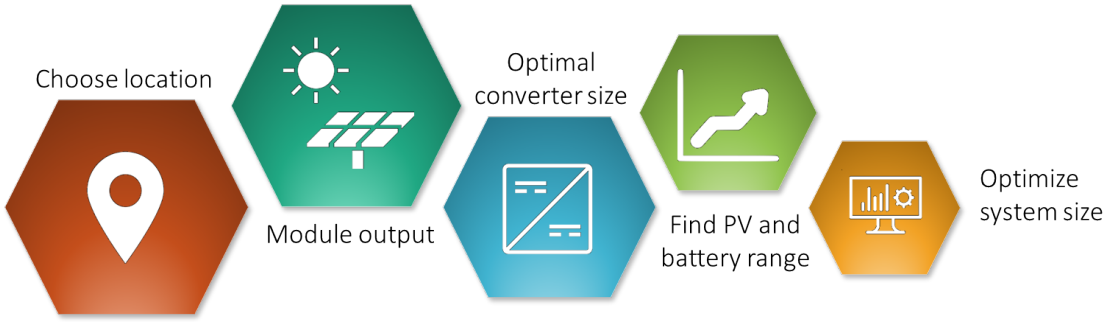

Figure 4.5: Modeling and optimization methodology

4.2.2. Iterative Optimization Method

The first optimization method employed in this study, is a classical iterative technique as discussed in section 2.3.2. The iterative technique consists of a nested for loop that runs the control strategy discussed in 3.4.1 over the whole range of both the battery size, and PV capacity. The increments in PV and battery capacity used are $20 W_p$ and 10 Wh respectively, in order to increase the accuracy of the solution, while abiding by the standard component sizes found in the markets and by manufacturers. The resulting output of this iterative approach is a set of matrices of dimensions $N \times C$ corresponding the range of PV capacity and battery size ranges respectively. The set of arrays will be the LLP, energy dump, system capital cost, and bundled parameter for each PV/Battery combination. The results are then plotted in order to select the optimal system size. The results for the system case used previously are shown below.

Iterative Method: Example study

The iterative method was first tested on the load profile and location mentioned in section 3.2, using equations 4.1 and 4.2, the minimum PV and battery capacity for the iteration range were obtained, and are as follows:

- P_{PV}: minimum value = 220 W; maximum value = 880 W at 20 W increments.
- C_B: minimum value = 670 Wh; maximum value = 2680 Wh at 20 Wh increments.

Then the cost of the different components was added as an input to the algorithm to compute the total system cost of every combination, the costs used are summarized in table 4.2 below. The iterative algorithm was run to obtain the LLP, battery lifetime and system upfront cost of each of the combinations and was plotted on MATLAB using contour lines as shown in the figures below.

Table 4.2: Normalized cost of solar home system components [29, 36, 65, 80]

Component	Normalized cost
PV array	1 $/Wp
Lead-acid battery	1.1 $/Wh
LiFePO4 battery	1.5 $/Wh
Charge controller	0.15 $/W

Figure 4.6 shows the LLP contour plot for the different PV and battery capacities, the LLP values from 0.01 to 0.05 are emphasized to put a threshold on the minimum reliability of the system, and to examine the change

in cost/capacity for each 1% decrease in LLP. The figure also shows the point with the minimum system cost for each LLP, along with the system size. The results are summarized in table 4.3.

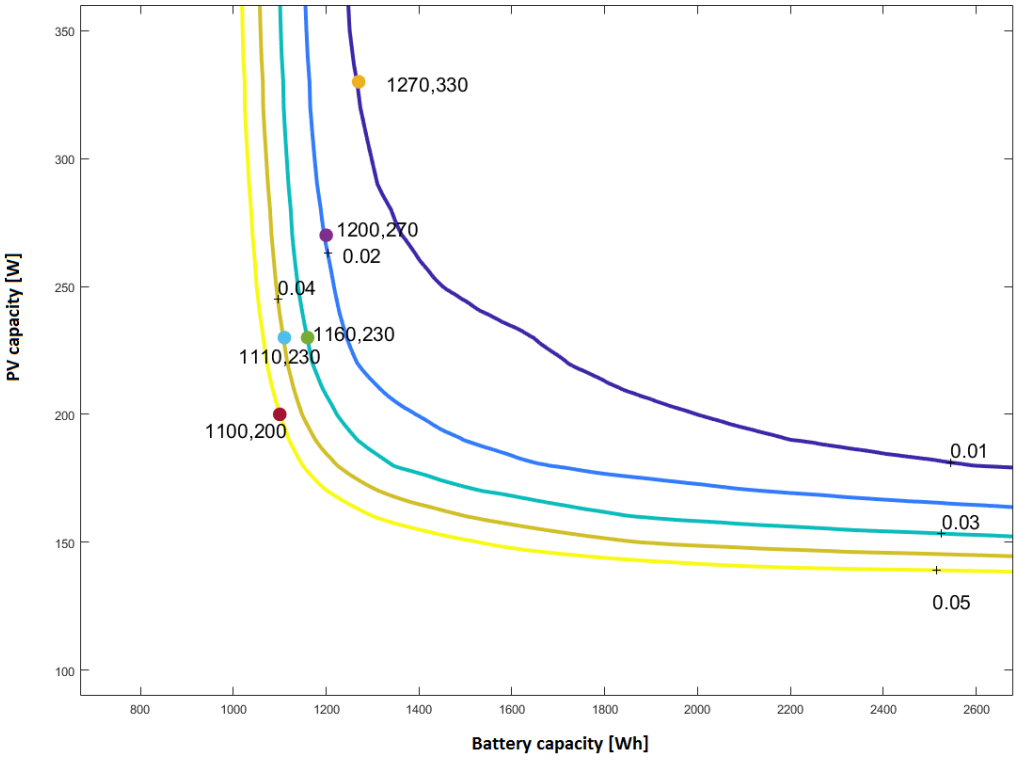

Figure 4.6: Iterative method example study: LLP for PV and battery combinations with optimal cost

In figure 4.7, the lead-acid battery lifetime is shown for increasing values of PV and battery capacities. It is clear that for increasing PV capacity, the battery lifetime decreases drastically which is due to the large increase in battery energy throughput. An increase in battery capacity however, increases its lifetime but not as severely. Hence, it can be concluded that for maximizing the lifetime, a low PV capacity and large battery should be selected, but it shouldn't be at the expense of the LLP, as shown in figure 4.8

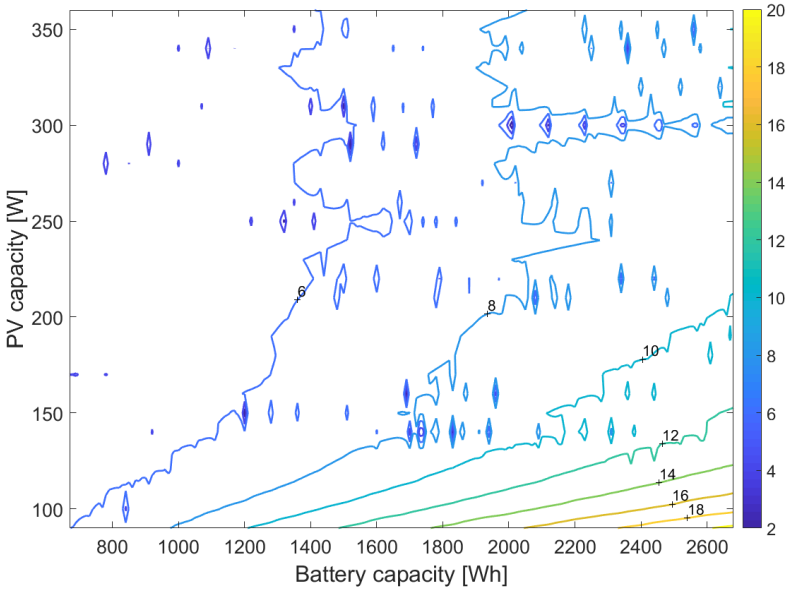

Figure 4.7: Iterative method example study: Battery lifetime for PV and lead-acid battery combinations

In the figure below, both the lifetime and LLP contours are plotted to illustrate the effect of system size on both parameters simultaneously. As mentioned before, a system with low PV and large battery seems like the ideal combination in terms of battery lifetime and cost, however, to maintain system reliability, the LLP should be 0.05 or lower. The colored scatter shows the minimum cost for each LLP as summarized table 4.3.

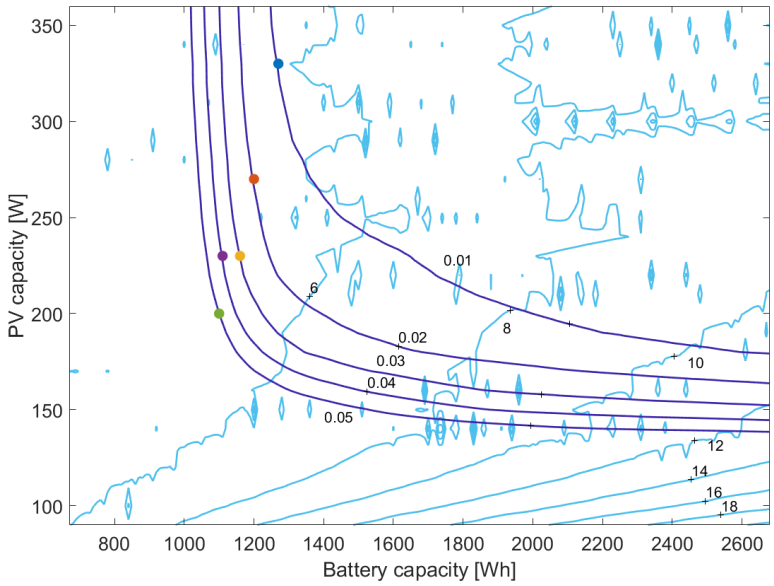

Figure 4.8: Example study iterative method: lead-acid battery Lifetime and LLP for PV and battery combinations

Table 4.3: Optimization values summary

LLP Values	PV Capacity [Wp]	Battery Capacity [Wh]	Cost]USD]	Lifetime [Years]
0,01	330	1270	5100	5.8
0,02	270	120	4764	5.5
0,03	230	1160	4553	5
0,04	230	1110	4405	4.6
0,05	200	1100	4272	4.8

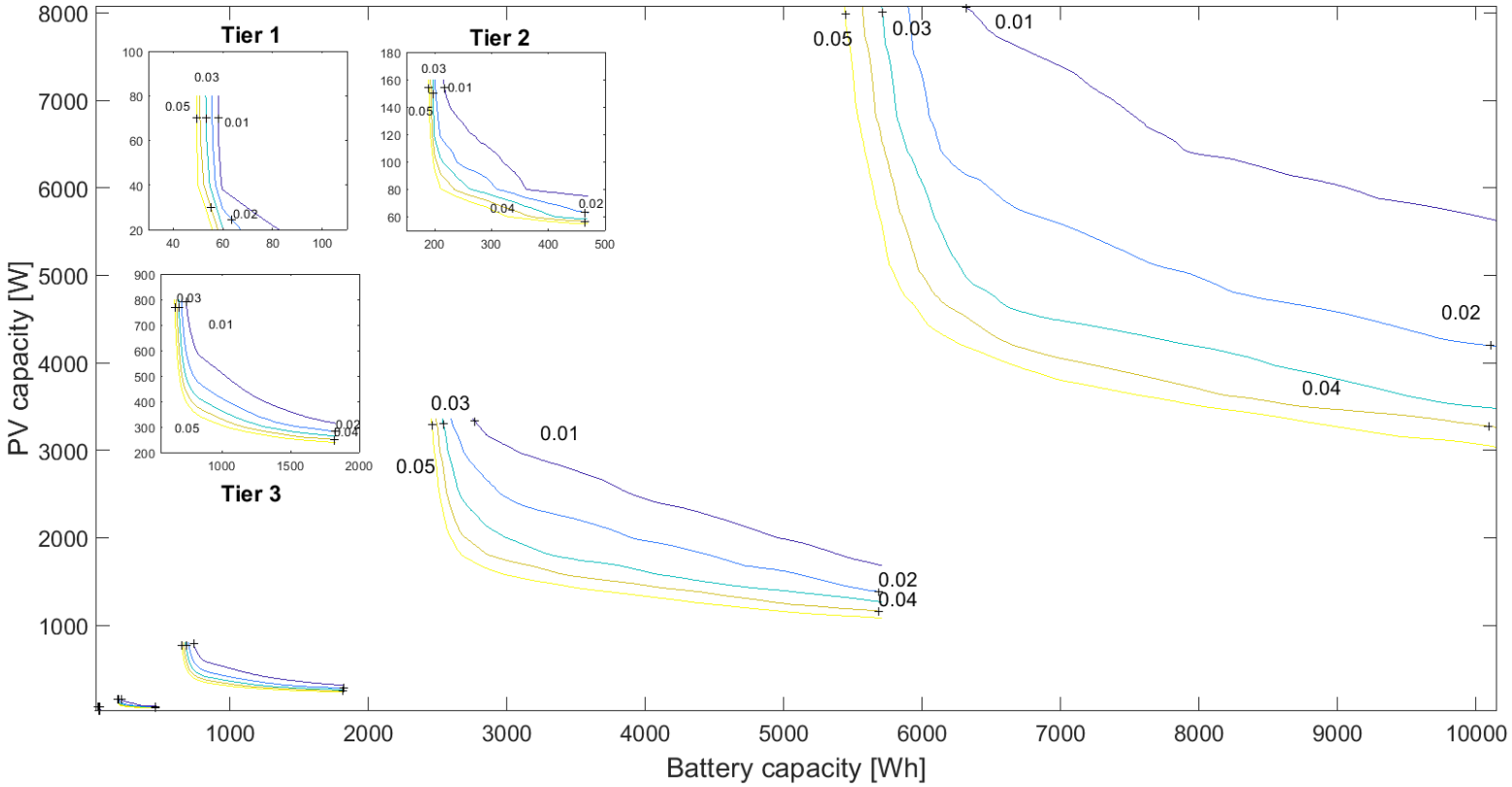

Figure 4.9: LLP for different tiers as a function of the PV and lead-acid battery combinations

As shown in the table and figure 4.9 above, with the iterative algorithm, an optimal system size can be found with respect to the cost. However, in this method, one of the parameters has to be fixed initially, and then optimize the other two parameters accordingly. In this case, the LLP value was fixed at first, with a value ranging from 0.01 to 0.05 as shown in table 4.3, then the optimal cost for each was obtained using the the cost function discussed in chapter 3. However, this method failed to provide optimal solutions taking all the parameters into consideration. Moreover, the computational time needed to run all the iterations proved to be excessively long. The Genetic Algorithm discussed in the following section was able to eliminate those restrictions, and was used to optimize the size for all tiers in the case studies.

4.2.3. Genetic Algorithm

Genetic Algorithm method: Example study

The GA was first run on the same example study as the iterative method, the algorithm was initialized with a population size of 50 particles, over 500 generations. The system objective functions and constraints are as follows:

- **Decision variables:**
  - PV array capacity in Wp: $W_{p,PV}$
  - Battery capacity in Wh: C_B
  - Converter rated capacity in W: $S_{C,Battery}; S_{C,PV}; S_{C,Load};$
- **Objective functions:**
  - *Minimize cost:* $\mathrm{W_{p,PV}} \times \mathrm{Q_{PV}} + \mathrm{C_B} \times \mathrm{Q_B} + (\mathrm{S_{C,Battery}} + \mathrm{S_{C,PV}} + \mathrm{S_{C,Load}}) \times \mathrm{Q_C}$
  - *Minimize LLP: LLP* $= \frac{t_{downtime}}{T_{total}}$
  - *Maximize Battery lifetime:* From battery lifetime polynomial.
- **Constraints:**
  - LLP $\leq 10\%$
  - $E_{Dump} \leq 2 \times$Yearly load

As mentioned in section 3.3.3, the charge controller chosen rated capacity is optimized at first using an iterative method, hence, it is a fraction of the PV array capacity, this allows the cost objective function to be reduced to: $W_{p,PV}.(Q_{PV} + f \times Q_C) + C_B \times Q_B + Q_C.(S_{C,Battery} + S_{C,Load})$, where $f = \frac{1}{R_s}$. After running the GA, a scatter plot of the obtained data points that represent the pareto front between pair of the three objective functions is plotted to illustrate the optimal points as shown below. Figure 4.10 shows the pareto front between the LLP and cost objective functions. Naturally, for a system with a lower LLP, a higher upfront cost is needed. The PV/battery combinations for each of the scatter points is also represented in the figure.

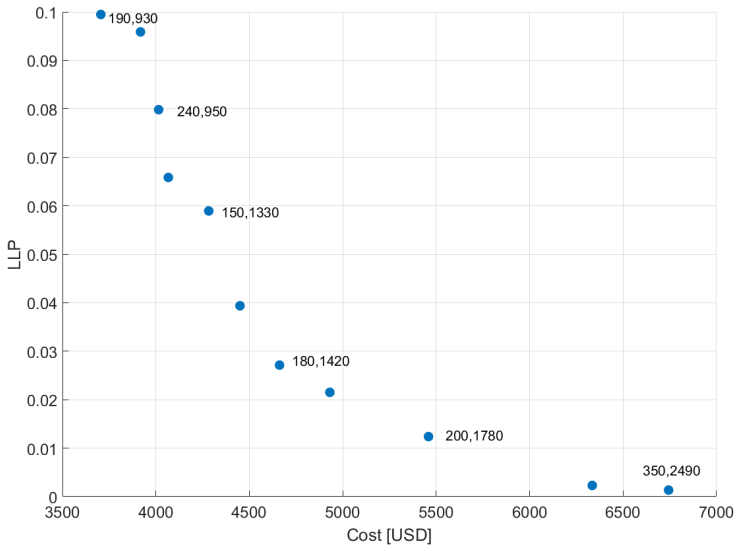

Figure 4.10: Test Case: Pareto front of LLP VS Cost with the PV/Battery combinations

In figure 4.13, the lead-acid battery lifetime VS LLP is shown. Unlike the LLP vs cost pareto front, in this plot, no clear pattern can be obtained. A high lifetime can be obtained even at low LLP values ($\leq 5\%$) and vice versa.

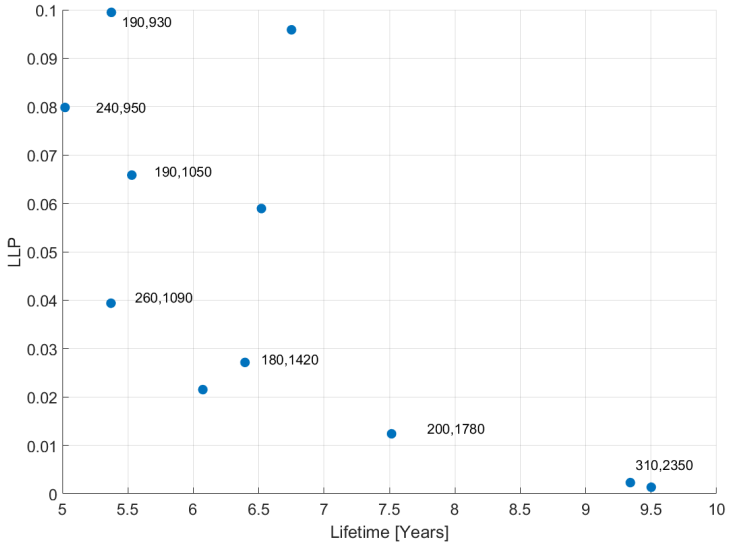

Figure 4.11: Test Case: Pareto front of lifetime VS LLP with the PV/Battery combinations

The lifetime VS cost pareto front in figure 4.12 doesn't show a clear pattern between the two objectives either.

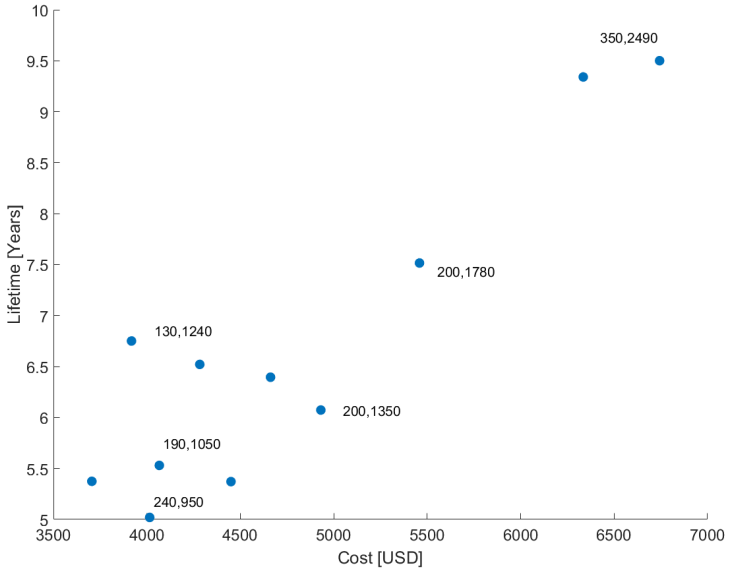

Figure 4.12: Test Case: Pareto front of lifetime VS Cost with the PV/Battery combinations

To get a better representation of all three objective functions, a contour plot using the scatter data was made where the LLP values were plotted as elevations for different lifetime and cost combinations. The data along with the SHS component sizes is summarized in table **??** in appendix **??**.

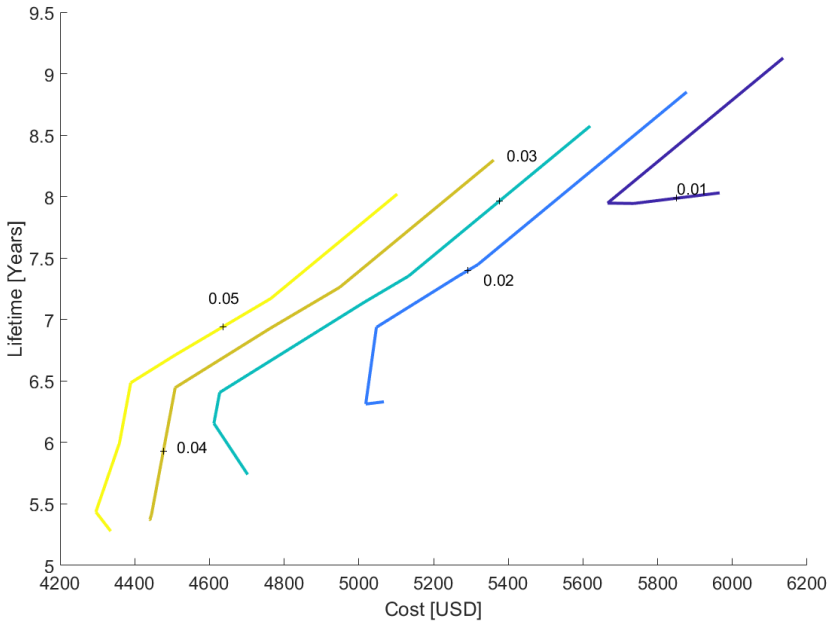

Figure 4.13: Test Case: Contour plot showing the different LLP levels at various lifetime and cost combinations

4.3. Case Studies

In this section, the optimization algorithms explained and tested will be implemented on case studies in three different locations. The optimal SHS sizing will be performed for each location over the load profiles of the five tiers discussed in section 4.1. The locations selected are in rural regions of developing countries where the electrification rates are some of the lowest worldwide. Moreover, these locations, as most rural un-electrified regions, have an abundance in solar irradiance making the implementation of SHS an even more attractive solution.

The first two locations of the case studies are the district of Pune and East Khasi Hills in India, where the overall electrification status of the country was 67% in 2011. Even after the launch of the Rajiv Gandhi Grameen Vidyutikaran Yojana (RGGVY) program in 2005, which is the scheme initiated by the government to supply continuous power to rural India, 17% of the households today still lack supply to electricity, and even more to continuous and reliable power supply [41, 62, 87]. According to the Times of India [62], the amount of un-electrified households is so high although it is claimed that India has already reached 100% electrification, is due to the simple definition of village electrification by the government. As of 2004, a village is considered electrified if the following occurs:

1. The public places in a village such as schools and hospitals have electricity access.
2. At least 10% of households have electricity.

With that definition, a village is considered electrified by the government even if up to 90% of households still lack access to reliable electricity. Table 4.4 below shows the states with more than 20% household un-electrification in India.

Table 4.4: States with over 20% un-electrified households in India, *Adapted from [62]*

State	Rate of un-electrified households [%]
Jharkhand	48
Uttar Pradesh	56
Assam	57
Odisha	64
Arunachal	66
Meghalaya	70
Tripura	72
Nagaland	74
Bihar	74
Manipur	77
Rajasthan	79
Jammu and Kashmir	79

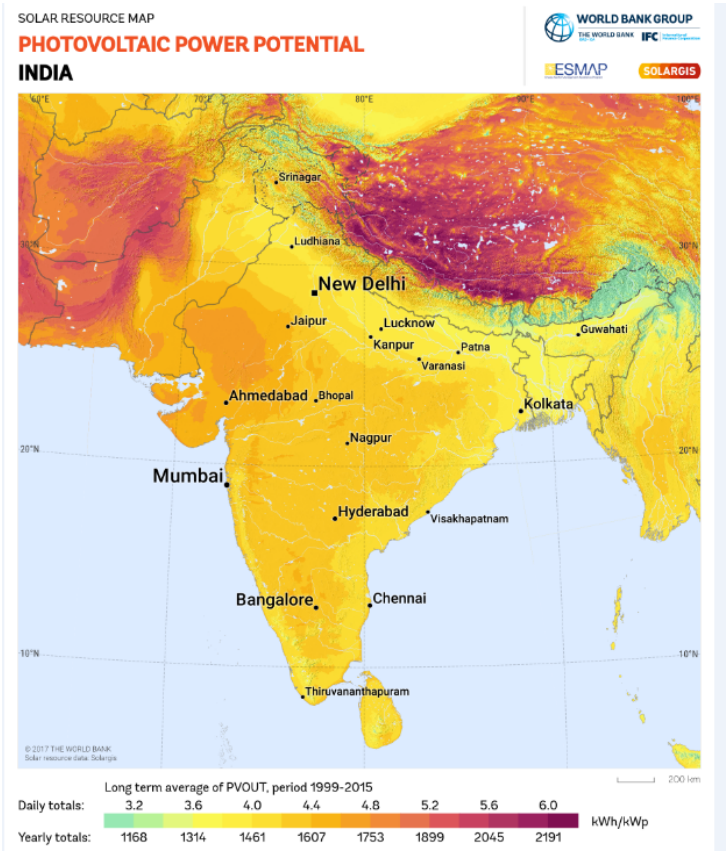

Figure 4.14: Photovoltaic solar potential in India in kWh/kW_p [84]

The third location is chosen to be the city of N'Djamena in the country of Chad, which is one of the countries with the least electrification rate worldwide, going from 0% in 1990 to 8.8% in 2016. The region, having on of the highest solar potentials worldwide makes the use of Solar Home Systems highly beneficial.

4.3.1. East Khasi Hills - Meghalaya

The first location for the case studies are the East Khasi hills, in the state of Meghalaya in India. The state is located in the north-east of India, and as shown in table 4.4 has 70% of its households still un-electrified. The figure below shows the electrical potential of Meghalaya as taken from the Solar Atlas map [84].

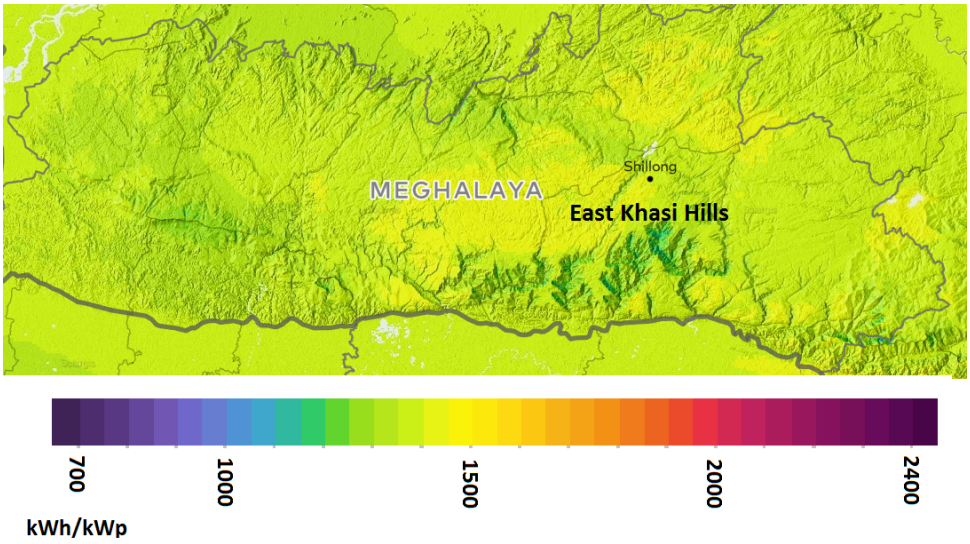

Figure 4.15: Photovoltaic solar potential in the district of the East Khasi Hills in kWh/kW_p [84]

The East Khasi hills was selected as a location due to the large amount of rural villages, and due to its presence near Shillong, a strong and well established city where a weather station is located. Due to the high similarity in meteorological data and solar insolation as shown in figure 4.15, the meteorological data of Shillong was extracted using Meteonorm, and was assumed to be the same for the whole district.

Solar module output

The solar module output for the East Khasi Hills was obtained using Meteonorm from the weather station in Shillong. At first, the optimal module orientation and tilt was found using the iterative method described in section 3.3.1, then the module output at this optimal point was calculated for the whole year. This output will be used to find the optimal size of the charge controller and SHS for each of the five tiers and is shown in figure 4.17. The optimal tilt angle and orientation found are 24 and 180 respectively as shown in figure 4.16

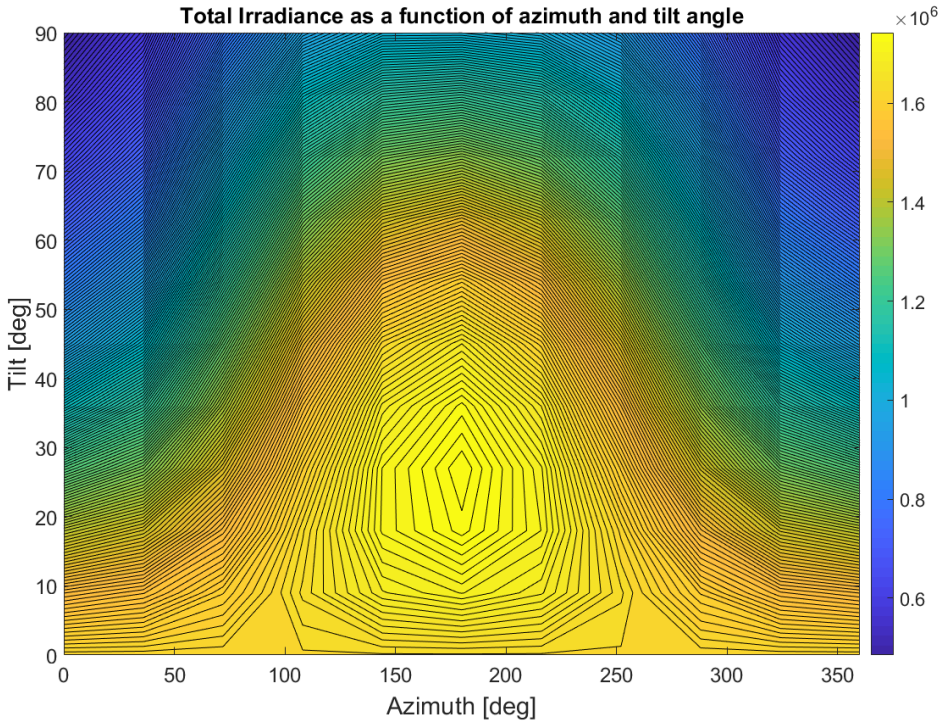

Figure 4.16: Optimal module orientation and tilt in East Khasi Hills: Azimuth: 180, Tilt: 24

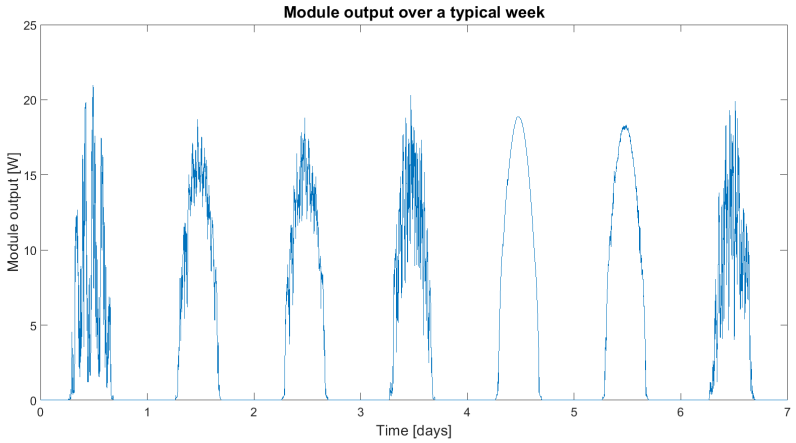

Figure 4.17: Module output in East Khasi Hills over a typical week

Optimal size of converters

From the module output and meteorological data, the optimal sizing ratio R_S for the PV converter was obtained as shown in 4.18. The maximum yield is obtained at $R_S = 1.14$, while 95% of that normalized maximum is obtained at $R_S = 1.43$.

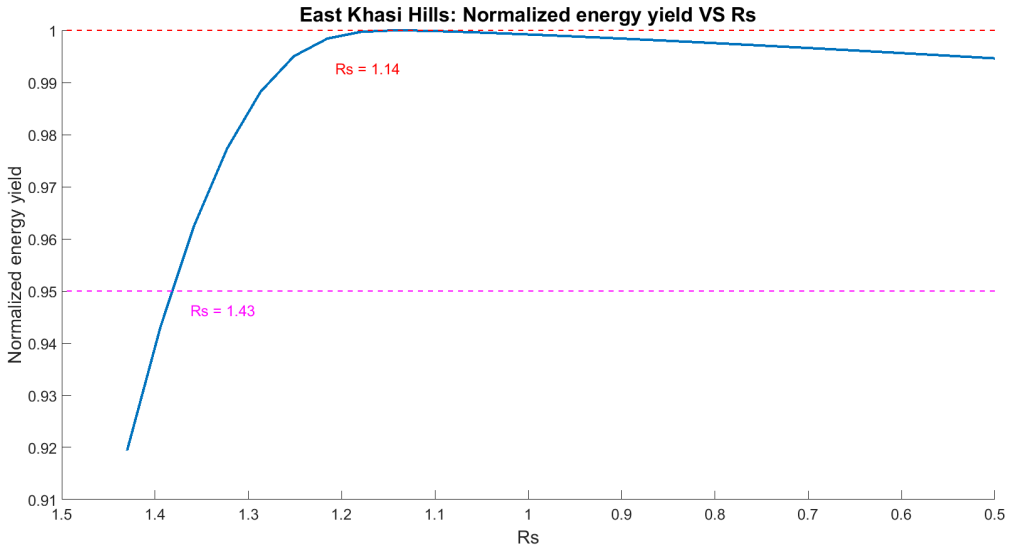

Figure 4.18: East Khasi Hills: Normalized energy yield VS Rs

As the rated size of the load converter depends on the maximum load during the tier, the size can be taken from the load data characteristics table 4.1 and is shown below.

Table 4.5: Converter P_{Nom} for different load tiers

Tier	**Load converter P_{Nom} [W]**
1	12
2	51
3	155
4	1670
5	3081

Capacity range of PV and battery

With the meteorological data, charge controller size, and PV module net output, the capacity range for the PV array and battery storage for each of the tiers can be found using equations 4.1 and 4.2 and are summarized

in table 4.6 below. For tiers 1 & 2, the maximum W_p was taken to be 10W instead of 20 since the loads are significantly smaller than in the last tiers, hence the smaller W_p increment increases the system size accuracy.

Table 4.6: East Khasi hills: Minimum and maximum PV and battery capacity range

	PV capacity [W]		**Battery capacity [Wp]**	
Tier	**Min**	**Max**	**Min**	**Max**
1	10	40	30	120
2	40	160	120	480
3	170	680	460	1840
4	690	2760	1430	5720
5	1650	6600	2550	10200

Running the optimization

Results: Tier 1

The figures below display the pareto fronts obtained after running the GA optimization algorithm for tier 1. Each figure shows the pareto front of two of the three objectives. Each scatter point in the pareto front represents a PV/battery combination as labeled in the figure. The component sizes are of the form Wp,Wh.

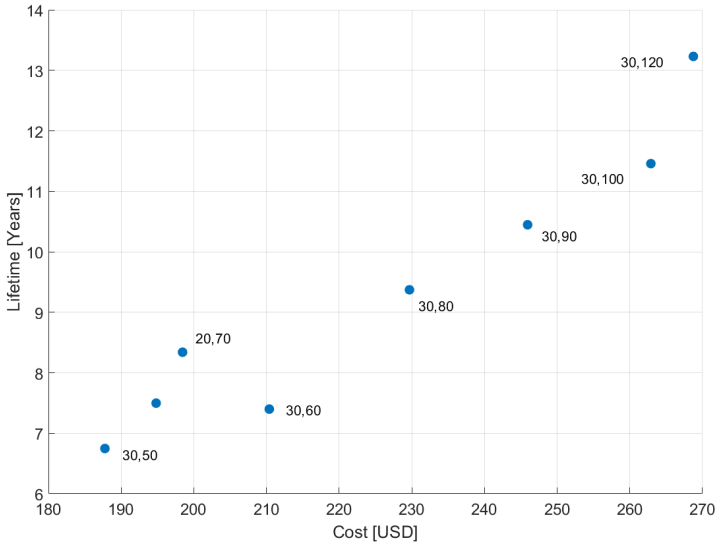

Figure 4.19: East Khasi Hills: Lifetime VS Cost (T1, GA, Lead-acid)

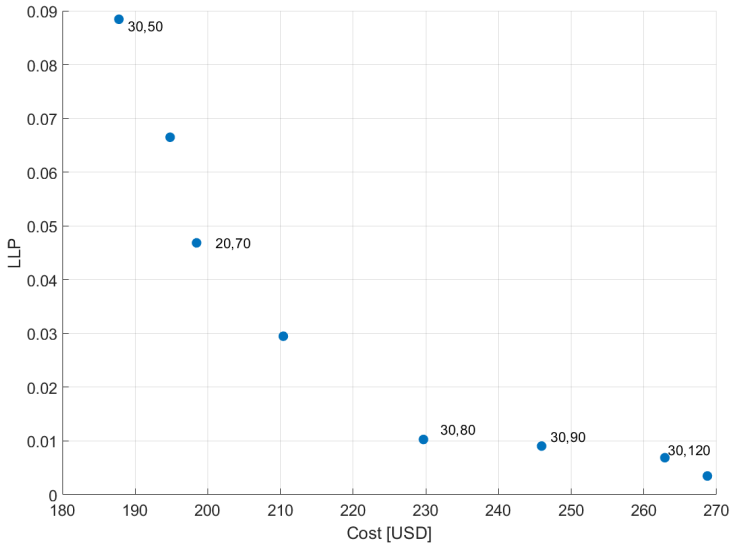

Figure 4.20: East Khasi Hills: LLP VS Cost (T1, GA, Lead-acid)

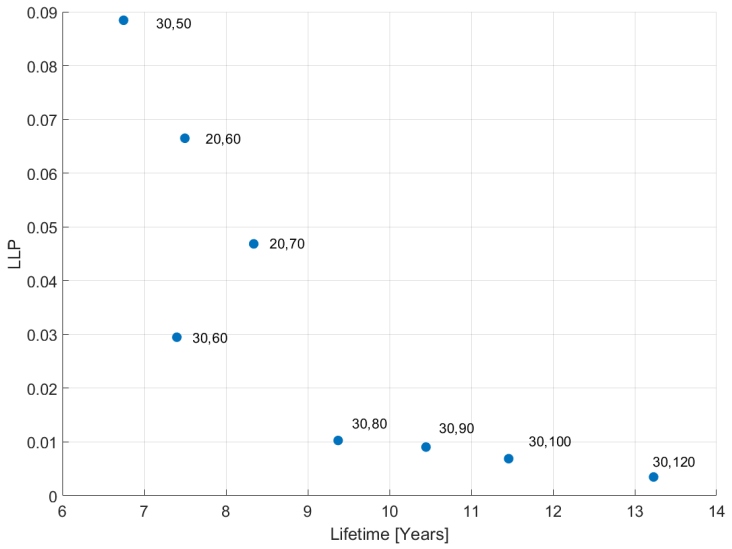

Figure 4.21: East Khasi Hills: LLP VS Lifetime (T1, GA, Lead-acid)

From the figures, a trend can be noticed in all the pareto fronts. The major contributor to the increase in cost, lifetime and decrease in LLP is the battery size. The PV capacities for all points are either 20 or 30 W_p, while the battery capacity ranges from 50 to 120 Wh. Moreover, the increase in price to go from 3.5% to almost 0% LLP is very low (around 20%).

Results: Tier 2

Tier 2 shows similar trends in the pareto fronts for the pairs of objectives that were obtained in tier one. The PV array capacity ranges from 80 to 150 W_p, while the battery capacity ranges from 200 to 480 Wh. The LLP VS Cost scatter shows an almost linear relation between the two objectives until LLP = 0.02 where the curve flattens to a plateau.

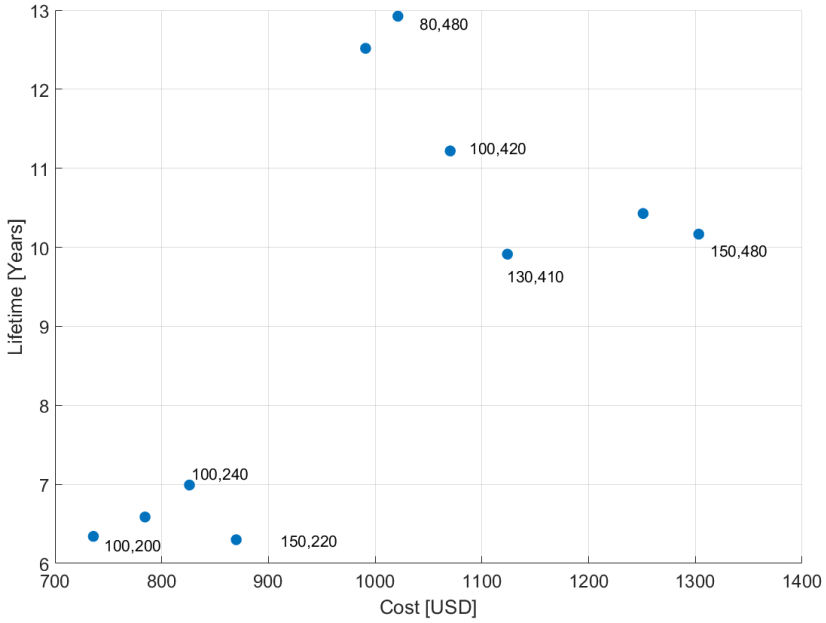

Figure 4.22: East Khasi Hills: Lifetime VS Cost (T2, GA, Lead-acid)

Figure 4.22 above shows that there is a broad range of LLPs that can be obtained for almost the same lifetime ≈ 6 years. To obtain higher battery lifetime, the PV array needs to tend towards the lower limits while the battery needs to be high. So a low PV, high battery combination is needed. However, this reflects greatly on the system cost as the battery is the most expensive component.

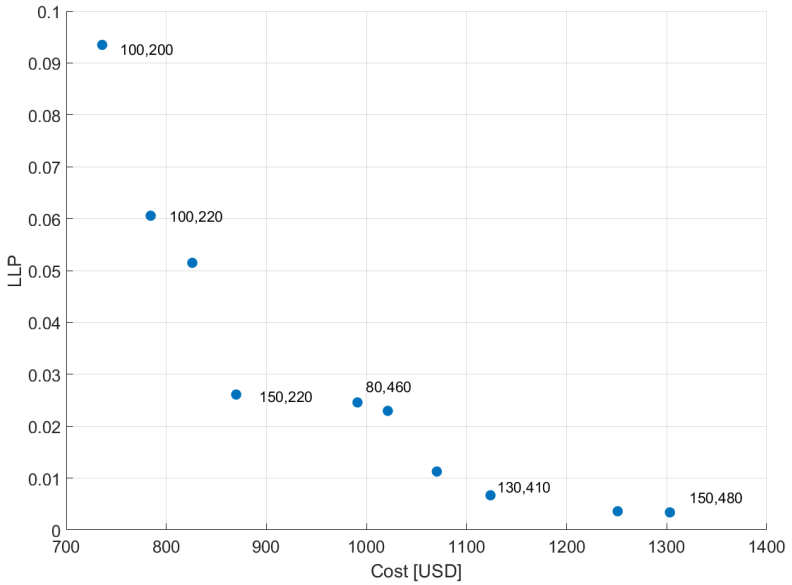

Figure 4.23: East Khasi Hills: LLP VS Cost (T2, GA, Lead-acid)

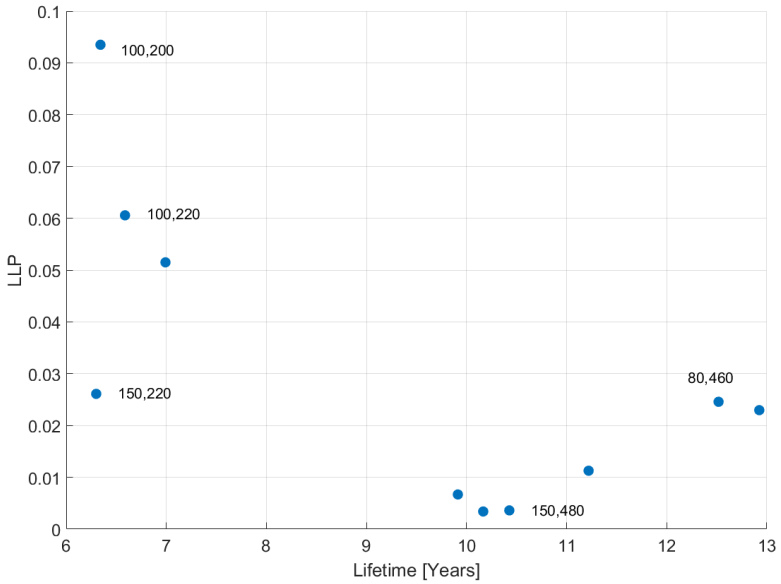

Figure 4.24: East Khasi Hills: LLP VS Lifetime (T2, GA, Lead-acid)

Results: Tier 3

Tier 3 shows the same behavior as the previous two years, where the battery capacity ranges from 400 to 1780, while the PV ranges from 360 to 680. It is worth noting that in these higher tiers, the broader capacity range initialized previously allows for more 20Wp/10Wh combinations, hence the pareto fronts plotted have more individuals than in the previous tiers.

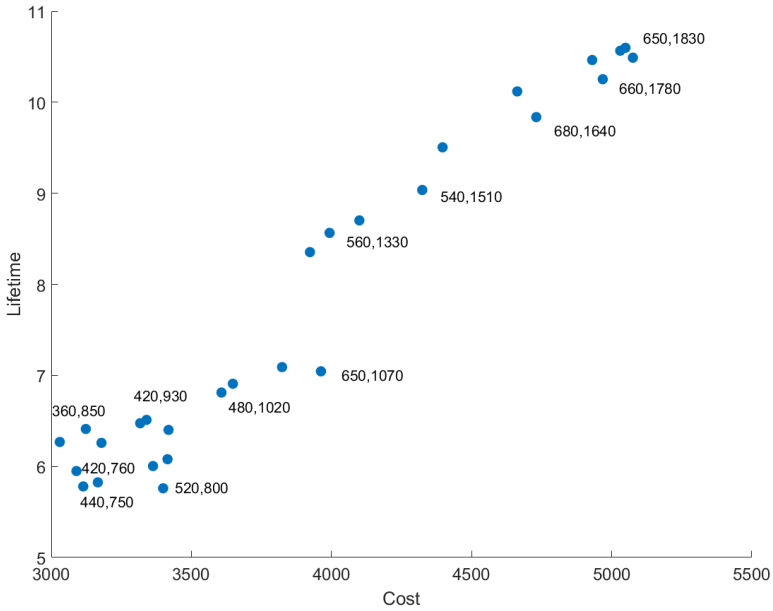

Figure 4.25: East Khasi Hills: Lifetime VS Cost (T3, GA, Lead-acid)

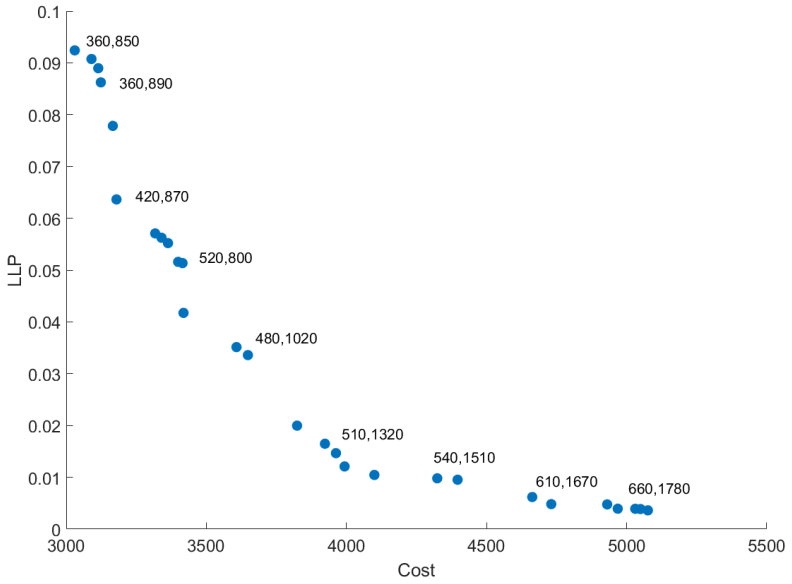

Figure 4.26: East Khasi Hills: LLP VS Cost (T3, GA, Lead-acid)

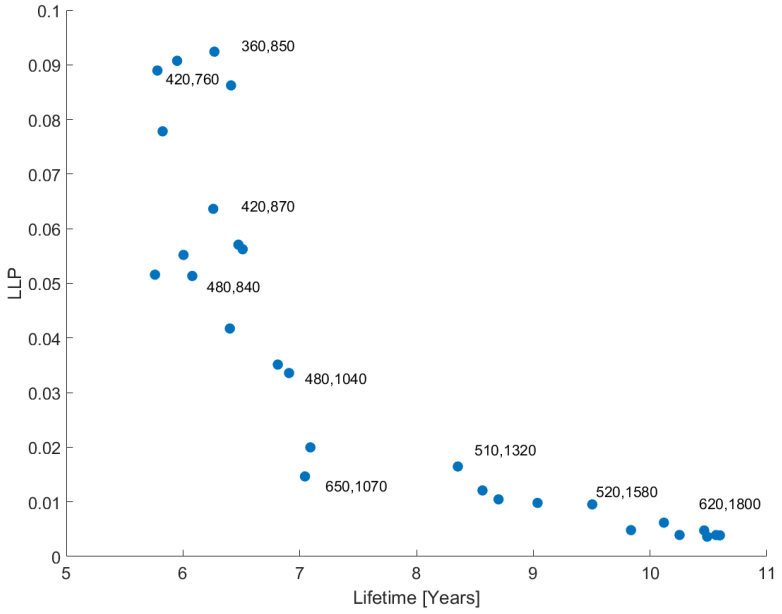

Figure 4.27: East Khasi Hills: LLP VS Lifetime (T3, GA, Lead-acid)

The pareto plots with the cost curves also show a steep increase in the system cost in this tier compared to tiers 1 & 2. While tier 1 had a system cost of 245$ for an LLP of 0.009 and a battery lifetime of 10 years, tier 3 has a system cost of 5000$ for an LLP or 0.009 and a battery lifetime of 9 years. This steep increase in cost trend becomes even more drastic in the remaining two tiers.

Results: Tier 4

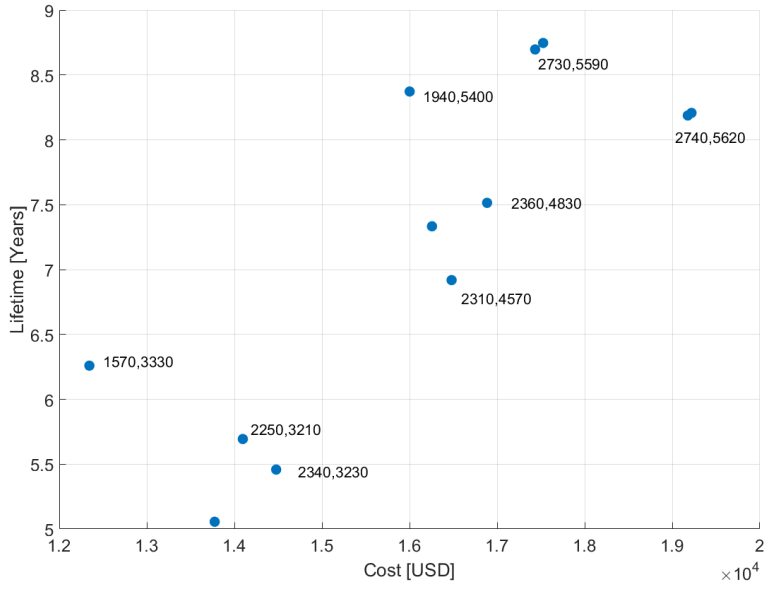

Figure 4.28: East Khasi Hills: Lifetime VS Cost (T4, GA, Lead-acid)

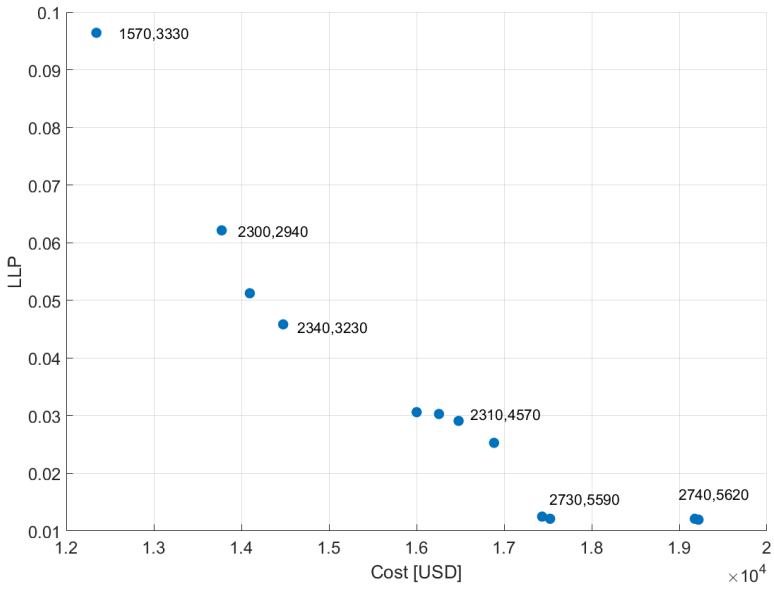

Figure 4.29: East Khasi Hills: LLP VS Cost (T4, GA, Lead-acid)

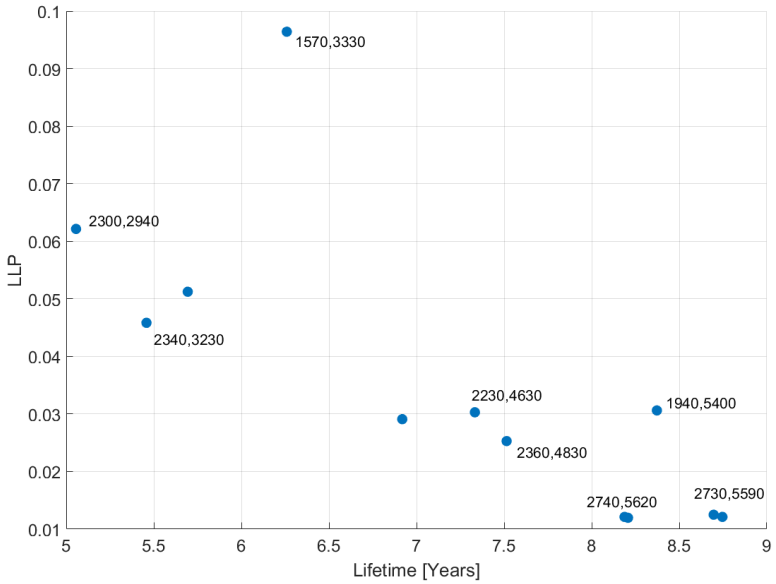

Figure 4.30: East Khasi Hills: LLP VS Lifetime (T4, GA, Lead-acid)

Results: Tier 5

In the last tier, the SHS cost increases drastically, the upfront cost ranges from 28000 to 40000 $ for a maximum battery life values of 7 years. The LLP VS Cost curve in figure 4.32 also shows an almost linear relation between the two objectives. Hence to decrease the LLP from 0.08 to 0.03, the cost increases by 20%.

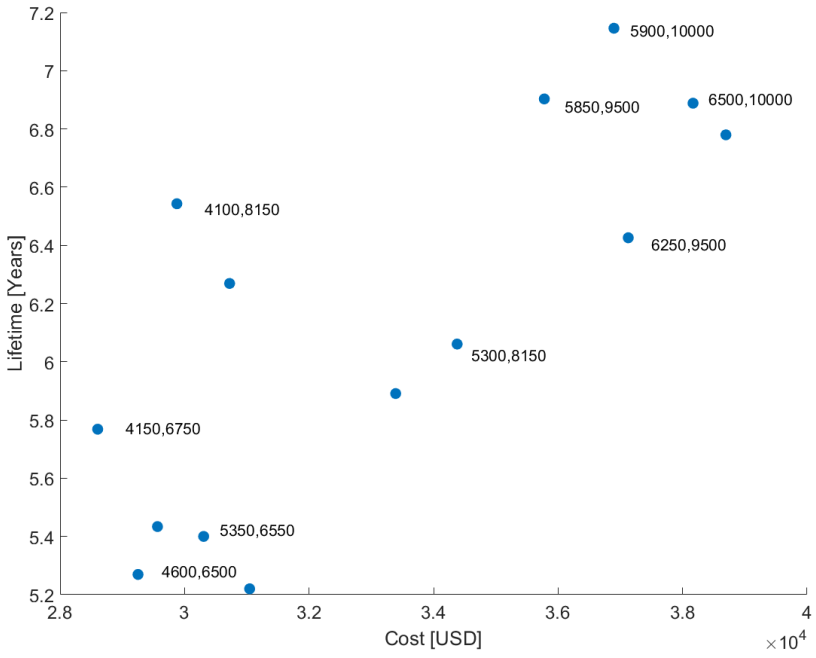

Figure 4.31: East Khasi Hills: Lifetime VS Cost (T4, GA, Lead-acid)

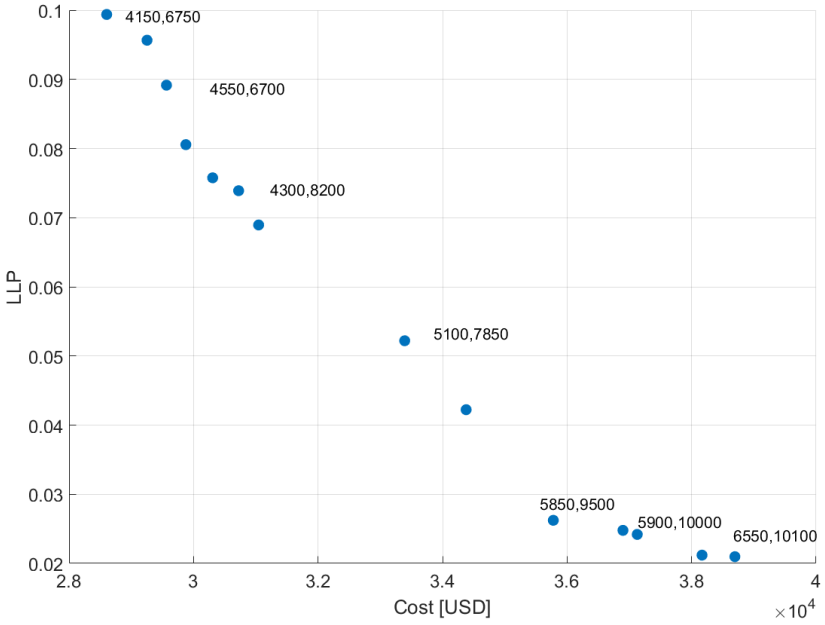

Figure 4.32: East Khasi Hills: LLP VS Cost (T4, GA, Lead-acid)

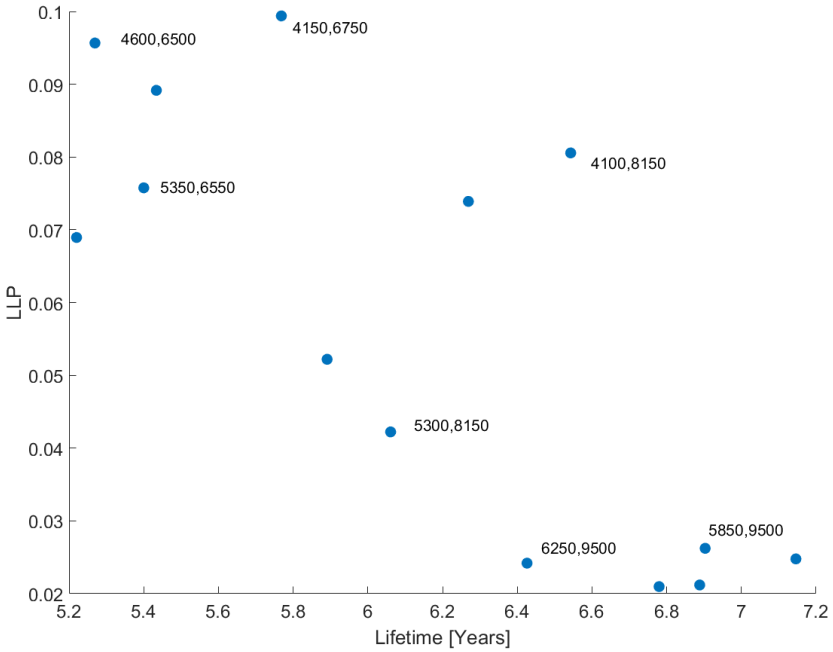

Figure 4.33: East Khasi Hills: LLP VS Lifetime (T4, GA, Lead-acid)

General results

In order to find the optimal system size for each tier, the LLP VS cost curve was examined. For most tiers, the curve has a steep slope for the lower cost values, and tends to flatten out at the end. Hence, the slope $\frac{\delta \text{LLP}}{\delta \text{Cost}}$ at each point of this curve was calculated and plotted as shown in the figure below.

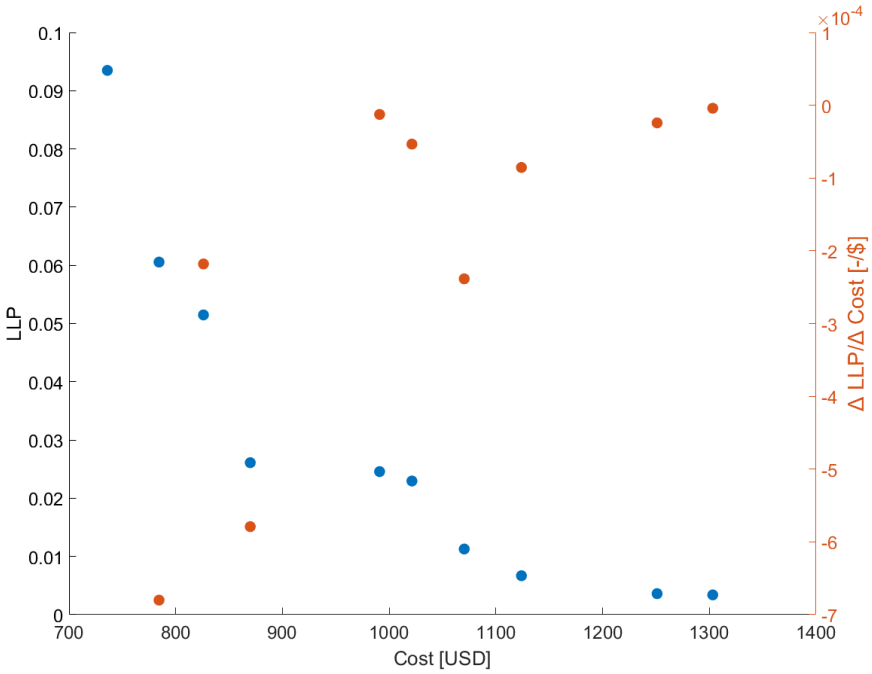

Figure 4.34: East Khasi Hills: LLP VS Cost with slope (T2, GA, Lead-acid)

In figure 4.34 showing the LLP VS cost for tier 2, the orange scatter points representing the slope seem to flatten out as the LLP reaches 0.02. Hence, at this point, the LLP becomes much less sensitive as the cost and system size increases. At each tier, the point where the slope flattens out, or where the LLP becomes less sensitive to the size increase, was considered as the chosen optimal point. The system size and objective function values were extracted from the GA matrix for these points for each tier and are shown in the table below.

Table 4.7: East Khasi Hills: Optimal SHS size per tier summary

Tier	PV [W_p]	Battery [Wh]	PV conv. [W]	Load conv. [W]	Battery conv. [W]	Cost [USD]	LLP [-]	Lifetime [Years]
1	30	80	26	12	25	230	0,010	9,4
2	80	460	69	51	67	991	0,025	12,5
3	580	1060	498	154	467	3824	0,020	7,1
4	1940	5400	1666	1670	1701	16001	0,031	8,4
5	5100	7850	4381	3081	4255	33392	0,052	5,9

4.3.2. District of Pune

The district of Pune in the state of Maharashtra has been chosen as the second location due to the fact that it has a large diversity in populations, some areas having access to reliable electricity, while some others have very low quality or no power supply. Moreover, The availability of the weather station in Pune allowed the retrieval of highly accurate yearly minute based data from Meteonorm, which increases the validity of the sizing done in the model. Figure 4.35 shows the solar abundance in the area, making it a great location for the use of SHSs.

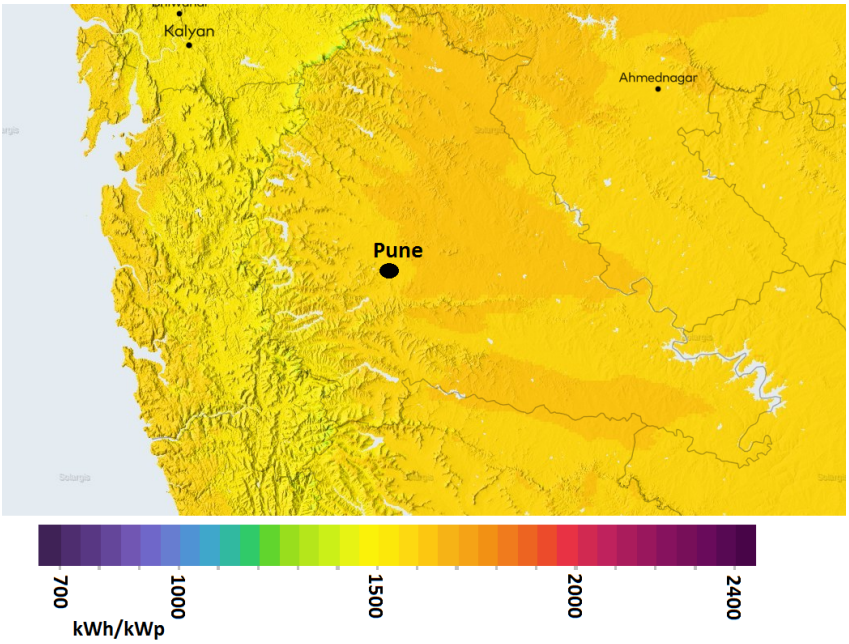

Figure 4.35: Photovoltaic solar potential in the district of Pune in kWh/kW_p [84]

Solar module output

The meteorological data used in the district of Pune is the same as was used in chapter 3 with the test case load profile. Hence, the net solar module output is also the same as the one in figure 3.9, it is shown again in the figure below for convenience.

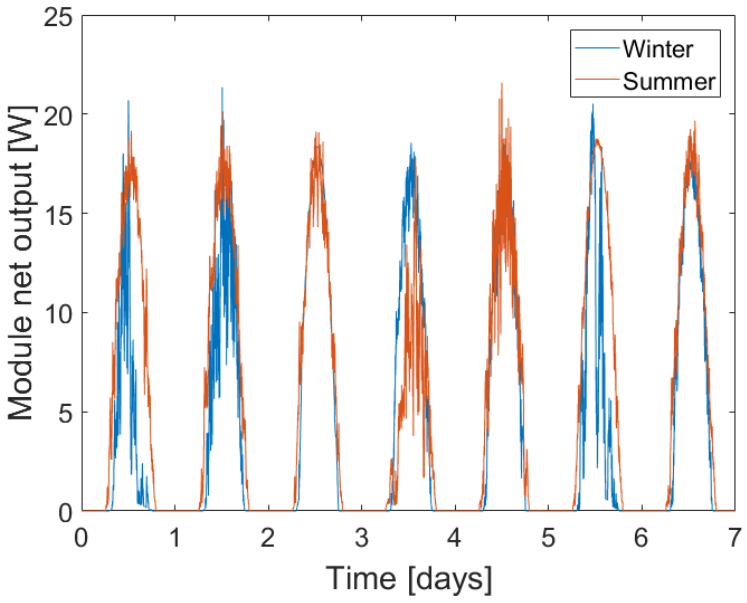

Figure 4.36: Module net output over a week in the summer and winter

Optimal size of converters

The PV converter optimal size is also dependent on both the meteorological data and solar module output, since those are the same as in the test case used in section 3.3.3, the optimal size is also chosen to be 72% of the PV array W_p size, or in other words $R_S = \frac{1}{0.72} = 1.39$. As for the load converter, table 4.5 shown in the East Khasi Hills case study shows the sizes for all the tiers.

Capacity range for PV array and batteries

Following the optimal sizing of the charge controller, the optimization range for the two other components: PV array and battery storage was performed as was done for the East Khasi Hills. The capacity range is shown in table 4.8 below.

Table 4.8: District of Pune: Minimum and maximum range of PV and battery capacities

	PV Array [W]		Battery Storage [Wh]	
Tier	**Min**	**Max**	**Min**	**Max**
1	10	40	30	120
2	30	120	110	440
3	140	560	450	1800
4	580	2320	920	3680
5	1400	5600	1500	6000

Running the optimization

Results: Tier 1

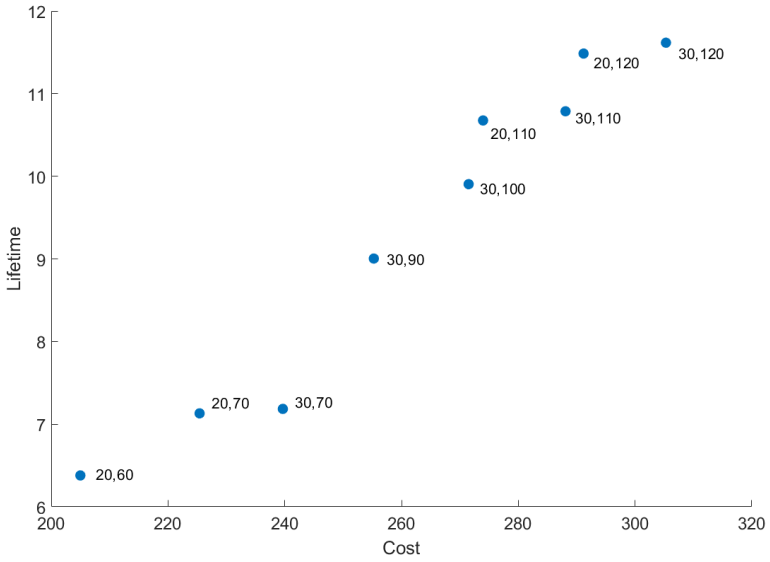

Figure 4.37: District of Pune: Lifetime VS Cost (T1, GA, Lead-acid)

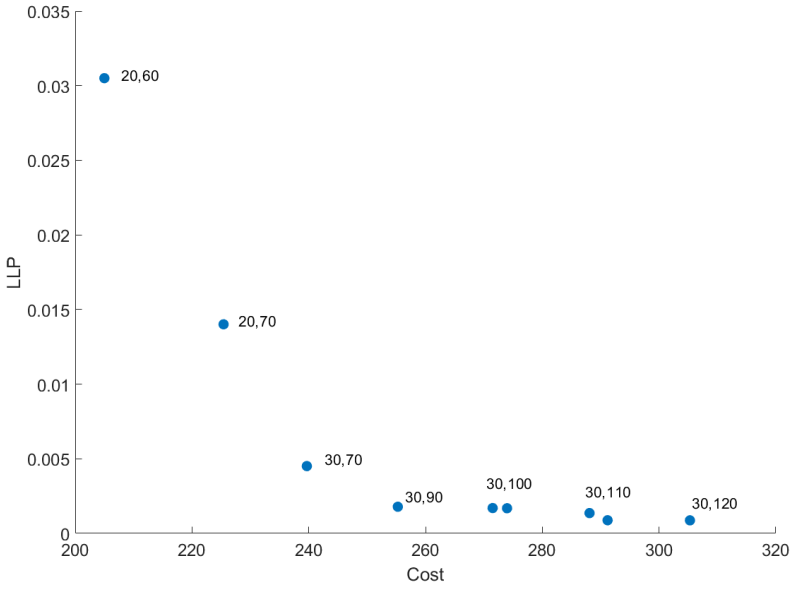

Figure 4.38: District of Pune: LLP VS Cost (T1, GA, Lead-acid)

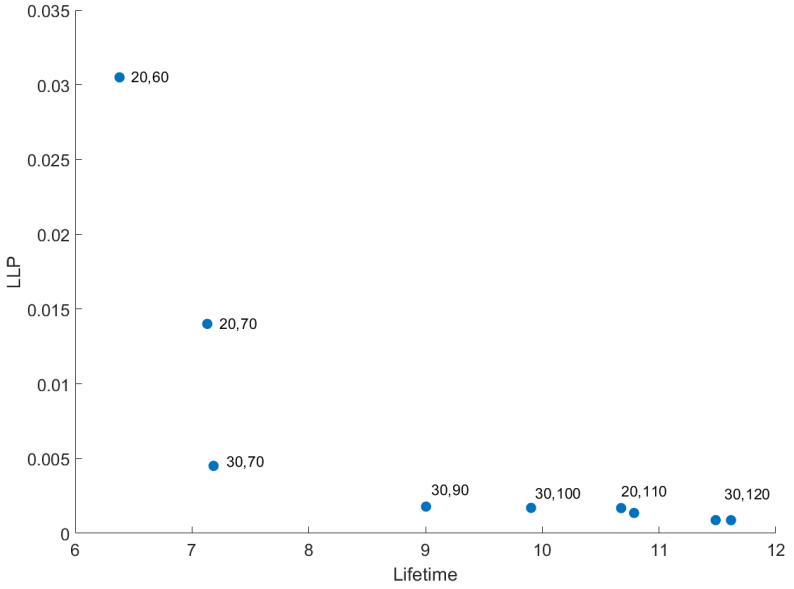

Figure 4.39: District of Pune: LLP VS Lifetime (T1, GA, Lead-acid)

Results: Tier 2

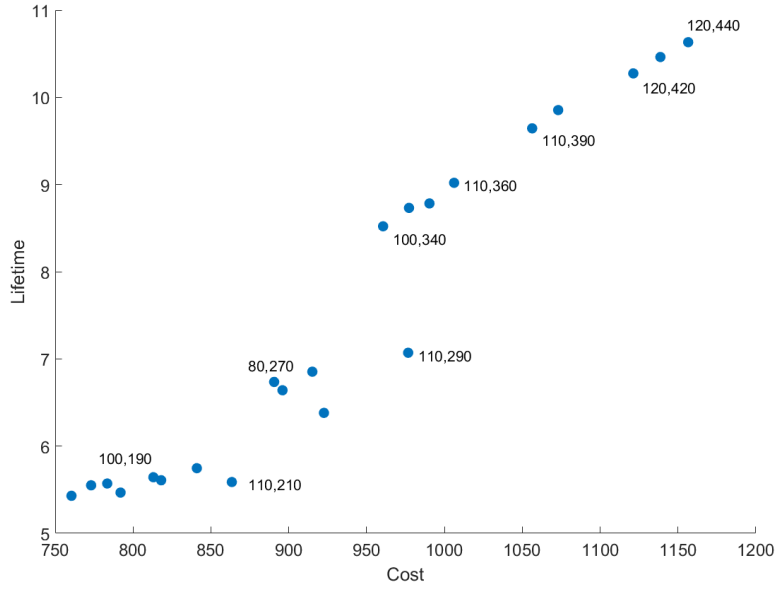

Figure 4.40: District of Pune: Lifetime VS Cost (T2, GA, Lead-acid)

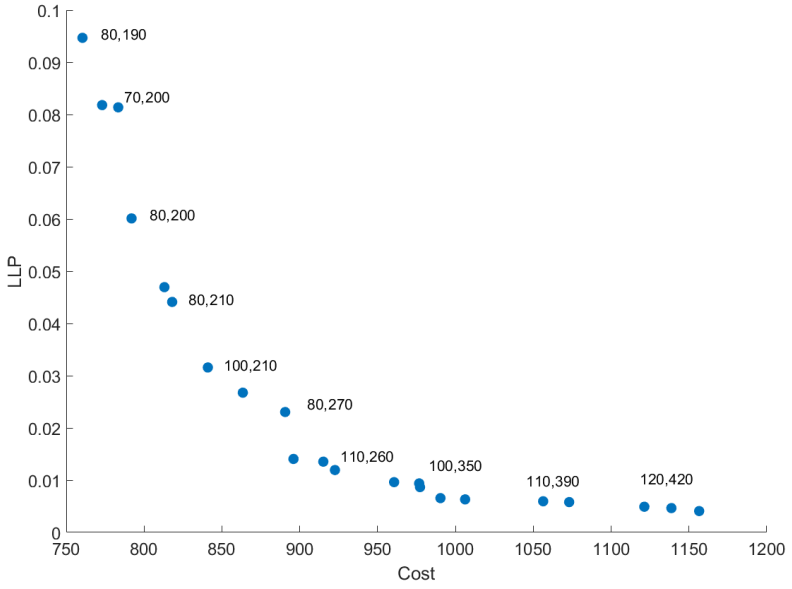

Figure 4.41: District of Pune: LLP VS Cost (T2, GA, Lead-acid)

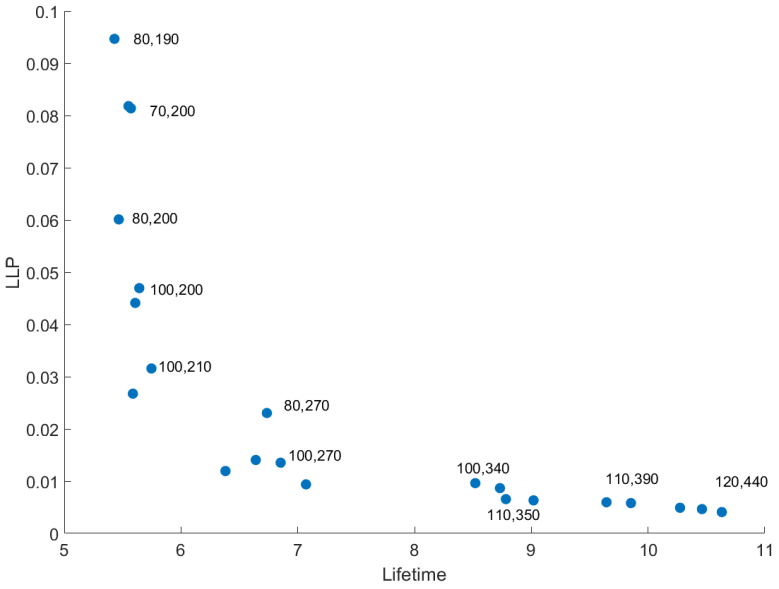

Figure 4.42: District of Pune: LLP VS Lifetime (T2, GA, Lead-acid)

Results: Tier 3

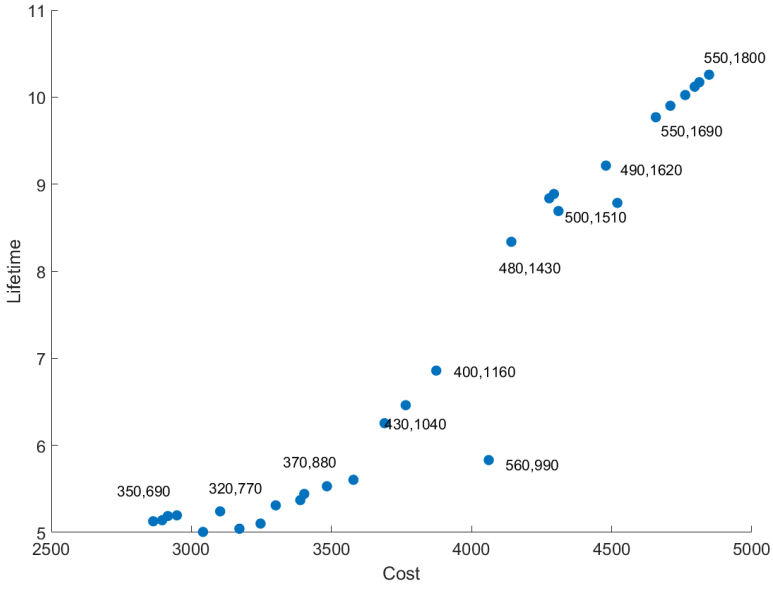

Figure 4.43: District of Pune: Lifetime VS Cost (T3, GA, Lead-acid)

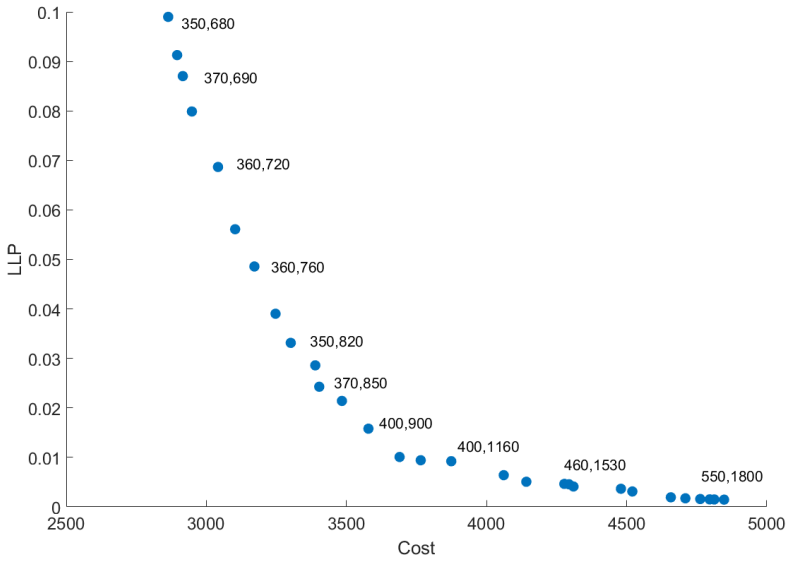

Figure 4.44: District of Pune: LLP VS Cost (T3, GA, Lead-acid)

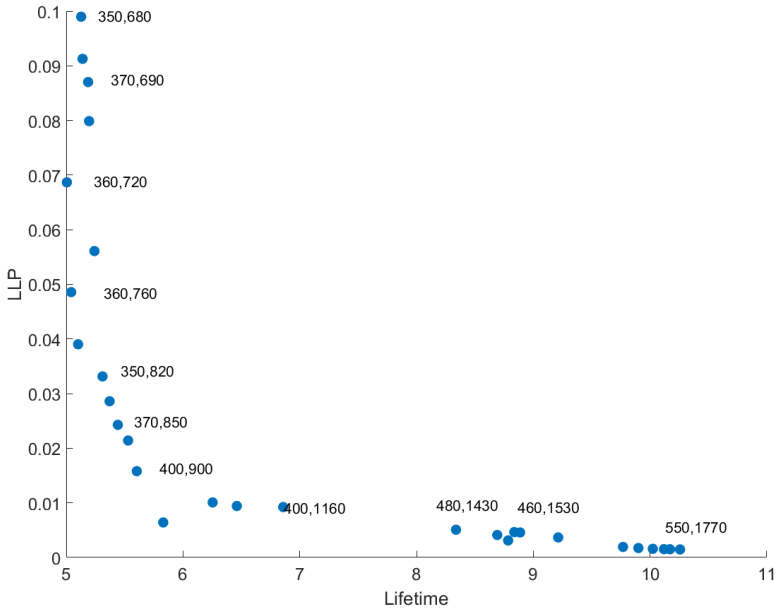

Figure 4.45: District of Pune: LLP VS Lifetime (T3, GA, Lead-acid)

Results: Tier 4

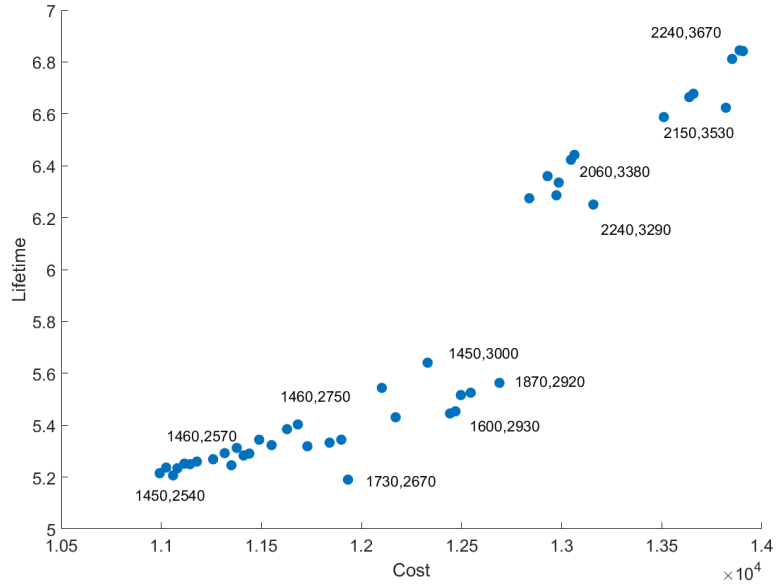

Figure 4.46: District of Pune: Lifetime VS Cost (T4, GA, Lead-acid)

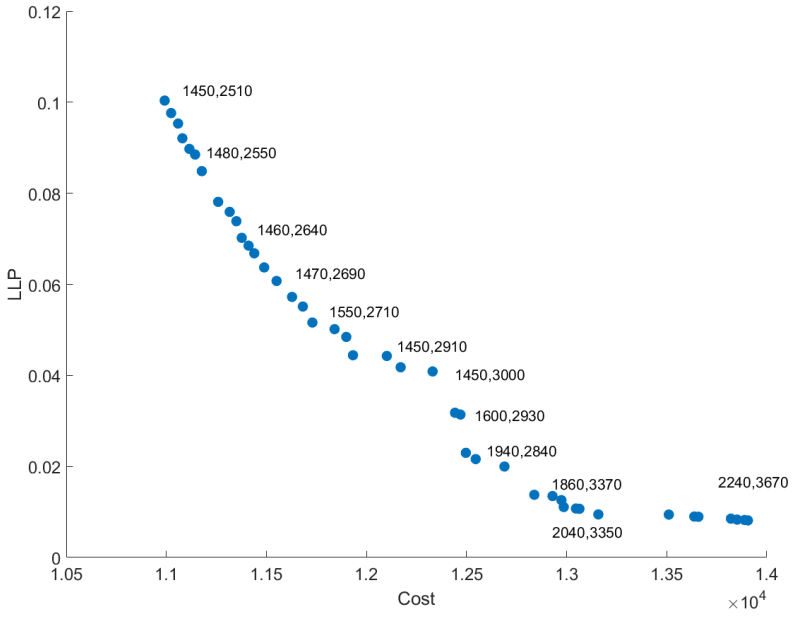

Figure 4.47: District of Pune: LLP VS Cost (T4, GA, Lead-acid)

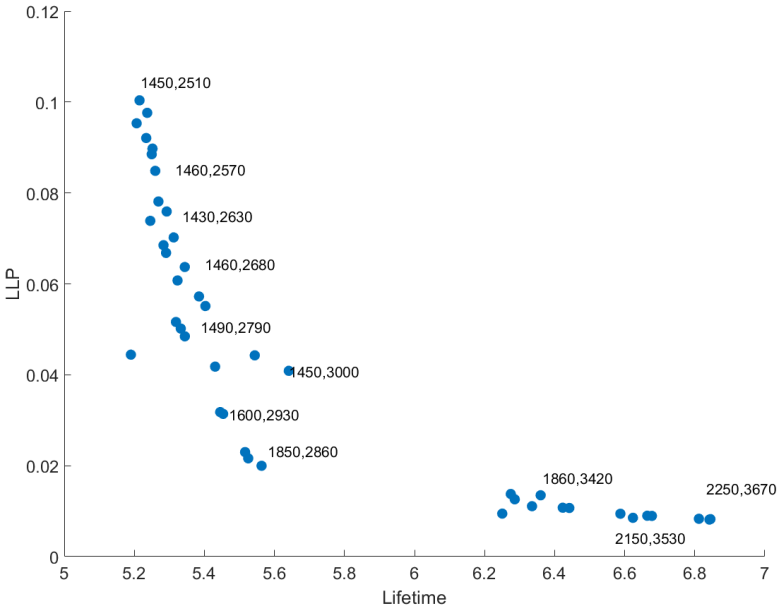

Figure 4.48: District of Pune: LLP VS Lifetime (T4, GA, Lead-acid)

Results: Tier 5

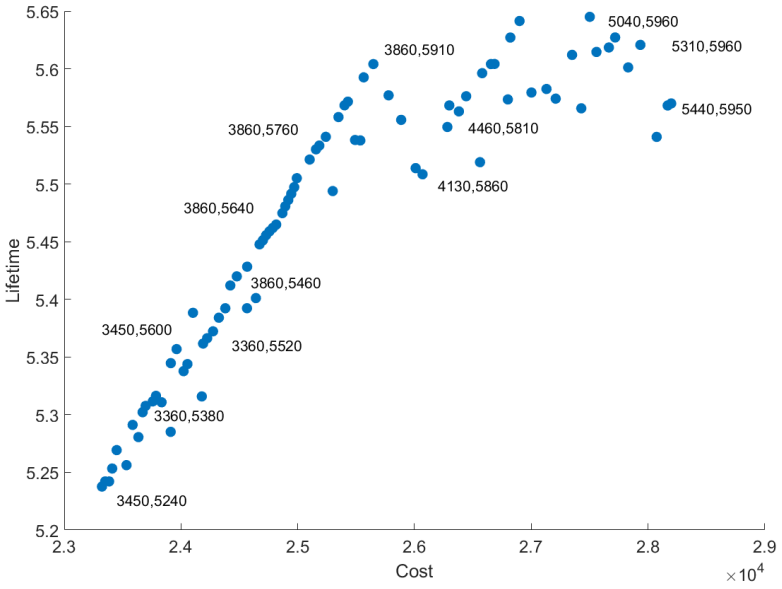

Figure 4.49: District of Pune: Lifetime VS Cost (T5, GA, Lead-acid)

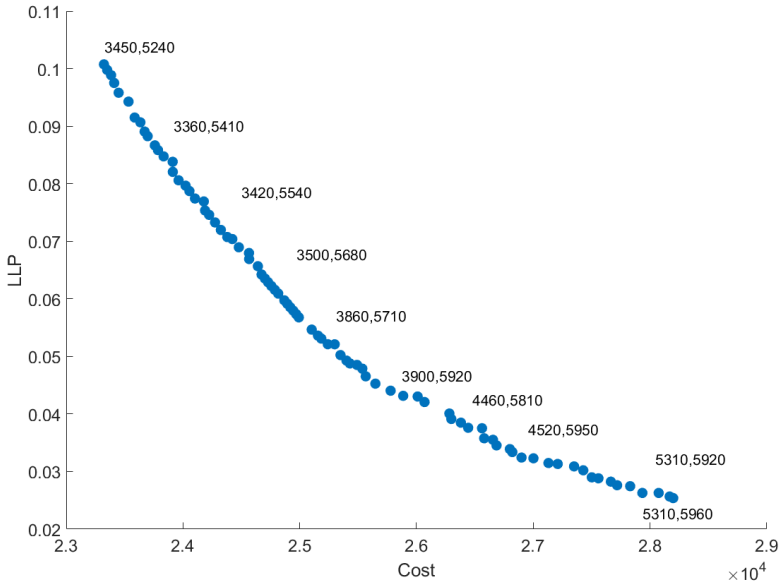

Figure 4.50: District of Pune: LLP VS Cost (T5, GA, Lead-acid)

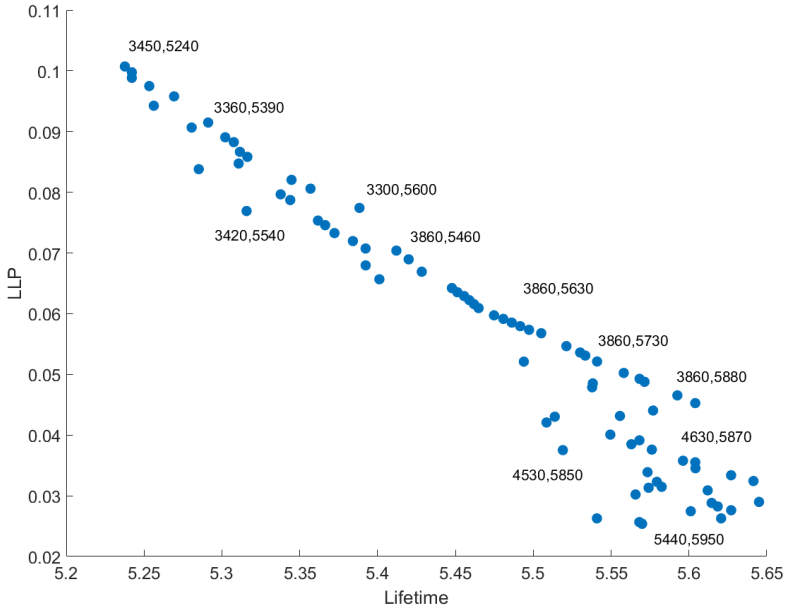

Figure 4.51: District of Pune: LLP VS Lifetime (T5, GA, Lead-acid)

The results from the five tiers in the previous figures show the same pattern observed for the case of the East Khasi Hills. There is a slow increase in the cost of the optimal system in the lower tiers, and then increases rapidly for the higher tiers with a certain loss in reliability (LLP of 1% in tier 1 VS 3$ in tier 5). Moreover, the same analysis to find the optimal system size was performed. Figure 4.52 below shows the $\frac{\delta \text{LLP}}{\delta \text{Cost}}$ for tier 1.

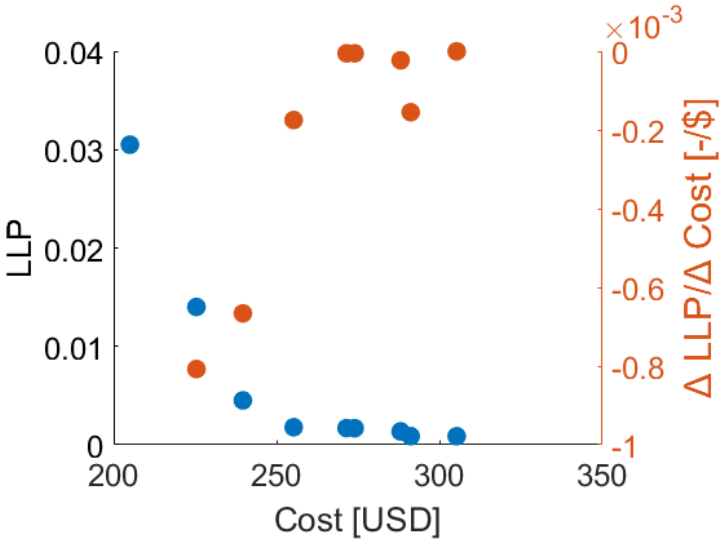

Figure 4.52: District of Pune: Lifetime VS Cost with changing slope (T1, GA, Lead-acid)

From the figure, a sudden gap in the slope is observed, and it is at the point of this gap that the optimal system size is taken. Table 4.9 in the general results below shows the optimal system size obtained for each tier.

General results

Table 4.9: District of Pune: Optimal SHS size per tier summary

Tier	PV [W_p]	Battery [Wh]	PV conv. [W]	Load conv. [W]	Battery conv. [W]	Cost [USD]	LLP [-]	Lifetime [Years]
1	30	90	25.71	12	25	255.3	0.002	9.0
2	110	260	94.29	51	93	922.6	0.012	6.4
3	430	1040	368.58	154	340	3689.5	0.010	6.3
4	1870	2920	1602.89	1670	1697	12689.3	0.020	5.6
5	3900	5740	3342.93	3081	3237	25299.3	0.052	5.5

4.3.3. N'Djamena, Chad

The third location for the case studies is the city of N'Djamena in Chad, a country located in central Africa, that despite being one of the countries with the strongest solar potential, has reached only 8.8% electrification rate in 2016 [8, 27]. Figures 4.53 and 4.54 show the geographical location of N'Djamena and increase of electrification rate in Chad from 1990 to 2016. Moreover, another reason for choosing N'Djamena as a case study location, is the fact that there is a large weather station located in Zalingei, Sudan, around 1,000 Km away and at a very similar latitude. The availability of the weather station allowed the retrieval of very accurate meteorological data using Meteonorm, and was assumed to be the same for both locations.

Figure 4.53: Geographical location of N'Djamena and Zalingei

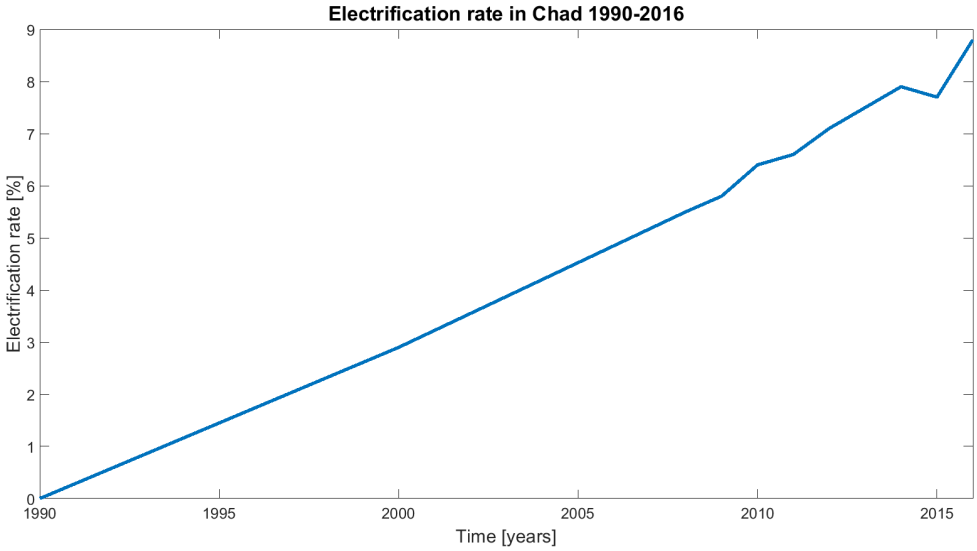

Figure 4.54: Electrification rate in Chad 1990 - 2016 *As Adopted from* [8]

Solar module output

With the location and meteorological data set, the output of a single 20 W_p solar module can be obtained for the whole year. This output will be used to find the optimal size of the charge controller in the next step, and as the unit for finding the optimal system size in later steps.

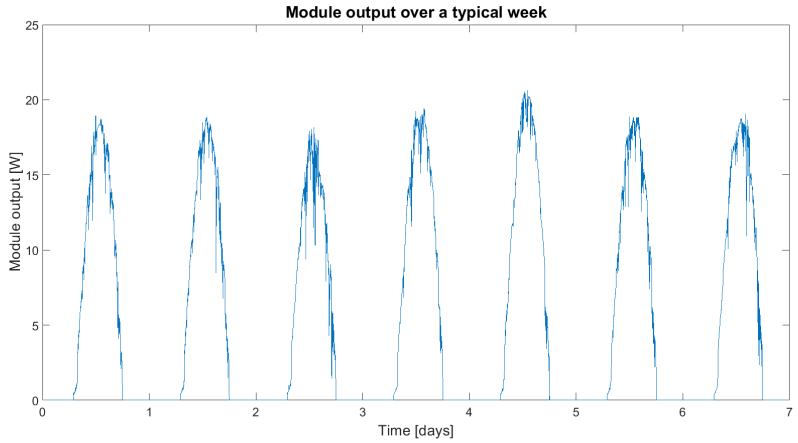

Figure 4.55: Module output in D'Jamena over a typical week

Optimal size of converters

After obtaining the module output, the optimal size of the PV converter can be found, prior to starting with the optimization simulations to find the best PV/battery size. Using the same method as in section 3.3.3, the normalized yearly energy yield of the module was obtained for charge controller $70\% \times 20W_p \leq P_{Nom} \leq 200\% \times 20W_p$ as shown in figure 4.56. The figure shows that for a sizing ratio $R_S = 1.25$ or for a $P_{Nom} = 80\% \times 20W_p$, the energy yield is 95% that of the maximum energy yield at an $R_S = 0.91$. Hence, a 27% decrease in the charge controller size and cost, only a 5% in energy yield is compromised. As for the load converters, the table 4.5 used previously is used.

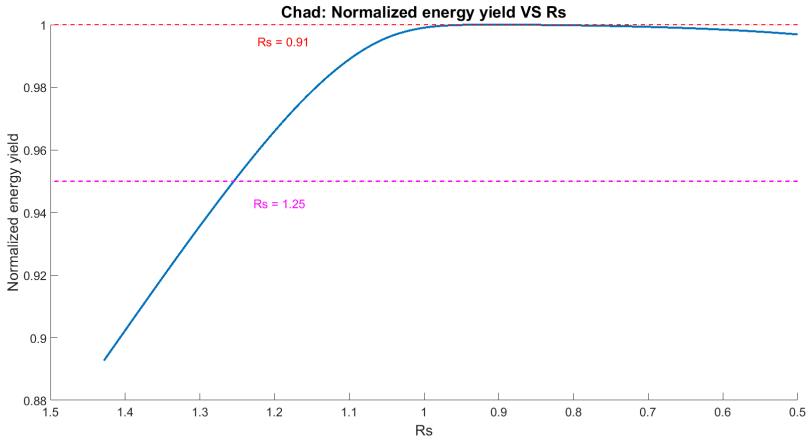

Figure 4.56: N'Djamena: Normalized energy yield VS Rs

Capacity range for PV array and batteries

With the meteorological data, charge controller size, and PV module net output, the capacity range for the PV array and battery storage for each of the tiers can be found using equations 4.1 and 4.2 and are summarized in table 4.10 below.

Table 4.10: N'Djamena: Minimum and maximum PV and battery capacity range

	PV Array [W]		Battery Storage [Wh]	
Tier	**Min**	**Max**	**Min**	**Max**
1	10	40	30	120
2	20	80	120	480
3	110	440	460	1840
4	460	1840	970	3880
5	1100	4400	1550	6200

Running the optimization

Results: Tier 1

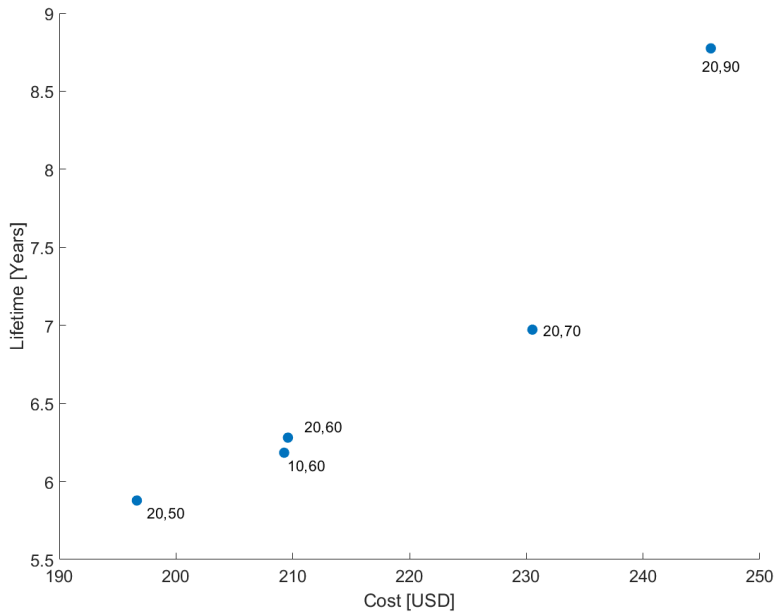

Figure 4.57: N'Djamena: Lifetime VS Cost (T1, GA, Lead-acid)

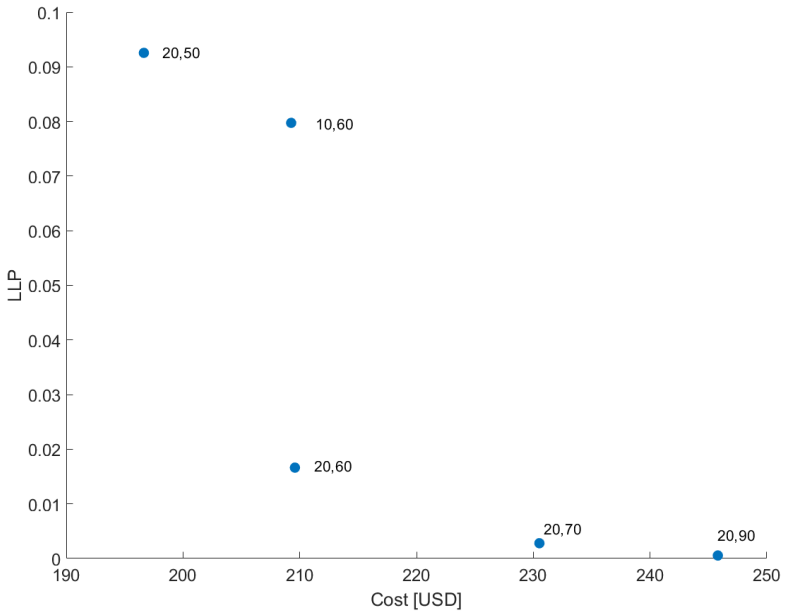

Figure 4.58: N'Djamena: LLP VS Cost (T1, GA, Lead-acid)

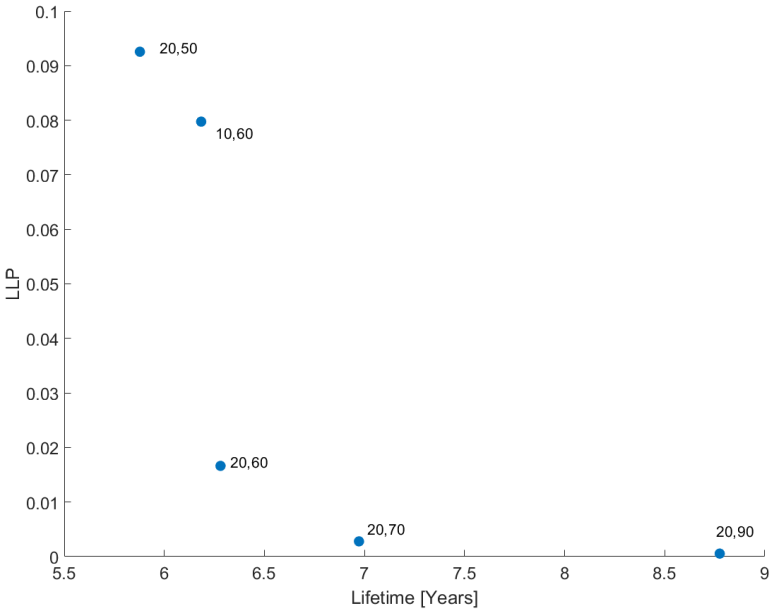

Figure 4.59: N'Djamena: LLP VS Lifetime (T1, GA, Lead-acid)

Results: Tier 2

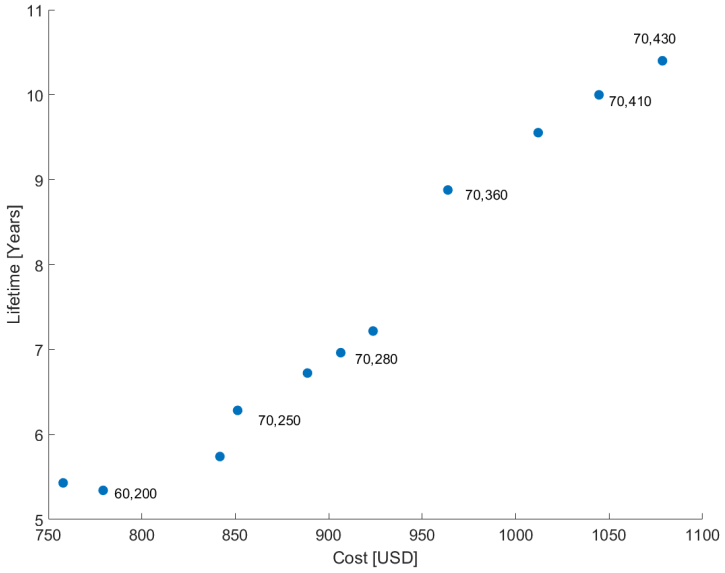

Figure 4.60: N'Djamena: Lifetime VS Cost (T2, GA, Lead-acid)

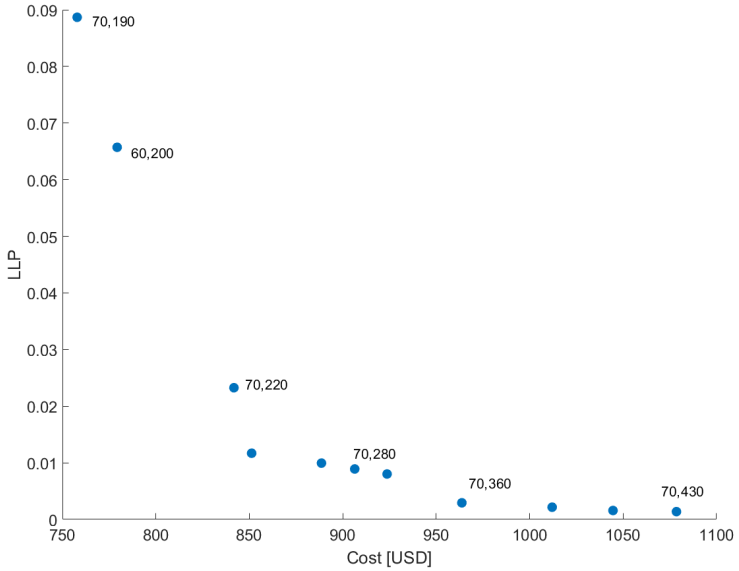

Figure 4.61: N'Djamena: LLP VS Cost (T2, GA, Lead-acid)

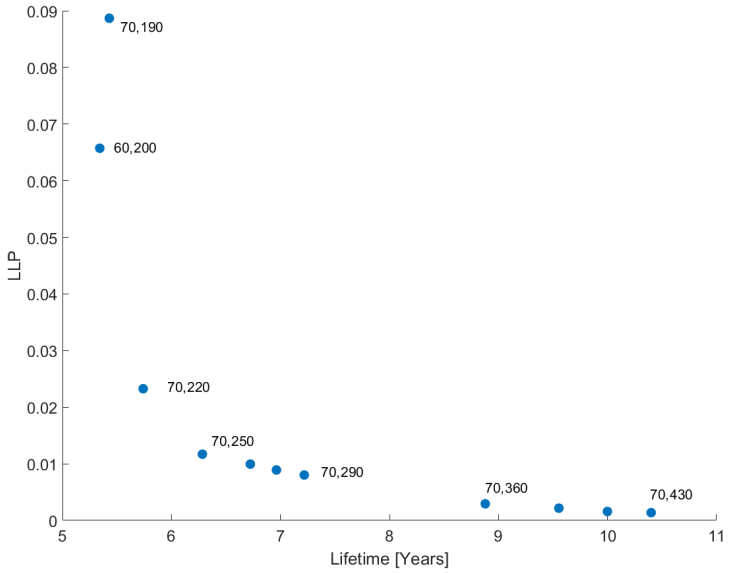

Figure 4.62: N'Djamena: LLP VS Lifetime (T2, GA, Lead-acid)

Results: Tier 3

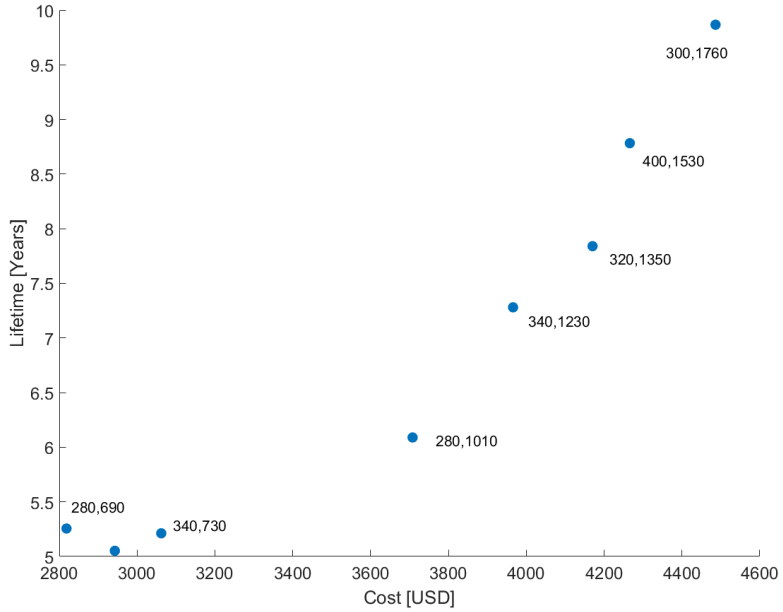

Figure 4.63: N'Djamena: Lifetime VS Cost (T3, GA, Lead-acid)

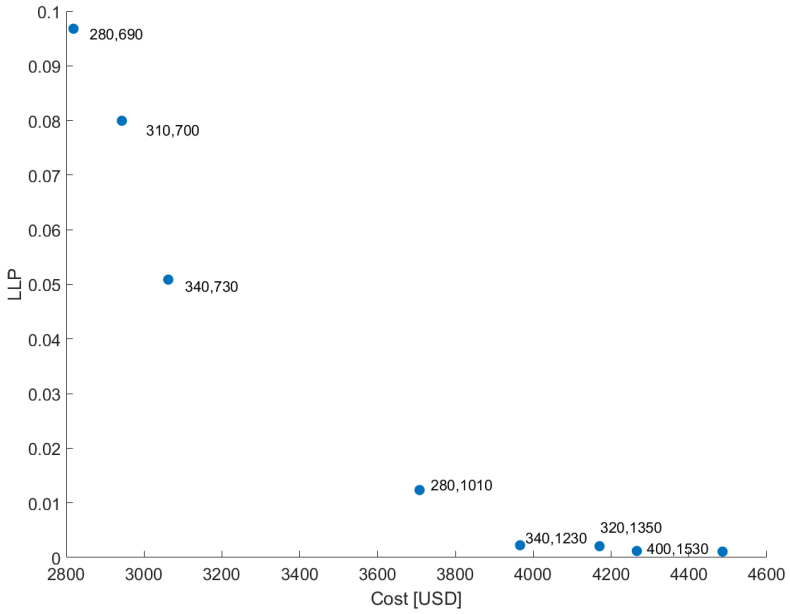

Figure 4.64: N'Djamena: LLP VS Cost (T3, GA, Lead-acid)

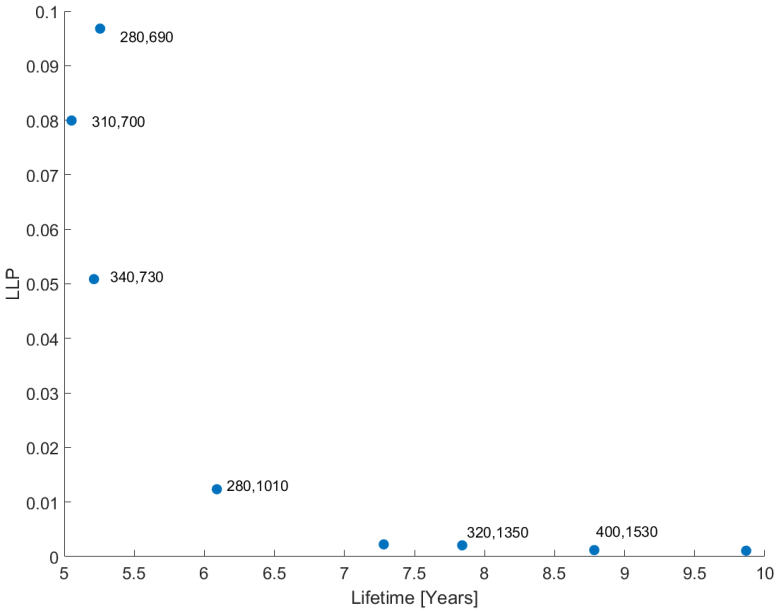

Figure 4.65: N'Djamena: LLP VS Lifetime (T3, GA, Lead-acid)

Results: Tier 4

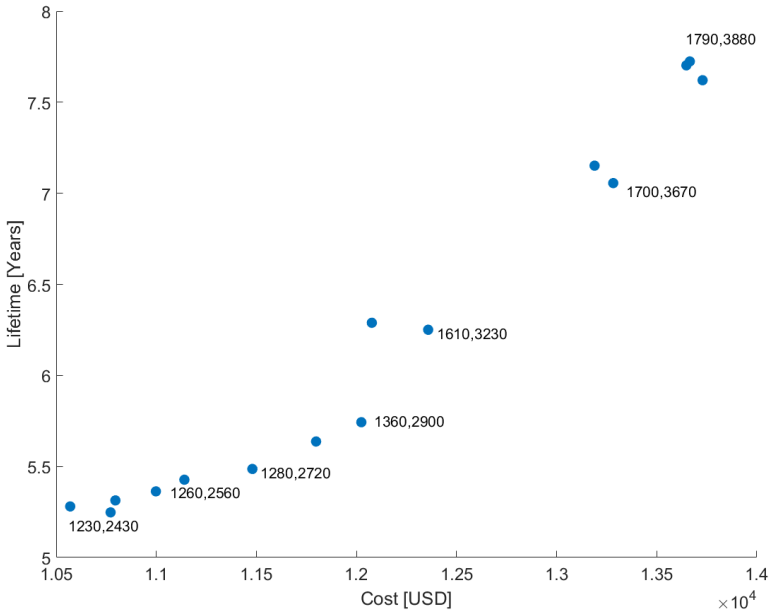

Figure 4.66: N'Djamena: Lifetime VS Cost (T4, GA, Lead-acid)

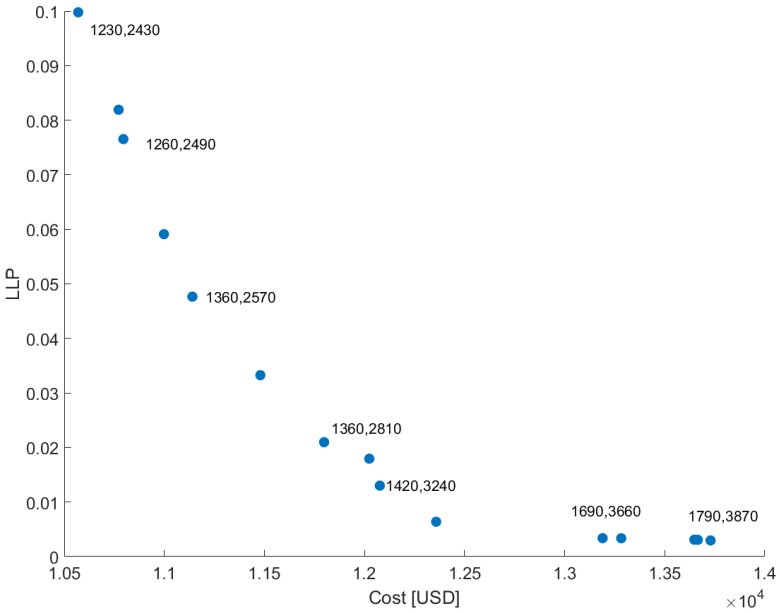

Figure 4.67: N'Djamena: LLP VS Cost (T4, GA, Lead-acid)

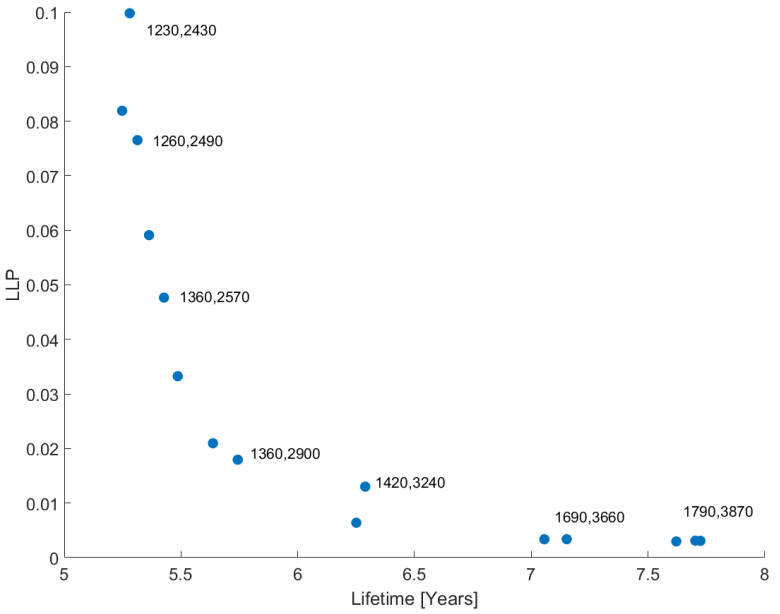

Figure 4.68: N'Djamena: LLP VS Lifetime (T4, GA, Lead-acid)

Results: Tier 5

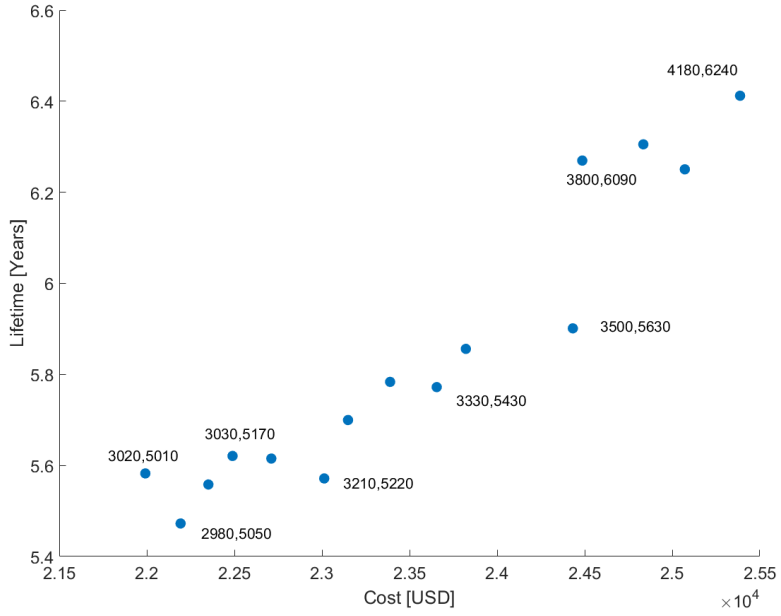

Figure 4.69: N'Djamena: Lifetime VS Cost (T5, GA, Lead-acid)

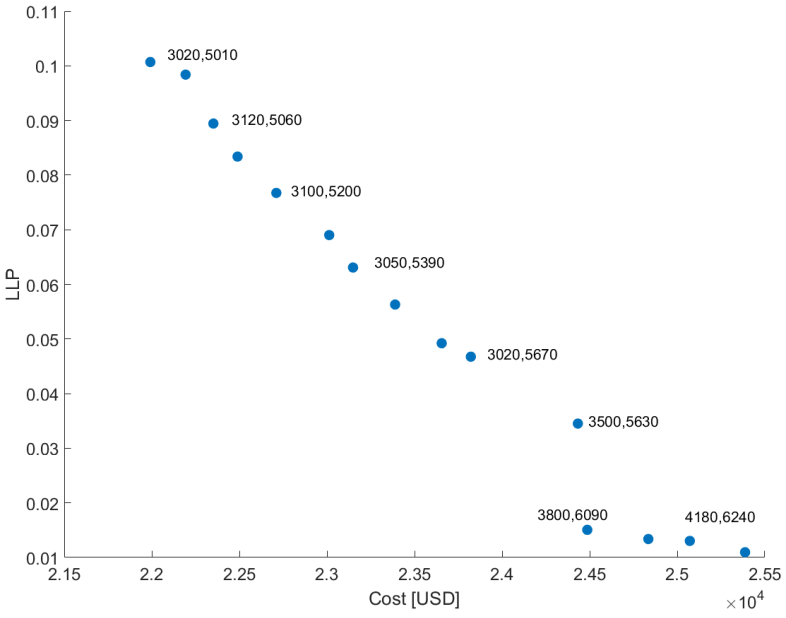

Figure 4.70: N'Djamena: LLP VS Cost (T5, GA, Lead-acid)

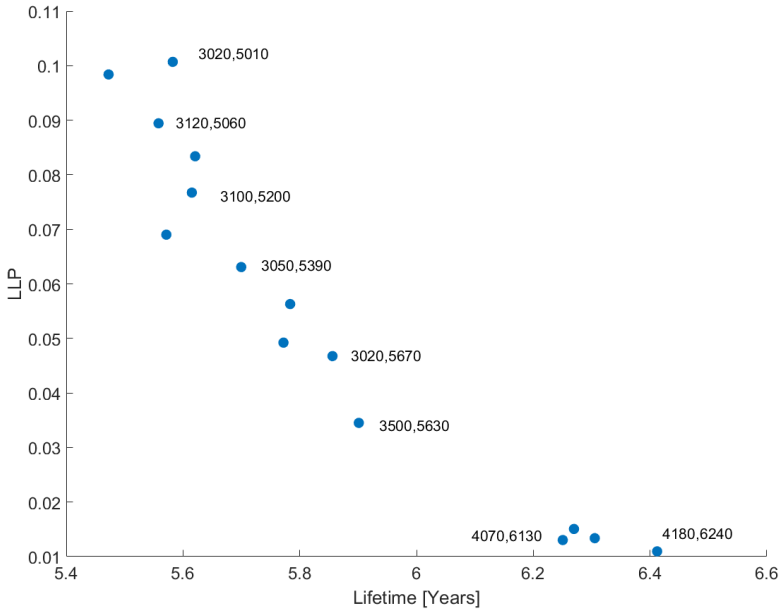

Figure 4.71: N'Djamena: LLP VS Lifetime (T5, GA, Lead-acid)

General results

In N'Djamena, the optimal system size resulted in a somewhat constant LLP throughout all tiers (around 0.013 %), and a battery lifetime of 6 years. The cost shows the same pattern as the previous locations. The large increase in cost is mostly due to the battery capacity, for which 4 replacements are required throughout the system lifetime.

Table 4.11: N'Djamena: Optimal SHS size per tier summary

Tier	PV [W_p]	Battery [Wh]	PV conv. [W]	Load conv. [W]	Battery conv. [W]	Cost [USD]	LLP [-]	Lifetime [Years]
1	20	60	19	12	19	209,6	0,017	6,3
2	70	250	67	51	66	851,2	0,012	6,3
3	280	1010	268	154	242	3707,8	0,012	6,1
4	1420	3240	1361	1670	1657	12076,6	0,013	6,3
5	3800	6090	3642	3081	3531	24486,3	0,015	6,3

4.4. System performance with Li-ion battery

As mentioned earlier in table 4.2, the major contributors to the cost of the SHS are the PV and battery, which are 1$/Wp and 1.1$/Wh respectively. Throughout this study, lead-acid batteries have been the choice of battery technology as they are the cheapest and most widely used for SHSs. In this section however, a performance analysis will be conducted to illustrate the change in system cost when changing the battery technology to Li-io that has a cost of 1.5$/Wh. By changing the technology, the upfront cost will change because of two factors: first, the Li-ion has a higher cost per Wh. Secondly, it has also typically a higher lifetime than the lead-acid batteries. The result of these changes are shown for the district on Pune in tier 3 in figures 4.72 through 4.74, East Khasi hills in tier 2 in figures 4.75 through 4.77.

District of Pune: Cost sensitivity using different battery technologies

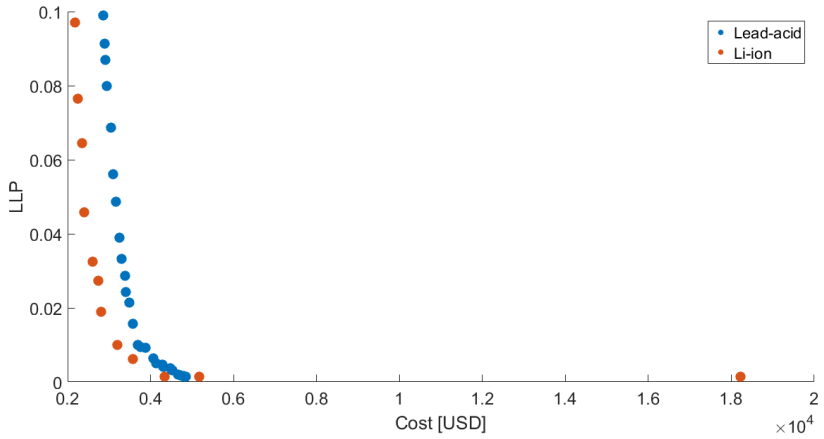

Figure 4.72: District of Pune: LLP VS Cost for different battery technologies (T3, GA, Lead-acid VS Li-ion)

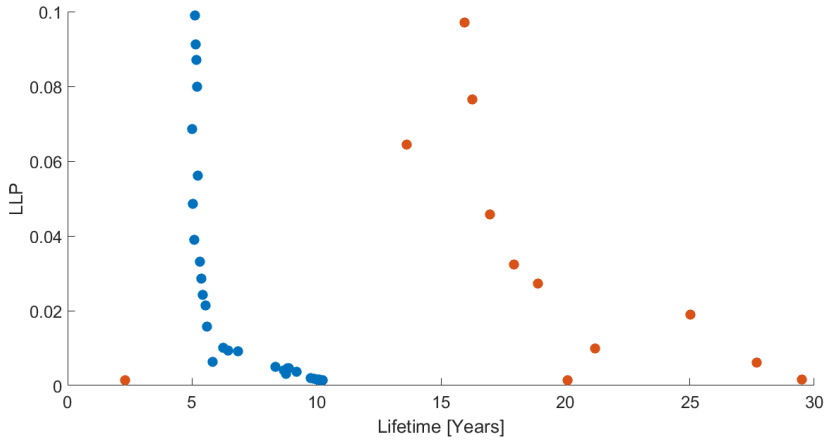

Figure 4.73: District of Pune: LLP VS Lifetime for different battery technologies (T3, GA, Lead-acid VS Li-ion)

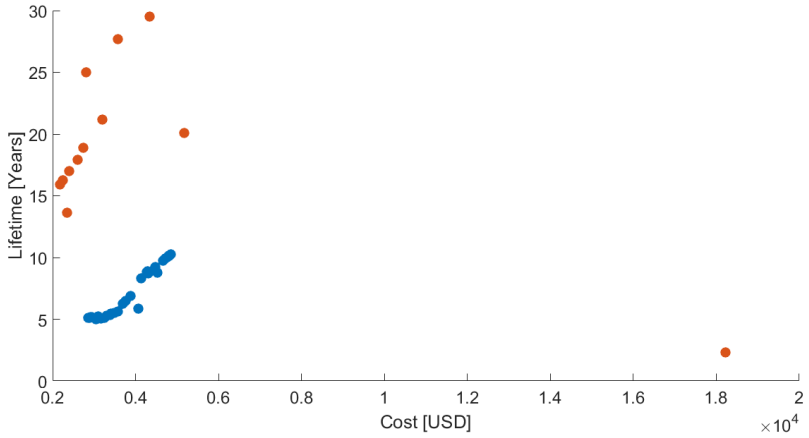

Figure 4.74: District of Pune: Lifetime VS Cost for different battery technologies (T3, GA, Lead-acid VS Li-ion)

The figures above show that for the district of Pune in tier 3, the use of Li-ion batteries proves to be a better choice. Even though the battery price increased from 1.1 to 1.5 (36%), the large improvement in battery life

reduced the total system upfront cost greatly, making it an even more affordable choice than with the lead-acid batteries. This fact is specifically highlighted in figure 4.74, where the battery lifetime VS cost curve shows that for the same cost range, the battery lifetime is 15-20 years for Li-ion, while being 5-10 years for lead-acid.

East Khasi Hills: Cost sensitivity using different battery technologies

The same comparison was done in the East Khasi Hills case study for tier 2.

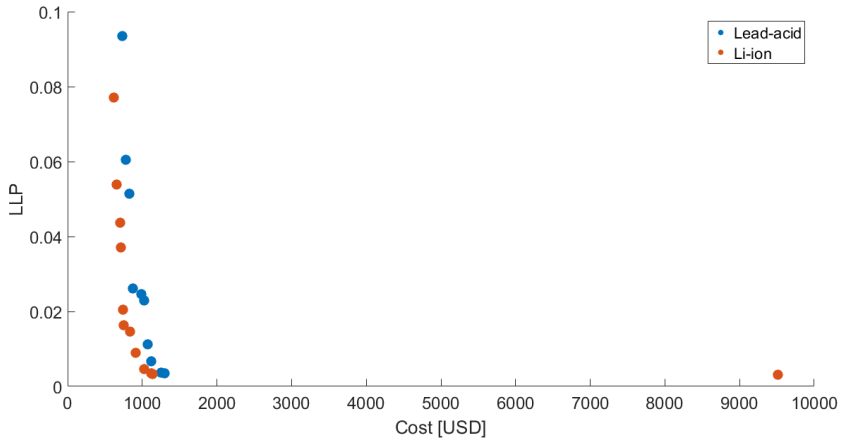

Figure 4.75: East Khasi Hills: LLP VS Cost for different battery technologies (T2, GA, Lead-acid VS Li-ion)

In figure 4.75 above, the choice of Li-ion appears to be also the preferable choice, although the variation of the total cost depending on the LLP is much smaller than in the case of Pune.

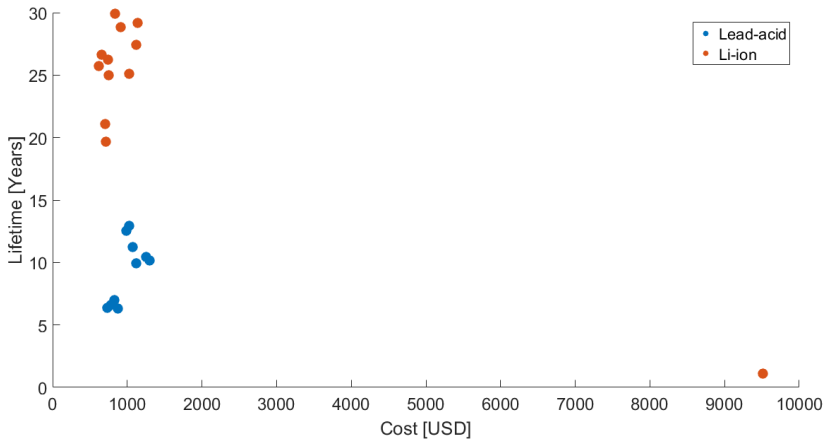

Figure 4.76: East Khasi Hills: Lifetime VS Cost for different battery technologies (T2, GA, Lead-acid VS Li-ion)

In the figure above however, the difference in battery lifetime is also highlighted greatly between the two technologies. The system cost of both systems is scattered around 1000$, but the battery life for Li-ion ranges from 20-30 years while it ranges from 5-10 years for lead-acid.

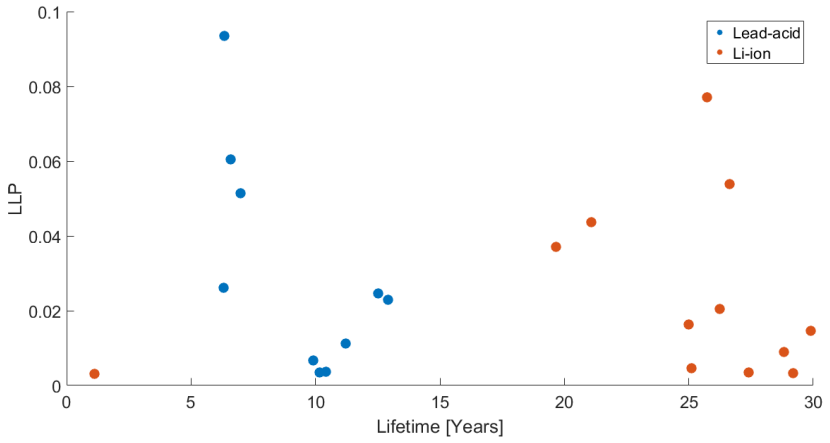

Figure 4.77: East Khasi Hills: LLP VS Lifetime for different battery technologies (T2, GA, Lead-acid VS Li-ion)

District of Pune: Cost sensitivity using with a variation of PV module price

In this section, a sensitivity analysis was performed after variating the price of the PV module from 1 to 2$/Wp. As the PV module has the highest lifetime in the system, which is equivalent to the system lifetime of 25 years, the increase in the PV module cost is especially highlighted in figure 4.78 below, where the total system cost shows a constant shift to the right.

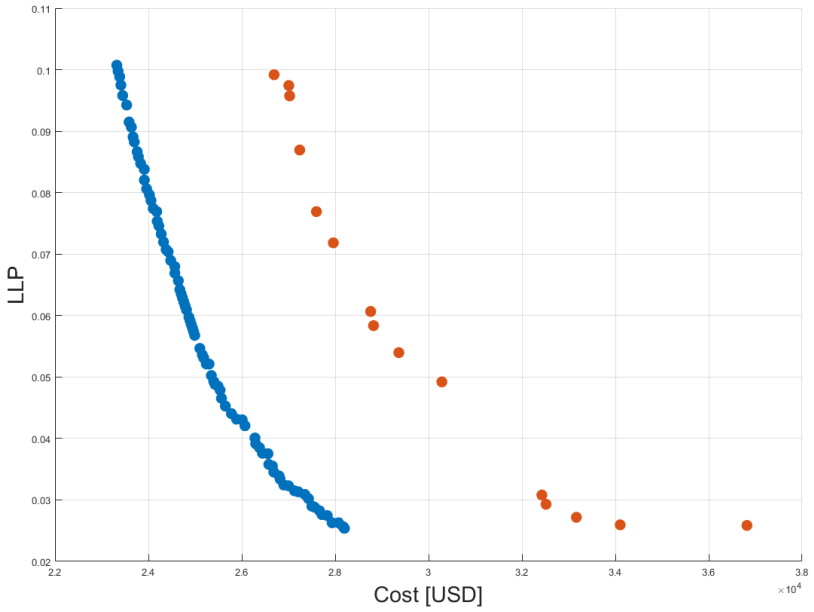

Figure 4.78: District of Pune: LLP VS Cost for different PV module prices (T5, GA, Lead-acid)

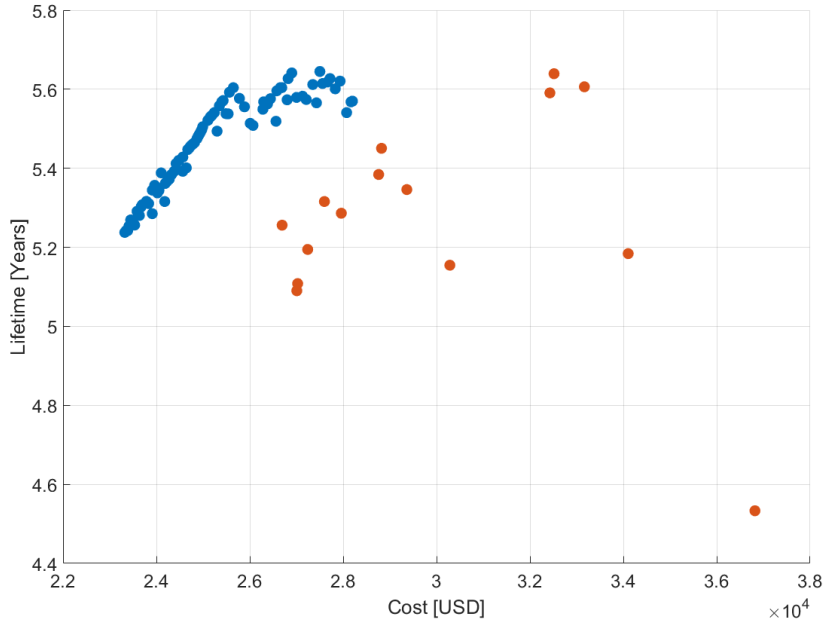

Figure 4.79: District of Pune: Lifetime VS Cost for different PV module prices (T5, GA, Lead-acid)

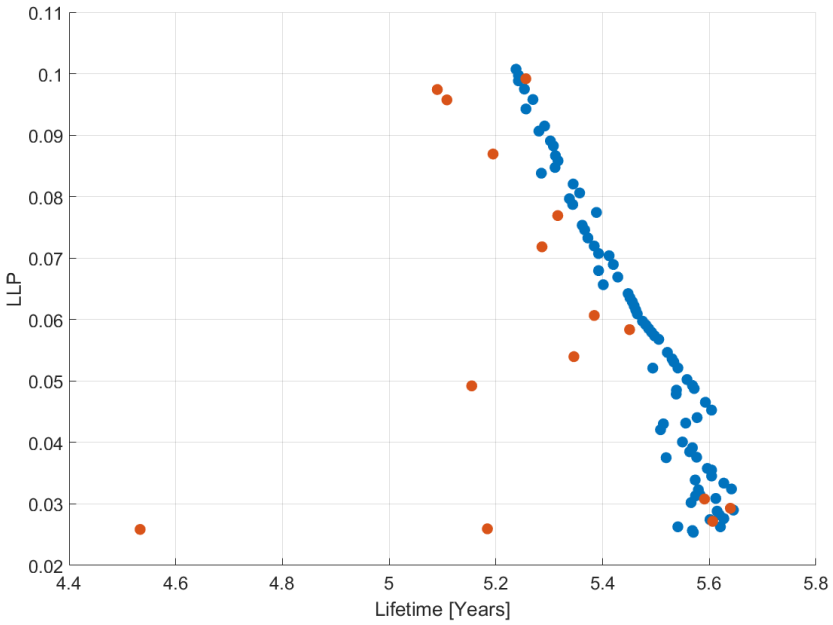

Figure 4.80: District of Pune: LLP VS Lifetime for different PV module prices (T5, GA, Lead-acid)

4.5. Conclusions

In this chapter, two optimization methods were tested on three different case studies to optimize the size of the stand-alone SHS while going up the 5 tier energy ladder. The first approach, using the iterative method, provided some insight on the optimal system size, but proved to require long computational time and required at least one of the three objectives to be fixed. The Genetic Algorithm however, an evolutionary heuristic algorithm, was able to plot the pareto fronts to optimize all three objectives simultaneously. Using the results obtained, the optimal system size for each tier was selected using the $\frac{\delta LLP}{\delta Cost}$ equation. Using this method, the sensitivity of the LLP to the system cost proved to be high at first for lower system cost and high LLPS, and

gradually decreased as the LLP Vs Cost curve flattened out, showing that to decrease the LLP requires a large increase in cost beyond a certain point. The point in which the curve shows a large shift was selected as the optimal point. Tables 4.7, 4.9 &4.11 show the optimal size for each case in each of the cases.

In this chapter, it was also concluded that the stand-alone architecture is feasible in the lower tiers, up until tier 3, but becomes expensive and less reliable in the higher tiers. This can be deducted from the summary tables mentioned above, where the total system cost shows a drastic increase between tiers 3 & 4, and tiers 4 & 5. For example, in the case of N'Djamena:

Tier	**Upfront cost [$]**	**LLP**
1	230	0,01
2	991	0,025
3	3824	0,02
4	**16000**	**0,03**
5	**33390**	**0,05**

This large gap in total system cost, going from under 5000$ to more than 15000$, at an even higher LLP makes the stand-alone architecture unfeasible for households with limited income who are trying to improve their quality of life.

Another method, the interconnectivity approach, where households interconnect and share their electricity was examined in chapter 5, and proved to be a potential solution to the problem.

5

Sizing interconnected SHS

In this chapter, an alternative approach towards full household electrification is presented. As seen in chapter 4, the upfront installation cost of stand-alone SHSs shows a substantial increase in the higher energy tiers. Hence, another option, household interconnectivity is analyzed. The modeling and methodology of this approach are presented at first, followed by the results and findings.

5.1. An Alternative Approach: Household interconnectivity

In chapter 4, it was concluded that the stand-alone SHS architecture is feasible in the lower tiers, but became less and less feasible in the higher tiers due to the large increase in cost and decrease in reliability (Higher LLP). In this approach, the overall system reliability and energy dump were examined in scenarios where several households are interconnected, hence sharing their energy in order to minimize dump and eliminate the energy deficit. The main idea is to compare the system's performance over a year as the number of interconnected households increases, to the performance of a single household over several tiers.

5.2. Modeling

The architecture and modeling of the interconnected households differs from the modeling of a single household. Due to the sharing of electricity between households, the number and rating of the converter increases to a safe and efficient power flow between the components in each household, and among the different households. In this section, the system topology and modeling of the components is explained.

5.2.1. System architecture

To interconnect different households, a common high voltage DC-bus needs to be installed to handle the accumulated power generation from the various PV arrays, the low voltage generated by each household is boosted to a higher voltage through a bi-directional HV/LV DC/DC converter. Meanwhile, within each household, a DC/DC converter connected to every component regulates and stabilizes the power flow to keep the system running at the best efficiency. Figure 5.1 below shows the typical topology for a household in an interconnected approach.

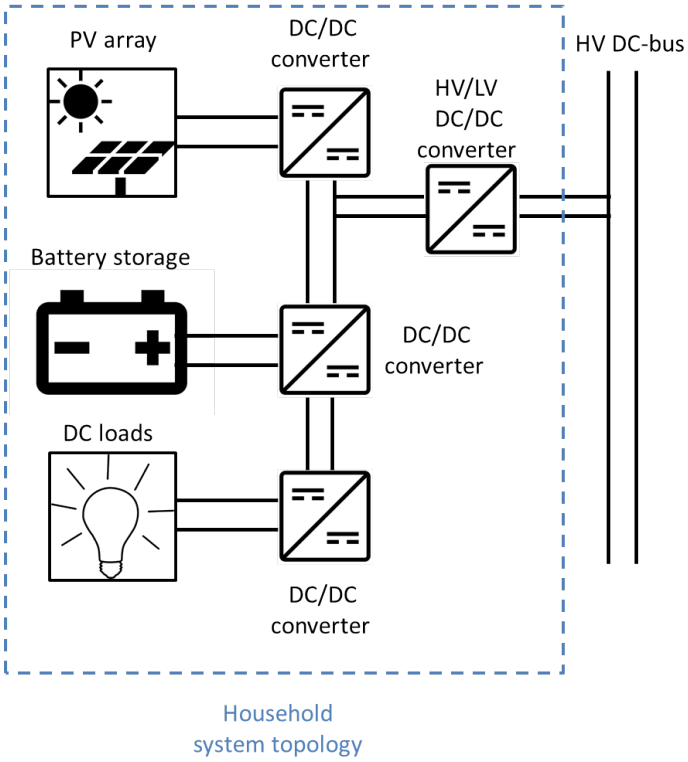

Figure 5.1: Household system topology during interconnectivity

5.2.2. System sizing

The first step in the performance modeling of interconnected households is to select the size of each based on certain criteria. In the previous chapter, an optimal size was obtained for each tier based on the $\frac{\delta \text{LLP}}{\delta \text{Cost}}$ slope showing that at a certain point, and was chosen as the operating system size. However, the pareto front obtained showed that there is a certain flexibility given to the user depending on which of the three objectives is the most important. For example, if the LLP is required to be 0% by the user, a certain optimal system size can be selected from the pareto front, at the expense of a high system upfront cost. If a high battery lifetime is the most crucial criteria, then the PV and battery combination with the highest battery lifetime can be chosen.

In this study, the component sizing for the interconnected approach was based on selecting the SHS size for each household where in the stand-alone case, an LLP = 10%, is achieved. The 10% LLP, which is the limit of the constraint set in section 4.2.3, is expected to drop as the number of households increase due to electricity sharing. The tables below show the system sizes for each location for all tiers where an LLP = 0.1 is obtained.

Table 5.1: District of Pune: System sizes with 0.1 LLP for all tiers

Tier	**PV** $[W_p]$	**Battery [Wh]**	**PV conv. [W]**	**Load conv. [W]**	**Battery conv. [W]**	**LLP [-]**
1	20	60	17	12	17	0.08
2	80	190	69	51	67	0.097
3	350	680	300	154	273	0.095
4	1450	2510	1243	1670	1697	0.1
5	3450	5240	2957	3081	2859	0.1

Table 5.2: East Khasi Hills: System sizes with 10% LLP for all tiers

Tier	PV [W_p]	Battery [Wh]	PV conv. [W]	Load conv. [W]	Battery conv. [W]	LLP [-]
1	30	50	26	12	25	0,088
2	100	200	86	51	85	0,093
3	360	850	3010	154	282,0	0,092
4	1570	3330	1350	1670	1700	0,096
5	4150	6750	3565	3081	3455	0,099

Table 5.3: N'Djamena: System sizes with 10% LLP for all tiers

Tier	PV [W_p]	Battery [Wh]	PV conv. [W]	Load conv. [W]	Battery conv. [W]	LLP [-]
1	20	50	19	12	19	0,093
2	70	190	67	51	66	0,089
3	280	690	268	154	242	0,097
4	1230	2430	1179	1670	1659	0,100
5	3020	5010	2894	3081	2797	0,101

Hence, in the case studies, the component sizes of each household were selected as shown in the tables, to study the effect of the interconnectivity on the system performance.

5.2.3. Control strategy

The main idea behind the interconnected approach, is to allow sharing of the electricity generated. This benefits the household community in several ways. First the energy dump that was getting produced by a household during the stand-alone case discussed in chapter 4, can now be sent to the DC HV-bus, and supply an other household that is at an energy deficit at that moment. Moreover, as the battery are also able to supply electricity, even if the aggregated energy dump by the households at a certain moment t is not able to satisfy all the energy deficits, the batteries from all the households can help satisfying it. As a result, at each time instant t, less households will be at an energy deficit, thus reducing their LLP. The equations and control methodology used in this approach are shown below:

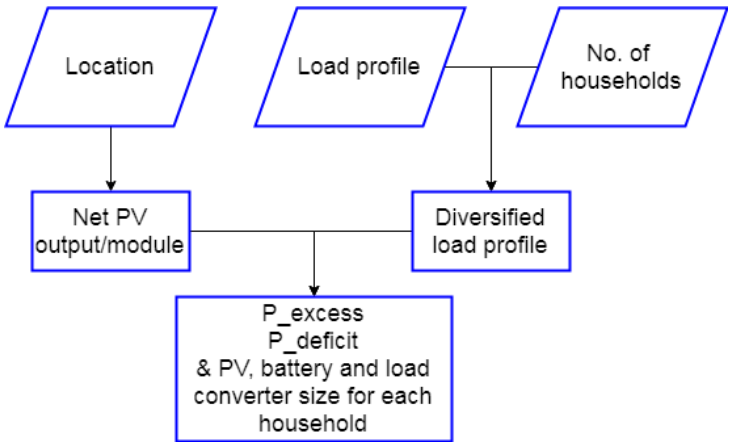

Figure 5.2: Interconnected approach: Case initialization flowchart

In flowchart 5.2 above, the first few steps in the algorithm are shown. First, the net output of the PV module P_{out} is obtained from the location and meteorological data. Then, the load profile for the tier and the number of households are taken as inputs to generate the diversified load profiles for each household. Finally, using the load profiles, module output, and PV array size for each household, the excess and deficit arrays at each instant *'t'* for each household can be obtained as shown in the stand-alone case. The rated power of the converter for the battery, PV array and DC loads is also obtained for each household.

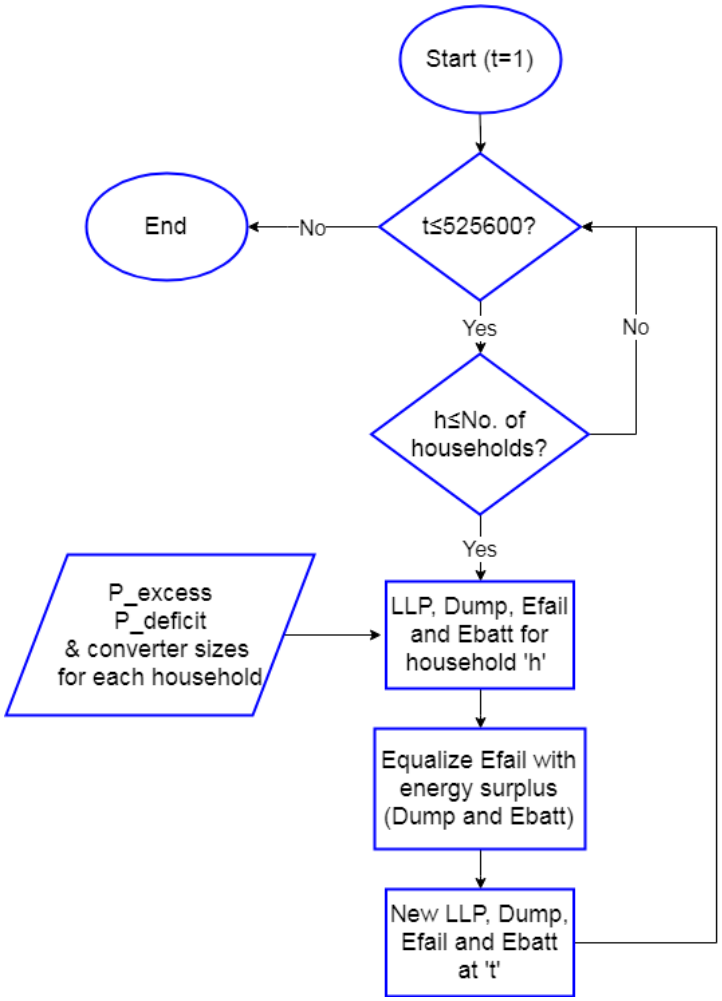

Figure 5.3: Interconnected approach: Iterative flowchart for parameter outputs

After the initialization of the model, the iterative loop over the range of time steps begins. As shown in 5.3, at every minute *'t'*, the LLP, energy dump and energy fail E_{fail} for each household *'h'* is calculated. The E_{fail}, as explained in flowchart 3.22, is the amount of energy deficit remaining that neither the household's PV array nor the battery E_{batt} can supply.

$$\text{For}: \quad P_{out,t} + E_{batt,t} - Load_t < 0; \qquad E_{fail,t} = Load_t - (P_{out,t} + E_{batt,t}) \tag{5.1}$$

Hence, every household that is not able to satisfy the whole load at that instant *'t'*, while output a certain amount of $E_{fail} \neq 0$, and an LLP value of 1 at that instant. Then, at that same time step, the energy surplus by the households is equalized with the energy deficits to reduce the energy dump and avoid having any household with a $E_{fail} \neq 0$ in the community, minimizing the average LLP. The equalization algorithm is explained below.

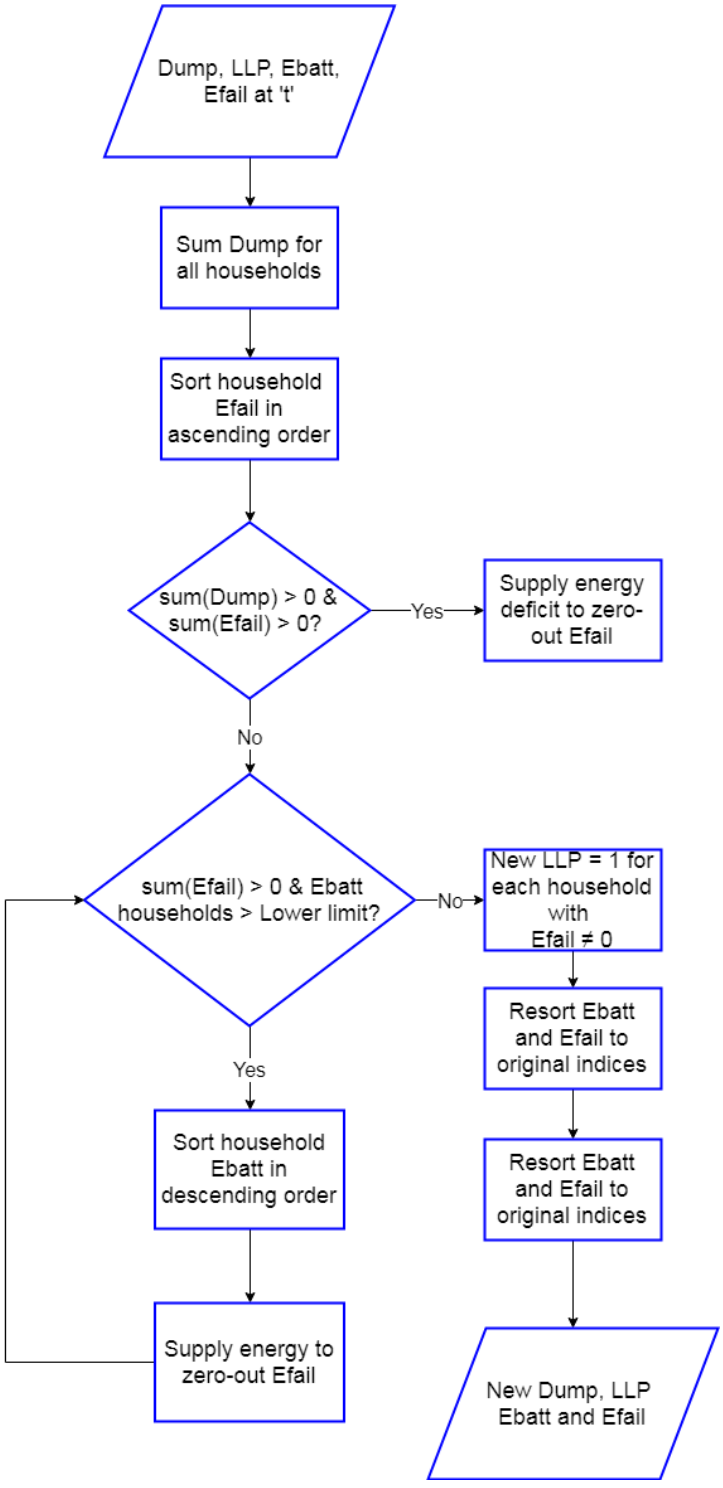

Figure 5.4: Interconnected approach: Energy surplus and deficit equalization flowchart

The energy equalization algorithm shown in the figure above is the most important step, and is the essence of the interconnected households topology. In this step, the energy sharing between households to zero-out the overall energy surplus and deficit is modeled. First, the different parameters that were calculated for each household in the previous step are taken as an input. Then, the dump of all the households is summed and acts as the primary measure to eliminate the energy deficit. In the modeled control strategy, an iterative approach is used where the energy dump feeds the households with an energy deficit in ascending order.

$$E_{fail} = [E_{fail,1}, E_{fail,2}, ...E_{fail,h}]; \qquad Where \quad E_{fail,i} \leq E_{fail,i+1} \tag{5.2}$$

Thus, the household with the lowest energy deficit is the first to be supplied with the surplus to zero-out its

E_{fail} and then check the next household. Prioritizing the households with the lowest E_{fail} minimizes the total number of households with an energy deficit, hence have an LLP = 0 at that instant. The secondary approach is employed when the total energy dump is consumed before all the energy deficit is satisfied. In this step, the available battery storage of the households that are able to supply energy is used to cover the remaining deficit. The household with the highest available energy in their battery is prioritized in energy supply.

$$E_{batt} = [E_{batt,1}, E_{batt,2}, ...E_{batt,h}]; \qquad Where \quad E_{batt,i} \geq E_{batt,i+1} \tag{5.3}$$

The equalization process ends either when the E_{fail} of all households is zeroed-out, or when E_{batt} reaches its lower limit and cannot supply any more. At that point, any household that still has an energy deficit keeps an LLP = 1, while the others have an LLP = 0. The process is then repeated for the next time step.

In figure 5.5 below, the performance of the control strategy is shown for a community of two households over a period of 1000 minutes, or 16 hours. The figure, split into 3 synchronized graphs. The top graph shows the change in battery capacity for each household $E_b$att1 & $E_b$att2, as the load of each household changes. The dynamic output of the PV modules is also plotted in green to evaluate the behaviour of the batteries. The middle graph simply represents the SoC of each of the batteries, where the lower limit is 0.2 as was set by the battery model. The bottom graph illustrates the output parameters of each household, which are the energy dump and energy fail E_{fail}.

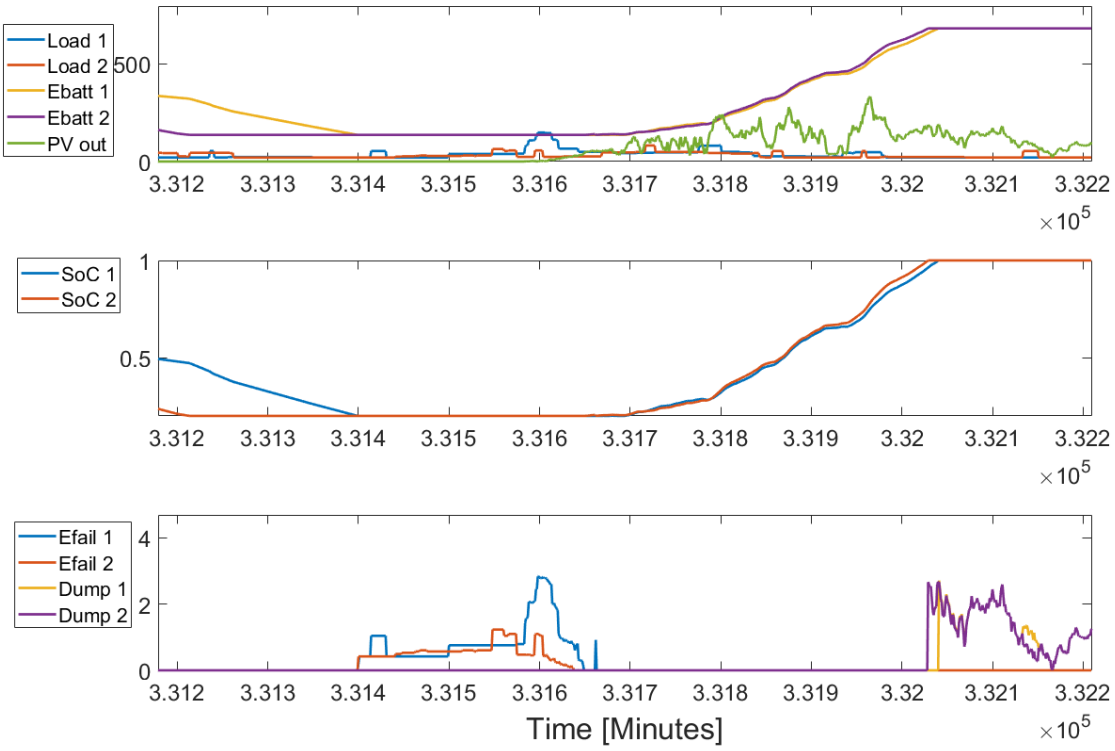

Figure 5.5: District of Pune: Graph showing the energy sharing between two households in tier 3

In the first part of the timeline, from minute 331200 to 331600, the PV output is zero, as it is night time. However, both households have a certain load represented by the blue and orange lines. The battery capacity and SoC of both batteries is decreasing until reaching the lower limit, where the energy fail goes from zero in the bottom graph to the same value of the load (blue and orange lines in the bottom graphs). On minute 331700, when the PV output becomes higher than the loads, E_{fail} drops to 0, and both batteries start charging using the excess energy. At time = 332000, both batteries reach full capacity, and the energy dump can be seen rising from its 0 value to match the value of excess energy (purple and yellow curves).

5.2.4. Assumptions

The interconnected architecture modeled in this study was based on the practical modeling of each of the components as shown in chapter 3, the control strategy explained in the previous section shows how the energy sharing takes place. However, some assumptions had to be taken during the modeling process and are as follows:

- No transmission losses were taken into account.
- No priority for energy sharing was given to houses in direct proximity, the hierarchy was based as shown in figure 5.4.
- The battery & battery converter efficiency were assumed to be constant.
- The battery lifetime was not taken into consideration.

5.3. Case Studies

In this section, some case studies were made to illustrate and analyze the effect of interconnectivity on the overall sizing, performance, and cost of the interconnected systems of the different households. The purpose of these studies is to examine the variation in the average system size and LLP of the different households when they are part of a microgrid as opposed to the stand-alone situation, and how the increase in the number of households affects the above-mentioned parameters.

5.3.1. Homogeneous inter-connected households

The first case study involves a set of n households that are all part of the same energy tier. For example, a microgrid consisting of 5 households that all have a tier 4 load profile as discussed in section 4.1. In order to avoid having the same load peaks and load profiles, the load profile was shifted by a number of days for each day, hence maintaining the same characteristics, but avoiding common peak points and patterns, hence creating some diversity in the household community. Figure 5.6 below shows an example of two weekly load profiles where the load was shifted by two days.

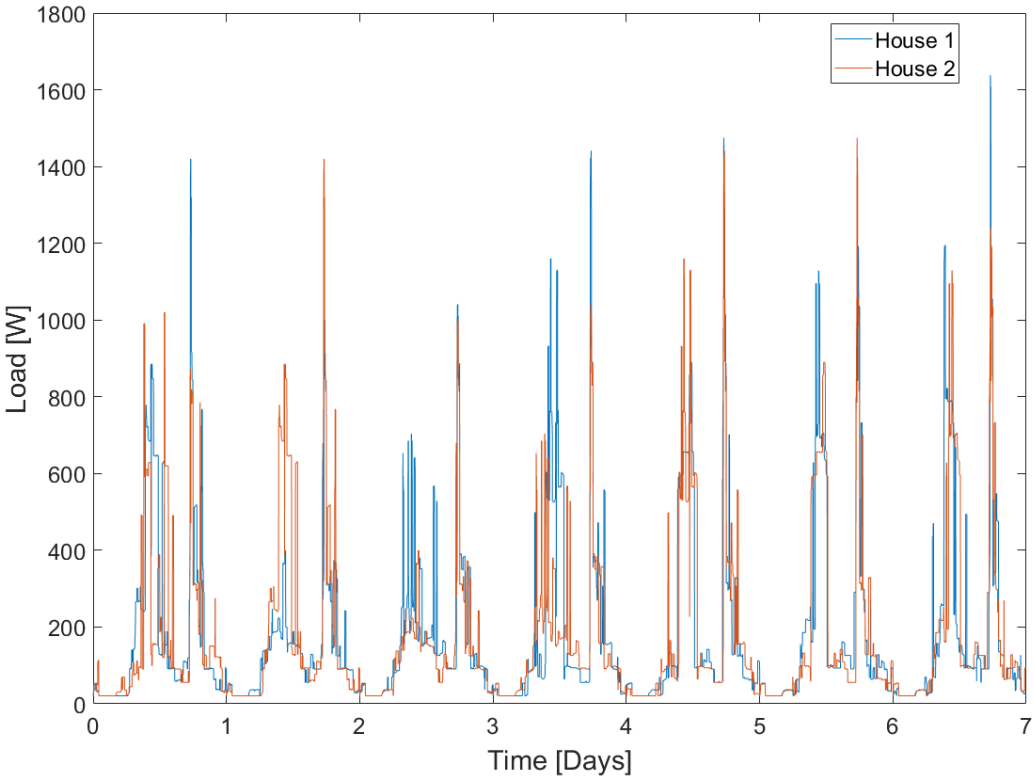

Figure 5.6: Two tier 4 households with a shift of a few days in the load profile

In the figures below, LLP, energy dump and E_{fail} are represented for the case of the district of Pune for each of the tiers. As summarized in table 5.1, the value of the households' SHS size for each tier was set to have an LLP of 10% in the stand-alone case to evaluate the change as the number of households grows until 50.

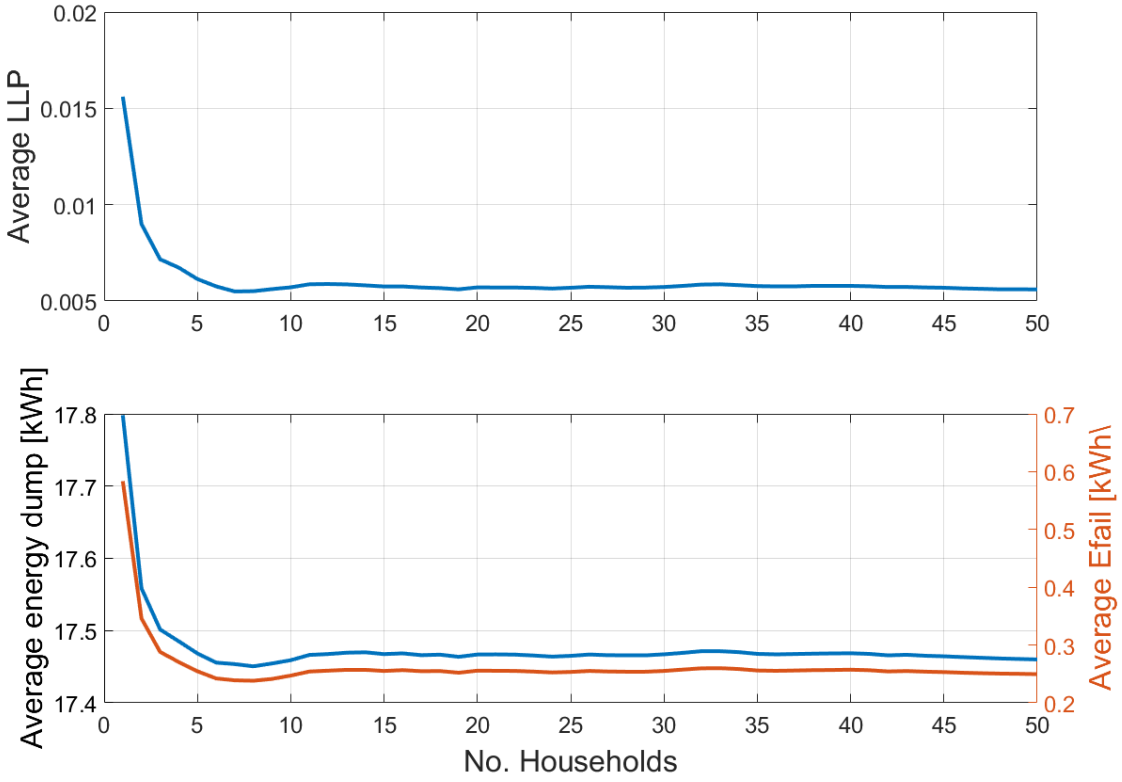

Figure 5.7: Homogeneous community Tier 1: LLP, Edump & Efail VS No. Households

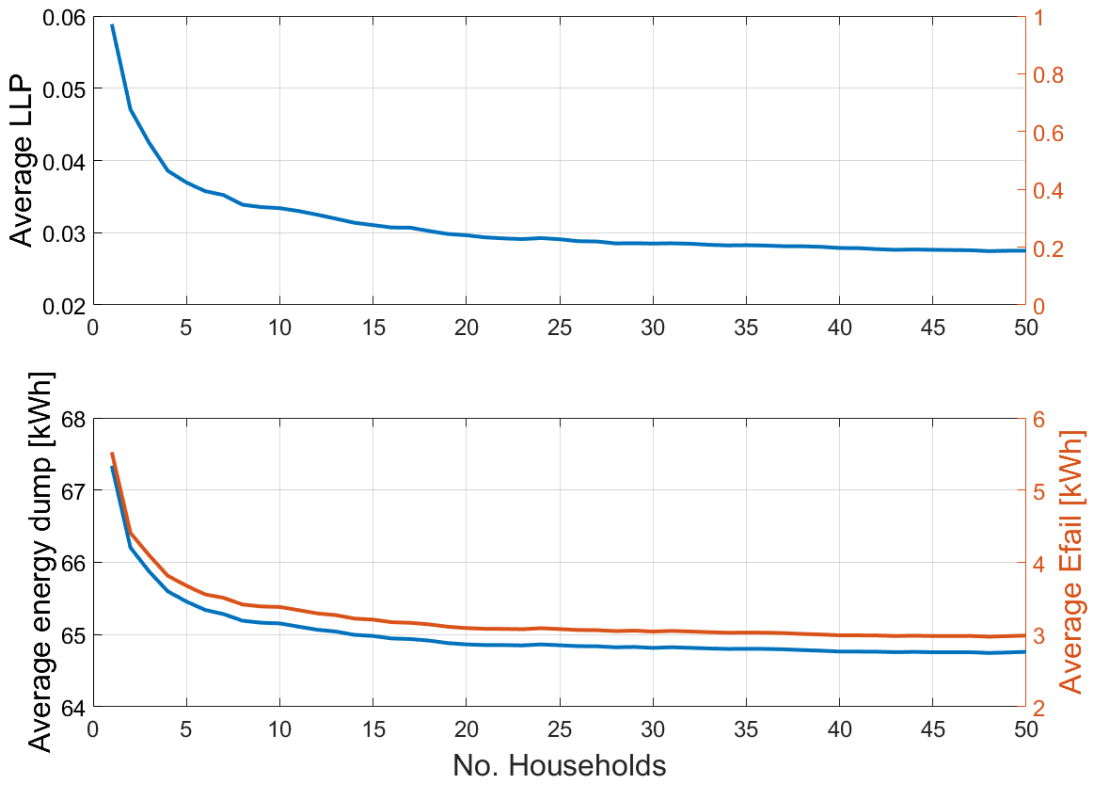

Figure 5.8: Homogeneous community Tier 2: LLP, Edump & Efail VS No. Households

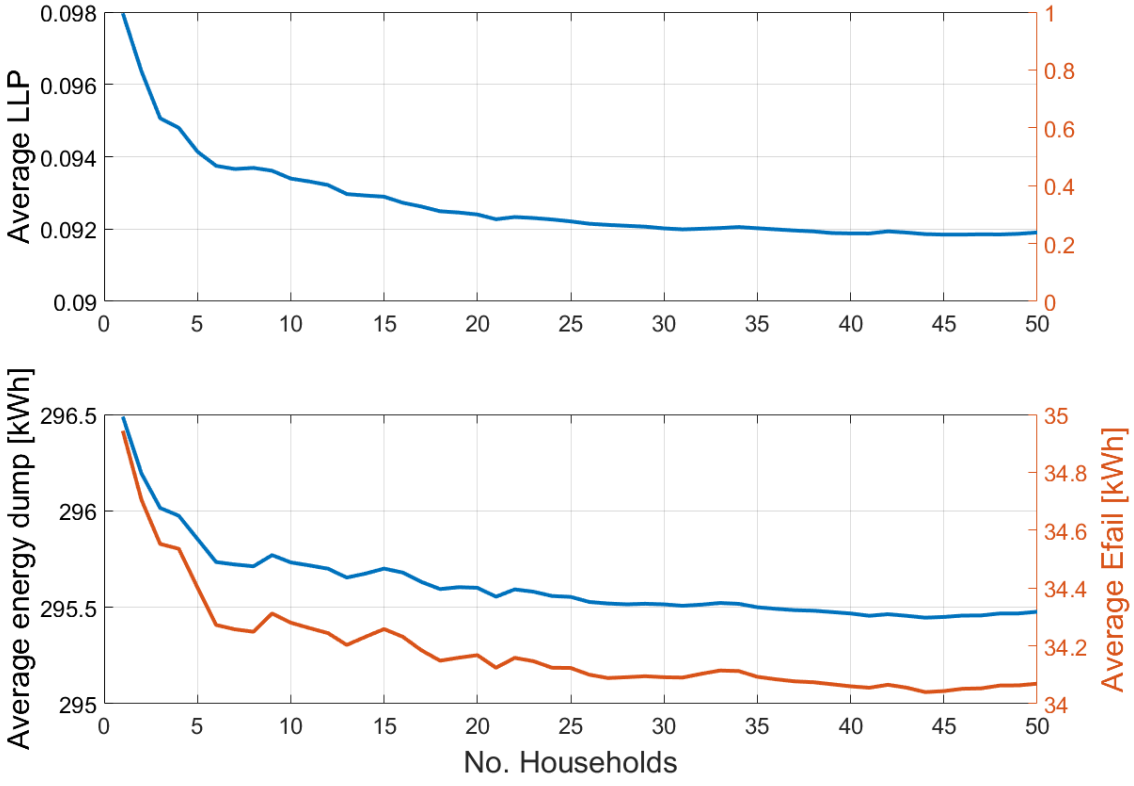

Figure 5.9: Homogeneous community Tier 3: LLP, Edump & Efail VS No. Households

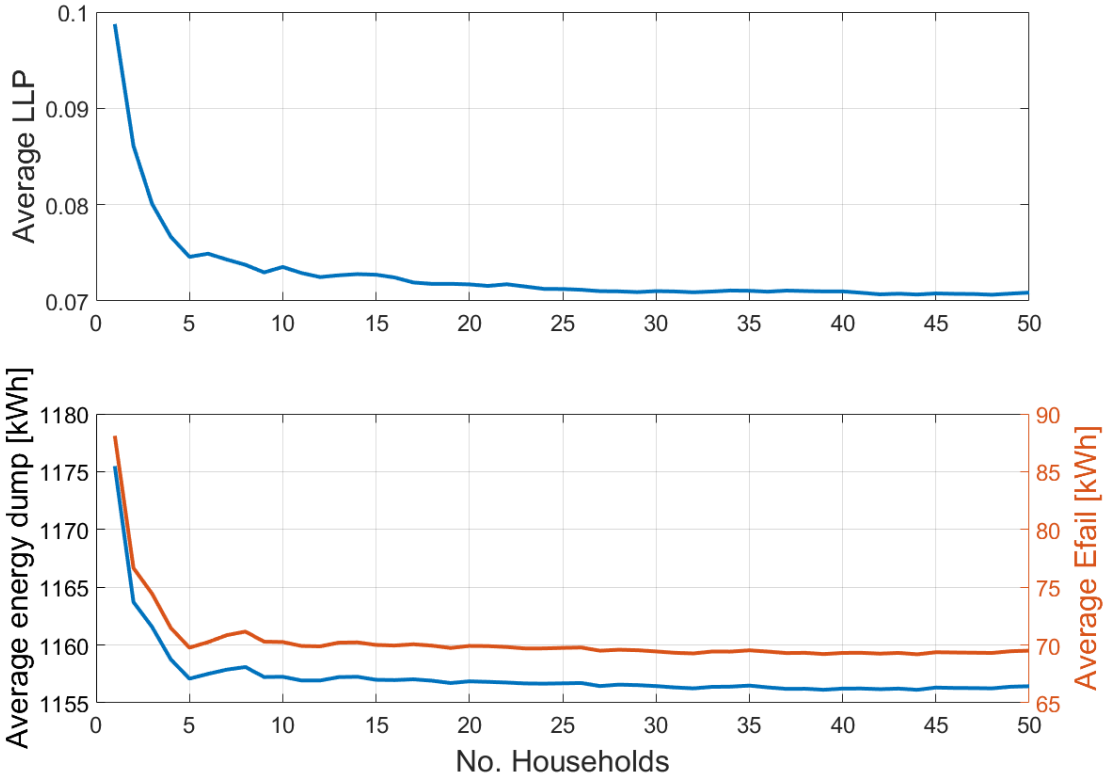

Figure 5.10: Homogeneous community Tier 4: LLP, Edump & Efail VS No. Households

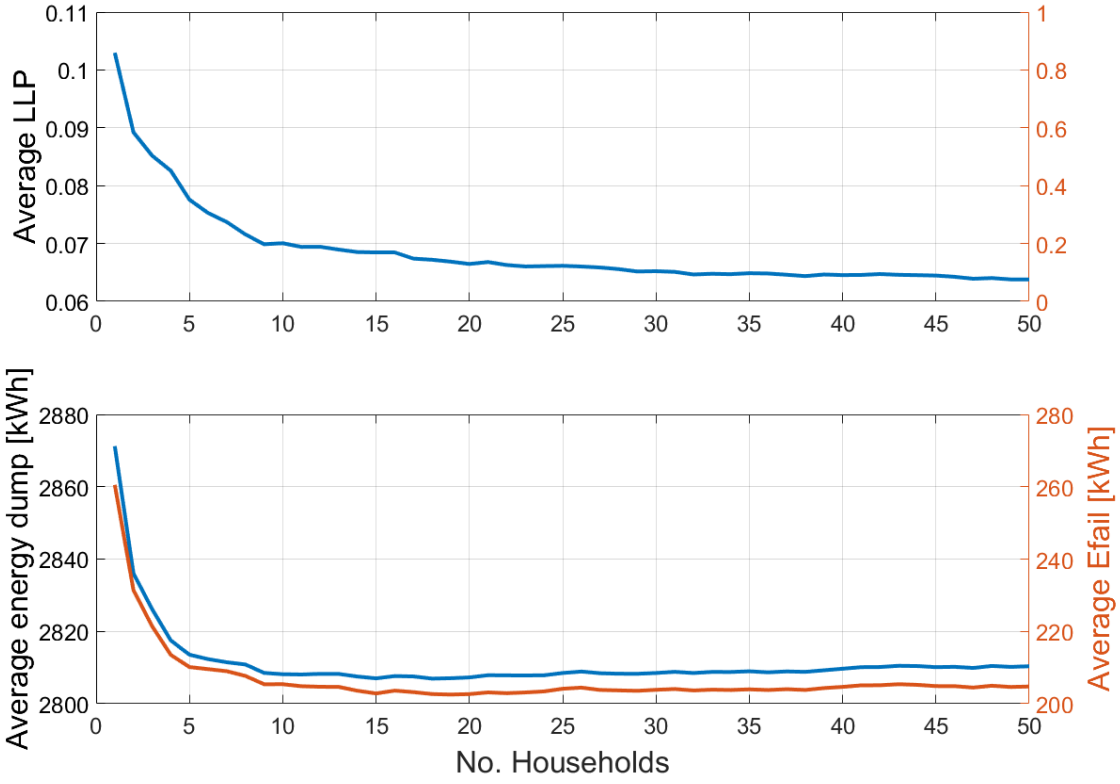

Figure 5.11: Homogeneous community Tier 5: LLP, Edump & Efail VS No. Households

Figures 5.7 through 5.11 show the same trend in the average LLP per household, average energy dump and E_{fail}. The LLP in all tiers decreases by around 30-40% from the range of 1 households up until 15-20 households. The average energy dump and E_{fail} show the same decreasing trend. However, the average energy dump decreases very little (maximum decrease of 5% in tier 2), which E_{fail} ranges greatly between 3 to 45%. Another important point is the saturation point of all parameters as the number of household increases. In all tiers, all three parameters seem to stabilize after reaching 25 households, showing that even with an even large community, the LLP and E_{fail} do not reach 0. A possible interpretation for this behavior is the high similarity between the household loads. The load profile is the same for all households, with a shift of a few days in between each. After a certain number of households, the aggregated load profile reaches a homogeneous pattern that even the load shift cannot diversify it greatly.

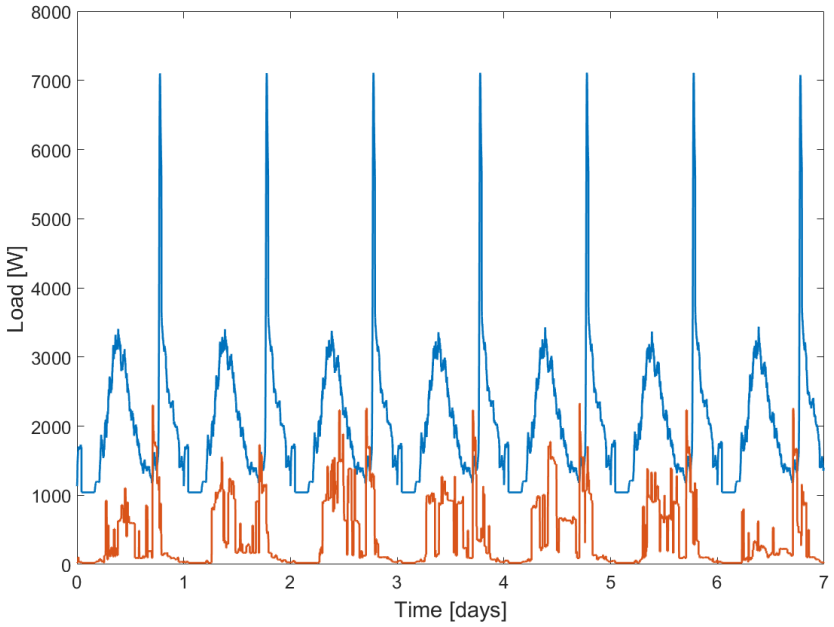

Figure 5.12: Load comparison between 1 household and 50 households.

Figure 5.12 above shows that pattern over a week. In blue, the aggregated shifted load of all households is plotted, while in orange, the load of one household is shown. Both load profiles show the same overall pattern where the single load is a fraction of the larger load, however, the peaks take place at almost the same time. Hence, the 50 household community can be compared to one large household with the aggregated load profile, explaining the reason for the saturation of the parameters.

5.3.2. Heterogeneous households

In this case study, an analysis on a set of interconnected and heterogeneous households is conducted. The case is similar to the homogeneous case, but in this situation, each of the households in the community is assigned a random load profile from the 5 tiers, and the system size to achieve a 10% LLP in that tier in a stand-alone architecture. As observed previously, the LLP and energy dump reach a saturation point after a certain No. of households. Hence, in this case, the number of households was limited from 1 to 15.

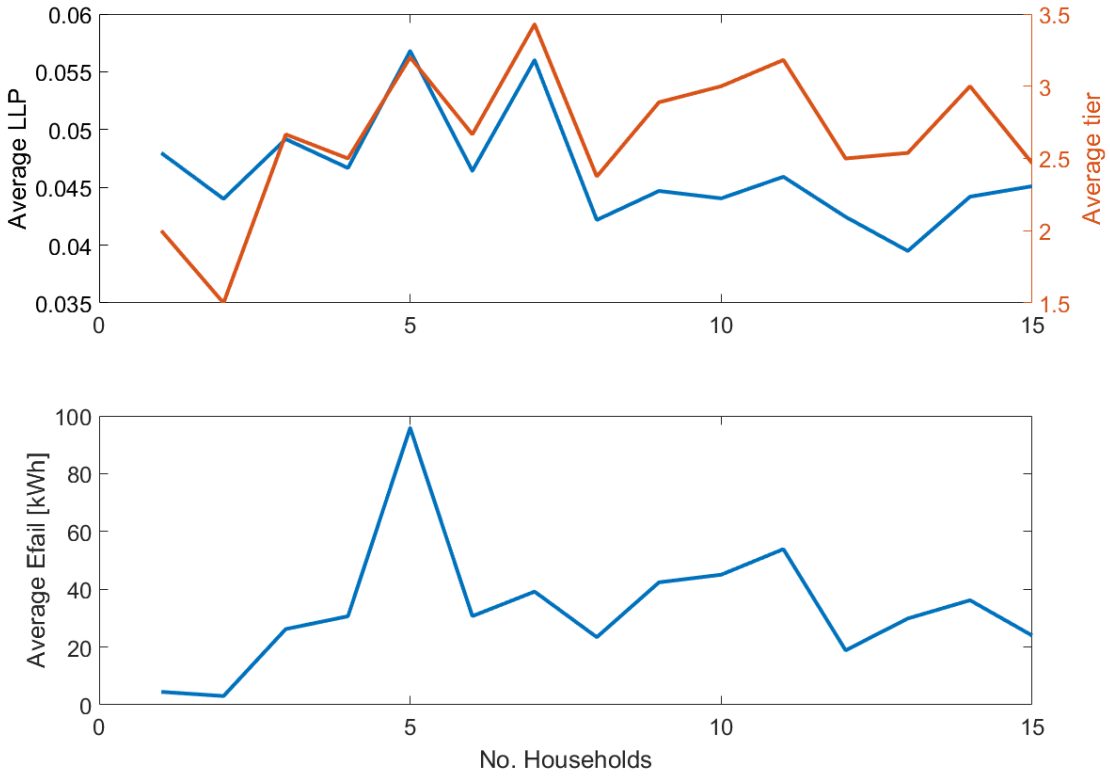

Figure 5.13: Heterogeneous interconnected case: average LLP and Efail for 1 - 15 households.

In the top graph in figure 5.13, the orange curve shows the average tier $\overline{\text{Ti}}$ per household. For example, for 5 households where two are of tier 2, and three are of tier 5, the average tier is $\overline{\text{Ti}} = \frac{19}{5} = 3.8$. The blue curve shows the average LLP per household. The average LLP seems to increase with an increasing $\overline{\text{Ti}}$ for a low number of households, but then stabilizes even if $\overline{\text{Ti}}$ increases when the No. of households is above 10. The same trend can be observed for E_{fail}, which is heavily affected by $\overline{\text{Ti}}$ at first, but then declines irrespective of the value of $\overline{\text{Ti}}$.

5.4. Conclusions

The interconnected methodology presented in this chapter showed that energy sharing among households, especially in the higher tiers, is highly beneficial. The homogeneous case study of the district of Pune, where the LLP, energy dump and E_{fail} were observed as the number of same-tier households increases showed a decrease in the average LLP per household, as well as the average E_{fail}. The decrease rate was the highest for tiers 4 & 5, where the LLP dropped by 30 and 45% respectively. Moreover, E_{fail} dropped by 28% in tier 5. In the higher tiers, this architecture proved to be a good alternative for the stand-alone approach. In tier five, in a stand-alone topology, a 3900 Wp array and 5920 Wh battery capacity is required to achieve a 6% LLP at a cost of 25500$. While a combination of 3450 Wp/5240 Wh, only is needed in an interconnected topology to achieve the same reliability while reducing the cost by 10%. The heterogeneous case showed similar results as the homogeneous study. Although, in this case, due to the variation of the household tiers, the average LLP and E_{fail} were highly affected by the average tier $\overline{\text{Ti}}$ when the total number of households is below 10.

6

Conclusions & Recommendations

In this thesis, two optimization methods were examined to optimize the SHS size in the multi-tier framework. Case studies were made to analyze the effect of the meteorological data on the system. Furthermore, the feasibility of the stand-alone SHS approach was examined for all the tiers, followed by a different approach: household interconnectivity. In this chapter, the conclusions of the study are presented, followed by recommendations for further research.

6.1. Conclusions

The conclusions of this thesis are drawn by answering the research questions raised in chapter 1:

What are the best modeling and optimization strategies to optimize the size of a SHS vis-à-vis the most important parameters, and optimization methods?

1. After having examined several electrical topologies used in renewable energy systems, the DC-coupled topology was opted for as the most feasible, due to the fact that all the system components in a SHS are DC, notably the PV array and battery storage. Moreover, most appliances nowadays are becoming highly efficient, DC powered devices.
2. The most important parameters identified in terms of optimizing the system were:
    - The system upfront cost, including the replacement costs throughout the project lifetime.
    - The system's reliability, quantified via the loss of load probability or LLP.
    - The battery lifetime, which takes the largest fraction of the system upfront cost.
    - The energy dump, which needs to be minimized to avoid over-sizing the system.
3. Conventional sizing methods typically rely on tough estimations based on the user's expertise, such as the sizing factor S_f and the Days of Autonomy (DOA). These methods were proved to be highly unreliable ineffective when proper system sizing is required as highlighted in section 3.5. The test study case in figure 3.27 showed that for 2 DOAs, a battery size of 3450 Wh is needed. During the optimization in chapter 4, the optimal battery size for a 1% LLP was found to be 1270 Wh, hence a decrease of 63%.
4. Two optimization methods were demonstrated in this study, the classical iterative technique, and an evolutionary heuristic multi-optimization technique called the Genetic Algorithm (GA). The iterative method, although more effective than conventional methods, became complicated when increasing the system sizing complexity and addition of parameters. Moreover, this approach proved to require a lot of computational time which depicted its impracticability. On the other hand, using the GA, the multiple parameters along with the constraints were implemented to find the optimal size that would abide to all the desired criteria.

What is the methodology that can be applied to all tiers to obtain the optimal system size that will be able to cope with the household demand? And at what point does the SHS stand-alone approach become unfeasible?

1. The methodology to obtain an optimal system size for the different tiers was organized as follows:

- Building practical models for the different components in the SHS which consist of the PV array, battery storage, and DC/DC converters.
- Designing a control strategy that links the different components and tests their performance over a yearly simulation to obtain the desired system parameters: LLP, dump, cost, and battery lifetime. As shown in flowchart 3.22.
- Formulate the objective functions and constraints for the system optimization:
  - **Objective functions:**
    - *Minimize cost:* $W_{p,PV} \times Q_{PV} + C_B \times Q_B + (S_{C,Battery} + S_{C,PV} + S_{C,Load}) \times Q_C$
    - *Minimize LLP: LLP* $= \frac{t_{downtime}}{T_{total}}$
    - *Maximize Battery lifetime:* From battery lifetime polynomial.
  - **Constraints:**
    - LLP $\leq 10\%$
    - $E_{Dump} \leq 2 \times$Yearly load
- Implementing the control strategy and system functions into the GA, through which the objective functions were targeted to find the optimal system size.

2. The optimal system sizes obtained from the three case studies, summarized in tables 4.7, 4.9 & 4.11 show that for the lower tiers, a stand-alone SHS is ideal to improve the quality of life of households at an affordable cost. While for higher tiers, due to the large increase in loads, this approach is unfeasible due to the large price and lower reliability. The table below highlights the results obtained. It can also be noted that the system sizes differ in each of the tiers due to the difference in sun abundance. N'Djamena, which has an ESH of 6.4, the highest among the areas, requires a smaller SHS compared to East Khasi Hills and Pune, which have an ESH of 4.7 and 5.6 respectively.

Table 6.1: Stand-alone SHS sizing summer for all locations in tiers 2 & 5

		PV [W_p]	**Battery** [Wh]	**PV conv.** [W]	**Battery conv.** [W]	**Cost** [USD]	**LLP** [-]	**Lifetime** [Years]
Tier 2	**N'Djamena**	70	250	67	66	851,2	0,012	6,3
	Pune	110	260	95	93	922,6	0,012	6,4
	East Khasi hills	80	460	69	67	991	0,025	12,5
Tier 5	**N'Djamena**	3800	6090	3642	3531	24486,3	0,015	6,3
	Pune	3900	5740	3345	3237	25299,3	0,052	5,5
	East Khasi hills	5100	7850	4381	4255	33392	0,052	5,9

3. The interconnectivity approach, was tested as an alternative to the stand-alone architecture, where several households are connected together to share their electricity generation and demand. This method proved to be very feasible in terms of reducing both the average LLP and energy dump among the households. Hence, for smaller SHS sizes per household, a more reliable and energy efficient system was obtained.
   - The homogeneous case where all the household community had the load profile from the same tier showed that for system sizes where 10% LLP would be achieved in a stand-alone architecture, the LLP could drop by as much as 45% and E_{fail} by 28% when energy sharing takes place.
   - In the heterogeneous case where the load tier of each household was set randomly and was different from the others, the average LLP and E_{fail} showed a low sensitivity to the number of households and high dependence on the average tier $\overline{\text{Ti}}$ when their total number is below ten, but then exhibited a similar behaviour to the homogeneous case.

6.2. Recommendations and future work

In the following section, recommendations on further research on the topic of SHS optimization are presented:

- First, in further work, it would be recommended to increase the complexity of the component models such as the battery storage, to improve the accuracy of their performance.
- The transmission and miscellaneous losses should be modeled in future works to improve the performance of the model.
- More cases should be examined in the interconnected approach, notable in the heterogeneous case, where not only the number of households is being changed, but also the load profile tiers and system

size of each household. The Genetic Algorithm could be also applicable in this case, where the optimal size of each household is obtained to minimize the average LLP, dump, E_{fail} and overall cost.

- The battery lifetime should be taken into account in the interconnected approach, which is expected to endure a large variation to the increase in throughput due to the energy sharing.
- The upfront cost depends heavily on the discount rate, and cost forecast for the battery technologies. A more accurate system cost study should be conducted where these two factors are addressed in more detail.
- A more elaborate cost sensitivity analysis should be performed, where the effect of changing the prices of the different system components would be analyzed.

A

Battery lifetime coefficients

Table A.1: Polynomial coefficients for Lead-acid and LifePO4 batteries lifetime curves [65].

Coefficients	Flooded Lead-acid	LifePO4
p_0	2,08E+04	5,00E+04
p_1	-9,83E+04	-7,03E+04
p_2	2,13E+05	2,13E+05
p_3	-2,19E+05	3,09E+05
p_4	8,66E+04	-1,56E+05
p_{l0}	-3,911	-2,81
p_{l1}	0,197	0,154
p_{d0}	2,45E+03	6,49E+03
p_{d1}	-1,17E+04	-9,14E+03
p_{d2}	2,54E+04	-1,69E+04
p_{d3}	-2,64E+04	4,02E+04
p_{d4}	1,07E+04	-2,03E+04

Bibliography

[1] World energy outlook 2017. *International Energy Agency*, 2017.

[2] Monaaf Al-falahi, Shantha Jayasinghe, and Hossein Enshaei. A review on recent size optimization methodologies for standalone solar and wind hybrid renewable energy system. 143, 07 2017.

[3] Greg Albright, Jake Edie, and Said Al-Halla. A comparison of lead acid to lithium-ion in stationary storage applications. 2012.

[4] Nicolina Angelou, Elizondo Azuela, Gabriela; Banerjee, Sudeshna Ghosh, Mikul Bhatia, Irina Bushueva, Javier Gustavo Inon, Ivan Jaques Goldenberg, Elisa Portale, and Ashok Sarkar. Global tracking framework. sustainable energy for all. washington, d.c. : World bank group. 2010.

[5] I. Baniasad Askari and M. Ameri. Techno-economic feasibility analysis of stand-alone renewable energy systems (pv/bat, wind/bat and hybrid pv/wind/bat) in kerman, iran. *Energy Sources, Part B: Economics, Planning, and Policy*, 7(1):45–60, 2012. doi: 10.1080/15567240903330384. URL https://doi.org/10.1080/15567240903330384.

[6] Solar Energy Industries Association et al. Rooftop solar panels: Benefits, costs, and smart policies, 2014.

[7] Abtin Ataei, Mojtaba Nedaei, Reza Rashidi, and Changkyoo Yoo. Optimum design of an off-grid hybrid renewable energy system for an office building. 7:053123, 09 2015.

[8] World Bank. Chad: Access to electricity (% of population). 2016.

[9] Ilaria Bendato, Andrea Bonfiglio, Massimo Brignone, Federico Delfino, Fabio Pampararo, R Procopio, and Mansueto Rossi. Design criteria for the optimal sizing of integrated photovoltaic-storage systems. 149, 02 2018.

[10] Hendrik Johannes Bergveld. Battery management systems : design by modelling, 6 2001.

[11] José L. Bernal-Agustín, Rodolfo Dufo-López, and David M. Rivas-Ascaso. Design of isolated hybrid systems minimizing costs and pollutant emissions. *Renewable Energy*, 31(14):2227 – 2244, 2006. ISSN 0960-1481. doi: https://doi.org/10.1016/j.renene.2005.11.002. URL http://www.sciencedirect.com/science/article/pii/S0960148105003356.

[12] F. A. Bhuiyan, A. Yazdani, and S. L. Primak. Optimal sizing approach for islanded microgrids. *IET Renewable Power Generation*, 9(2):166–175, 2015. ISSN 1752-1416. doi: 10.1049/iet-rpg.2013.0416.

[13] MMH Bhuiyan and M Ali Asgar. Sizing of a stand-alone photovoltaic power system at dhaka. *Renewable Energy*, 28(6):929–938, 2003.

[14] Hanieh Borhanazad, Saad Mekhilef, Velappa Gounder Ganapathy, Mostafa Modiri-Delshad, and Ali Mirtaheri. Optimization of micro-grid system using mopso. *Renewable Energy*, 71:295 – 306, 2014. ISSN 0960-1481. doi: https://doi.org/10.1016/j.renene.2014.05.006. URL http://www.sciencedirect.com/science/article/pii/S0960148114002572.

[15] Xavier Camps, Guillermo Velasco, Jordi de la Hoz, and Helena Martín. Contribution to the pv-to-inverter sizing ratio determination using a custom flexible experimental setup. *Applied Energy*, 149:35 – 45, 2015. ISSN 0306-2619. doi: https://doi.org/10.1016/j.apenergy.2015.03.050. URL http://www.sciencedirect.com/science/article/pii/S0306261915003347.

[16] Jenna Carr. An introduction to genetic algorithms. *Senior Project*, 1:40, 2014.

[17] Santosh Chalise, Jason Sternhagen, Timothy M. Hansen, and Reinaldo Tonkoski. Energy management of remote microgrids considering battery lifetime. *The Electricity Journal*, 29(6):1 – 10, 2016. ISSN 1040-6190. doi: https://doi.org/10.1016/j.tej.2016.07.003. URL http://www.sciencedirect.com/science/article/pii/S1040619016300987.

[18] A. Chaurey and T.C. Kandpal. A techno-economic comparison of rural electrification based on solar home systems and pv microgrids. *Energy Policy*, 38(6):3118 – 3129, 2010. ISSN 0301-4215. URL http://www.sciencedirect.com/science/article/pii/S0301421510000807.

[19] A. Chaurey and T.C. Kandpal. A techno-economic comparison of rural electrification based on solar home systems and pv microgrids. *Energy Policy*, 38(6):3118 – 3129, 2010. ISSN 0301-4215. doi: https://doi.org/10.1016/j.enpol.2010.01.052. URL http://www.sciencedirect.com/science/article/pii/S0301421510000807. The Role of Trust in Managing Uncertainties in the Transition to a Sustainable Energy Economy, Special Section with Regular Papers.

[20] Kalyanmoy Deb and Deb Kalyanmoy. *Multi-Objective Optimization Using Evolutionary Algorithms*. John Wiley & Sons, Inc., New York, NY, USA, 2001. ISBN 047187339X.

[21] Charis Demoulias. A new simple analytical method for calculating the optimum inverter size in grid-connected pv plants. *Electric Power Systems Research*, 80(10):1197 – 1204, 2010. ISSN 0378-7796. doi: https://doi.org/10.1016/j.epsr.2010.04.005. URL http://www.sciencedirect.com/science/article/pii/S0378779610000866.

[22] Rodolfo Dufo-López and José L. Bernal-Agustín. Design and control strategies of pv-diesel systems using genetic algorithms. *Solar Energy*, 79(1):33 – 46, 2005. ISSN 0038-092X. doi: https://doi.org/10.1016/j.solener.2004.10.004. URL http://www.sciencedirect.com/science/article/pii/S0038092X04003020.

[23] Rodolfo Dufo-López, Juan M. Lujano-Rojas, and José L. Bernal-Agustín. Comparison of different lead–acid battery lifetime prediction models for use in simulation of stand-alone photovoltaic systems. *Applied Energy*, 115:242 – 253, 2014. ISSN 0306-2619. doi: https://doi.org/10.1016/j.apenergy.2013.11.021. URL http://www.sciencedirect.com/science/article/pii/S0306261913009148.

[24] Rodolfo Dufo-López, Iván R. Cristóbal-Monreal, and José M. Yusta. Optimisation of pv-wind-diesel-battery stand-alone systems to minimise cost and maximise human development index and job creation. *Renewable Energy*, 94:280 – 293, 2016. ISSN 0960-1481. doi: https://doi.org/10.1016/j.renene.2016.03.065. URL http://www.sciencedirect.com/science/article/pii/S096014811630249X.

[25] Orhan Ekren and Banu Yetkin Ekren. Size optimization of a pv/wind hybrid energy conversion system with battery storage using response surface methodology. *Applied Energy*, 85(11):1086 – 1101, 2008. ISSN 0306-2619. doi: https://doi.org/10.1016/j.apenergy.2008.02.016. URL http://www.sciencedirect.com/science/article/pii/S0306261908000524.

[26] Adel El-Menchawy, Hesham Bassioni, and A-Aziz Farouk. Photovoltaic systems in existing residential building in egypt.

[27] Sustainable Energy for All (SE4ALL. Country data: Chad.

[28] L. R. Foulds. *Classical Optimization*, pages 257–309. Springer New York, New York, NY, 1981. ISBN 978-1-4613-9458-7. doi: 10.1007/978-1-4613-9458-7_7. URL https://doi.org/10.1007/978-1-4613-9458-7_7.

[29] Ran Fu, David J Feldman, Robert M Margolis, Michael A Woodhouse, and Kristen B Ardani. Us solar photovoltaic system cost benchmark: Q1 2017. 2017.

[30] M.K. Fuentes, Sandia Laboratory, and United States. Department of Energy. *A Simplified Thermal Model for Flat-plate Photovoltaic Arrays*. SAND (Series) (Albuquerque, N.M.). Sandia Laboratories, 1987. URL https://books.google.com.lb/books?id=tUXWQQAACAAJ.

[31] Karina Garbesi, Vagelis Vossos, and Hongxia Shen. Catalog of dc appliances and power systems, 12 2017.

[32] Mahmoud Ghofrani and Negar Niromand Hosseini. Optimizing hybrid renewable energy systems: A review. 12 2016.

[33] Anjela Govan. Introduction to optimization. In *North Carolina State University, SAMSI NDHS, Undergraduate workshop*, 2006.

[34] S. Harrington and J. Dunlop. Battery charge controller characteristics in photovoltaic systems. *IEEE Aerospace and Electronic Systems Magazine*, 7(8):15–21, Aug 1992. ISSN 0885-8985.

[35] Randy L Haupt, Sue Ellen Haupt, and Sue Ellen Haupt. *Practical genetic algorithms*, volume 2. Wiley New York, 1998.

[36] Hoeppecke. Installation, commissioning and operating instructions for valve-regulated stationary lead-acid batteries - solar battery data sheet. 2015.

[37] Ramin Hosseinalizadeh, Hamed Shakouri G, Mohsen Sadegh Amalnick, and Peyman Taghipour. Economic sizing of a hybrid (pv–wt–fc) renewable energy system (hres) for stand-alone usages by an optimization-simulation model: Case study of iran. *Renewable and Sustainable Energy Reviews*, 54: 139 – 150, 2016. ISSN 1364-0321. doi: https://doi.org/10.1016/j.rser.2015.09.046. URL http://www.sciencedirect.com/science/article/pii/S1364032115010163.

[38] International Renewable Energy Agency (IRENA). Solar pv in africa: Costs and markets. 2016.

[39] International Renewable Energy Agency IRENA. Renewable power generation costs in 2017, 2017.

[40] Saiful Islam, Achim Woyte, Ronnie Belmans, and Johan Nijs. Undersizing inverters for grid connection what is the optimum? 07 2018.

[41] Ammu Susanna Jacob, Rangan Banerjee, and Prakash Chandra Ghosh. Modelling and simulation of a pv battery grid backup system for various climatic zones of india. In *Photovoltaic Specialist Conference (PVSC), 2017 IEEE 44th*, pages 1–6. IEEE, 2017.

[42] M. Jantsch, H. Schmidt, and J. Schmid. Results on the concerted action on power conditioning and control. In *11th European photovoltaic Solar Energy Conference*, pages 1589–1592, 1992.

[43] Richard H Jones. Energy poverty: How to make modern energy access universal. *Special early excerpt of the World Energy Outlook*, 2010.

[44] Azadeh Kamjoo, Alireza Maheri, Arash M. Dizqah, and Ghanim A. Putrus. Multi-objective design under uncertainties of hybrid renewable energy system using nsga-ii and chance constrained programming. *International Journal of Electrical Power Energy Systems*, 74:187 – 194, 2016. ISSN 0142-0615. doi: https://doi.org/10.1016/j.ijepes.2015.07.007. URL http://www.sciencedirect.com/science/article/pii/S0142061515002938.

[45] Cornelia R. Karger and Wilfried Hennings. Sustainability evaluation of decentralized electricity generation. *Renewable and Sustainable Energy Reviews*, 13(3):583 – 593, 2009. ISSN 1364-0321. doi: https://doi.org/10.1016/j.rser.2007.11.003. URL http://www.sciencedirect.com/science/article/pii/S1364032107001517.

[46] M. N. I. Khan, M. Z. Khan, D. F. Noor, A. Nahiyan, M. E. Haque, S. S. Saha, M. R. K. Rachi, and M. Z. R. Khan. Modelling and simulation of an efficient charge controller for photovoltaic system with maximum power point tracking. In *2014 3rd International Conference on the Developments in Renewable Energy Technology (ICDRET)*, pages 1–5, May 2014. doi: 10.1109/ICDRET.2014.6861672.

[47] Tamer Khatib, Ibrahim A. Ibrahim, and Azah Mohamed. A review on sizing methodologies of photovoltaic array and storage battery in a standalone photovoltaic system. *Energy Conversion and Management*, 120: 430–448, 7 2016. ISSN 0196-8904. doi: 10.1016/j.enconman.2016.05.011.

[48] S.A. Klein and W.A. Beckman. Loss-of-load probabilities for stand-alone photovoltaic systems. *Solar Energy*, 39(6):499 – 512, 1987. ISSN 0038-092X. doi: https://doi.org/10.1016/0038-092X(87)90057-0. URL http://www.sciencedirect.com/science/article/pii/0038092X87900570.

[49] Jing Li, Wei Wei, and Ji Xiang. A simple sizing algorithm for stand-alone pv/wind/battery hybrid microgrids. 5:5307–5323, 12 2012.

[50] Akbar Maleki and Fathollah Pourfayaz. Optimal sizing of autonomous hybrid photovoltaic/wind/battery power system with lpsp technology by using evolutionary algorithms. *Solar Energy*, 115(Complete):471–483, 2015. doi: 10.1016/j.solener.2015.03.004.

[51] Vasileios Marioleas. Sip ii project: Cycle life analysis and cost evaluation of the main battery technologies for off-grid pv systems. unpublished.

[52] MATLAB. *gamultiobj Algorithm*. The MathWorks Inc., Natick, Massachusetts, 2018.

[53] MATLAB. *Genetic Algorithm Terminology*. The MathWorks Inc., Natick, Massachusetts, 2018.

[54] Meteonorm. Meteonorm data sources. URL http://www.meteonorm.com/en/features/features.

[55] Morningstar. Heat dissipation of the tristar tristar mppt controllers inside enclosures. 2014.

[56] T. Morstyn, B. Hredzak, and V. G. Agelidis. Network topology independent multi-agent dynamic optimal power flow for microgrids with distributed energy storage systems. *IEEE Transactions on Smart Grid*, 9 (4):3419–3429, July 2018. ISSN 1949-3053. doi: 10.1109/TSG.2016.2631600.

[57] N. Narayan, T. Papakosta, V. Vega-Garita, J. Popovic-Gerber, P. Bauer, and M. Zeman. A simple methodology for estimating battery lifetimes in solar home system design. In *2017 IEEE AFRICON*, pages 1195–1201, Sept 2017. doi: 10.1109/AFRCON.2017.8095652.

[58] N Narayan, Z Qin, J Popovic, P Bauer, and M Zeman. Evaluating the techno-economic feasibility of battery technologies in the context of solar home systems. Unpublished.

[59] Nishant Narayan. Stochastic load profile construction for the multi-tier framework for household electricity access using off-grid dc appliances. 2018.

[60] Nishant Narayan, Thekla Papakosta, Victor Vega-Garita, Zian Qin, Jelena Popovic-Gerber, Pavol Bauer, and Miroslav Zeman. Estimating battery lifetimes in solar home system design using a practical modelling methodology. *Applied Energy*, 228:1629 – 1639, 2018. ISSN 0306-2619. doi: https://doi.org/10.1016/j.apenergy.2018.06.152. URL http://www.sciencedirect.com/science/article/pii/S0306261918310225.

[61] FDJ Nieuwenhout, A Van Dijk, PE Lasschuit, G Van Roekel, VAP Van Dijk, D Hirsch, H Arriaza, M Hankins, BD Sharma, and H Wade. Experience with solar home systems in developing countries: a review. *Progress in Photovoltaics: Research and Applications*, 9(6):455–474, 2001.

[62] Times of India. Learning with the times: Why 17% homes have no electricity in 100% electrified india. 2018.

[63] Ayodeji Ogunjuyigbe, Raphael Ayodele, and Olayinka Akinola. Optimal allocation and sizing of pv/wind/split-diesel/battery hybrid energy system for minimizing life cycle cost, carbon emission and dump energy of remote residential building. 171:153–171, 06 2016.

[64] Gregoris Panayiotou, Soteris Kalogirou, and Savvas Tassou. Design and simulation of a pv and a pv–wind standalone energy system to power a household application. *Renewable Energy*, 37(1):355 – 363, 2012. ISSN 0960-1481. doi: https://doi.org/10.1016/j.renene.2011.06.038. URL http://www.sciencedirect.com/science/article/pii/S0960148111003752.

[65] Thekla Papakosta. Investigating hybrid battery configuration for solar home systems. Unpublished.

[66] K. Peippo and P.D. Lund. Optimal sizing of solar array and inverter in grid-connected photovoltaic systems. *Solar Energy Materials and Solar Cells*, 32(1):95 – 114, 1994. ISSN 0927-0248. doi: https://doi.org/10.1016/0927-0248(94)90259-3. URL http://www.sciencedirect.com/science/article/pii/0927024894902593.

[67] Amol A. Phadke, Arne Jacobson, Won Young Park, Ga Rick Lee, Peter Alstone, and Amit Khare. Powering a home with just 25watts of solar pv: Super-efficient appliances can enable expanded off-grid energy service using small solar power systems. Technical report, 04/2015 2015.

[68] Sabine Piller, Marion Perrin, and Andreas Jossen. Methods for state-of-charge determination and their applications. *Journal of Power Sources*, 96(1):113 – 120, 2001. ISSN 0378-7753. doi: https://doi.org/10.1016/S0378-7753(01)00560-2. URL http://www.sciencedirect.com/science/article/pii/S0378775301005602. Proceedings of the 22nd International Power Sources Symposium.

[69] V. Pop, H.J. Bergveld, P.P.L. Regtien, J.H.G. Op het Veld, D. Danilov, and P.H.L. Notten. Battery aging and its influence on the electromotive force. *Journal of the Electrochemical Society*, 154(8):A744–A750, 2007. ISSN 0013-4651. doi: 10.1149/1.2742296.

[70] D R George and Iain Macgill. Solar home systems vs. the grid in rural india: A balancing act of risk and reward, 12 2016.

[71] M R. Vervaart and Frans Nieuwenhout. Manual for the design and modification of solar home system components. 01 2001.

[72] *20W Monocrystalline Solar Panel*. Renogy.

[73] Paul Ruetschi. Aging mechanisms and service life of lead–acid batteries. *Journal of Power Sources*, 127(1): 33 – 44, 2004. ISSN 0378-7753. doi: https://doi.org/10.1016/j.jpowsour.2003.09.052. URL http://www.sciencedirect.com/science/article/pii/S0378775303009340. Eighth Ulmer Electrochemische Tage.

[74] Sarangthem Sanajaoba and Eugene Fernandez. Maiden application of cuckoo search algorithm for optimal sizing of a remote hybrid renewable energy system. *Renewable Energy*, 96:1 – 10, 2016. ISSN 0960-1481. doi: https://doi.org/10.1016/j.renene.2016.04.069. URL http://www.sciencedirect.com/science/article/pii/S0960148116303718.

[75] Dirk Sauer, Georg Bopp, Andreas Jossen, Juergen Garche, Martin Rothert, and Michael Wollny. State of charge - what do we really speak about ?, 06 1999.

[76] O Schmidt, A Hawkes, A Gambhir, and I Staffell. The future cost of electrical energy storage based on experience rates. *Nature Energy*, 2(8):17110, 2017.

[77] Vinod Kumar Sharma, Antonio Colangelo, and Giuseppe Spagna. Photovoltaic technology: basic concepts, sizing of a stand alone photovoltaic system for domestic applications and preliminary economic analysis. *Energy Conversion and Management*, 36(3):161–174, 1995.

[78] Rajanna Siddaiah and R.P. Saini. A review on planning, configurations, modeling and optimization techniques of hybrid renewable energy systems for off grid applications. *Renewable and Sustainable Energy Reviews*, 58:376 – 396, 2016. ISSN 1364-0321. doi: https://doi.org/10.1016/j.rser.2015.12.281. URL http://www.sciencedirect.com/science/article/pii/S1364032115016640.

[79] Arno Smets, Klaus Jäger, Olindo Isabella, R.A.C.M.M. Van Swaaij, and Miro Zeman. *Solar Energy - The physics and engineering of photovoltaic conversion, technologies and systems*. 02 2016. ISBN 9781906860325.

[80] Jessika Trancik, Patrick Brown, Joel Jean, Goksin Kavlak, Magdalena Klemun, Morgan Edwards, James Mcnerney, Marco Miotti, Joshua Mueller, and Zachary Needell. Technology improvement and emissions reductions as mutually reinforcing efforts: Observations from the global development of solar and wind energy. 11 2015.

[81] IT Power (UK) and AETS (France). Evaluation of the financial and economic combination of shs and mini-grid systems. 2015.

[82] John Voelcker. Electric car battery warranties compared. *R GreenCar Reports*, 2016.

[83] H.X. Wang, M.A. Muñoz-García, G.P. Moreda, and M.C. Alonso-García. Optimum inverter sizing of grid-connected photovoltaic systems based on energetic and economic considerations. *Renewable Energy*, 118 (C):709–717, 2018. doi: 10.1016/j.renene.2017.11. URL https://ideas.repec.org/a/eee/renene/v118y2018icp709-717.html.

[84] Global Solar Atlas World Bank. Photovoltaic solar potential - india, 2017.

[85] Wai Kean Yap and Vishy Karri. An off-grid hybrid pv/diesel model as a planning and design tool, incorporating dynamic and ann modelling techniques. *Renewable Energy*, 78:42–50, 6 2015. ISSN 0960-1481. doi: 10.1016/j.renene.2014.12.065.

[86] K Yumkella and C Holiday. Sustainable energy for all: a global action agenda. *New York: The*, 2012.

[87] Brian Min Zachary O'Keeffe Fan Zhang. *Whose Power Gets Cut? Using High-Frequency Satellite Images to Measure Power Supply Irregularity*. The World Bank, 2017. doi: 10.1596/1813-9450-8131. URL https://elibrary.worldbank.org/doi/abs/10.1596/1813-9450-8131.

[88] Bo Zhao, Xuesong Zhang, Peng Li, Ke Wang, Meidong Xue, and Caisheng Wang. Optimal sizing, operating strategy and operational experience of a stand-alone microgrid on dongfushan island. *Applied Energy*, 113:1656 – 1666, 2014. ISSN 0306-2619. doi: https://doi.org/10.1016/j.apenergy.2013.09.015. URL http://www.sciencedirect.com/science/article/pii/S0306261913007629.

[89] Ghassan Zubi, Rodolfo Dufo-López, Nicolás Pardo, and Guzay Pasaoglu. Concept development and techno-economic assessment for a solar home system using lithium-ion battery for developing regions to provide electricity for lighting and electronic devices. *Energy Conversion and Management*, 122: 439 – 448, 2016. ISSN 0196-8904. doi: https://doi.org/10.1016/j.enconman.2016.05.075. URL http://www.sciencedirect.com/science/article/pii/S0196890416304538.